ABSTRACT

Lithospheric Magmatism in Southern Colorado and Northern New Mexico

Daniel James Wegert, Ph.D.

Mentor: Don F. Parker, Ph.D.

This dissertation looks at the formation of three different volcanic centers throughout southern Colorado and northern New Mexico to evaluate potential sources for their subduction-like trace element signatures. These subduction signatures are found in volcanic rocks formed well away from concurrent subduction and are, in many cases, rift related.

The Laramide-age McDermott Formation is a lahar deposit deposited into the San Juan Basin formed through melting of Proterozoic subduction-modified lithospheric mantle. Near zero εNd_t values (-1.94 and 0.47) rule out a crustal source for these magmas, while trace element ratios suggest a subduction-modified continental lithosphere source. Geochemical analyses suggest a possible relationship to the La Plata Mountains intrusive complex, though weathering and sericitization have made confirming this hypothesis impossible.

The Nathrop domes are crustal melts formed due to partial melting associated with crustal extension along the Arkansas Valley Graben segment of the Rio Grande Rift. εNd_t values (-10.1, Bald Mountain and -13.9, Precambrian granite) suggest that the magmas ancestral to those of the Nathrop Domes were largely the result of partial melting of Precambrian crustal rock. These crustal melts then evolved through protracted crystal fractionation of observed phenocrysts, yielding the large enrichment/depletion patterns observed in incompatible element diagrams.

The Raton-Clayton volcanic field lies on the Jemez Lineament, on the eastern flank of the Rio Grande Rift. The Jemez Lineament coincides with the ancient Proterozoic boundary between the Matzatzal and Yavapai terranes, which have been interpreted as accreted arc complexes. The subduction signature present in the RCVF lavas is attributed to modification during this event. The RCVF magmas show evidence that both assimilation and fractional crystallization played significant roles in their evolution. εNd values for all samples indicate derivation from lithospheric mantle. Olivine back-calculation results were used to determine that magmas ancestral to Raton-Clayton basalts were formed between 50 and 217 km inside the Earth.

Lithospheric Magmatism in Southern Colorado and Northern New Mexico

by

Daniel James Wegert, B.S., M.S.

A Dissertation

Approved by the Department of Geology

_____

Stacy C. Atchley, Ph.D., Chairperson

Submitted to the Graduate Faculty of
Baylor University in Partial Fulfillment of the
Requirements for the Degree
of

Doctor of Philosophy

Approved by the Dissertation Committee

_____

Don F. Parker, Ph.D., Chairperson

_____

Steve Dworkin, Ph.D.

_____

Vincent Cronin, Ph.D.

_____

Steven Driese, Ph.D.

_____

Darrin Bellert, Ph.D.

Accepted by the Graduate School

August 2014

_____

J. Larry Lyon, Ph.D., Dean

Page bearing signatures is kept on file in the Graduate School.

TABLE OF CONTENTS

LIST OF FIGURES

LIST OF TABLES

ACKNOWLEDGMENTS

There are numerous people that I would like to thank. First, I owe a great debt to my advisor, Dr. Don Parker. His guidance and assistance in the lab, classroom, and field have been invaluable to me throughout this entire process. Second, I would like to thank my committee members, Dr. Steve Dworkin, Dr. Vincent Cronin, Dr. Steven Driese, and Dr. Darrin Bellert for their support and guidance. Third, I want to thank the professors and staff of the Baylor University Department of Geology for their support, patience, and assistance. Fourth, I would like to thank Charles Chapin, Nancy McMillan, Eric Christiansen, Donald Burt, Art Snoke, and Brendon Orr for their assistance in editing my first two manuscripts. Fifth, the National Park Service for their permission to collect samples from Capulin Volcano for use in this dissertation. Finally, I would like to thank my family and friends for their support, patience, understanding and love.

DEDICATION

To my wonderful wife Jennifer whose love and support kept me sane

CHAPTER ONE

Introduction

Numerous volcanic rocks, throughout Colorado and New Mexico, exhibit trace element patters similar to subduction-related volcanic rocks. These volcanic centers are located far from areas of concurrent subduction, which raises the question of the origin of these subduction-like trace element signatures. This dissertation uses a variety of geochemical techniques to look at three different volcanic centers to determine the source for these trace element signatures. These three locations were chosen to look at specific aspects of the Cenozoic age volcanism in southern Colorado and northern New Mexico.

Chapter Two is a reproduction of an article on the McDermott Formation, which was published in Rocky Mountain Geology. The McDermott Formation was formed from volcanic debris being shed off of a late Cretaceous volcanic complex that was likely centered to the north of the San Juan Basin. Cobble to small boulder size trachyandesite fragments are preserved in this formation. Chemically, these trachyandesites are very similar, with the main variations being the result of potassium metasomatism. This metasomatism is also present in intrusive rocks from the hypothesized source region: the La Plata Mountains. Analyses of the volcanic material clearly shows the subduction-like trace element signature. This volcanic center provided us with the opportunity to evaluate pre-Rio Grande Rift volcanism.

Chapter Three is a reproduction of an article on the Nathrop Domes in Colorado, which was published in Rocky Mountain Geology. The Nathrop Domes are a group of

four lava dome volcanoes erupted along the eastern side of the Arkansas Valley Graben, which is the northernmost segment of the Rio Grande Rift. These domes are examples of "topaz rhyolite", which is commonly reported to be the result of melting crustal material. Geochemical data suggests that these domes were the result of partial melting of crustal material that mixed with some mantle generated melt associated with the Rio Grande Rift. These rift related samples do not display the subduction-like signature present in the other locations. This gave us the chance to evaluate lower crustal material as a source for the subduction-like trace element signatures.

Chapter Four is a reproduction of a journal article on the Raton-Clayton volcanic field in New Mexico, which has been submitted to a journal for review. The Raton-Clayton volcanic field is located on the eastern flank of the Rio Grande Rift and sits on the Jemez Lineament. This field contains a wide range of lava compositions extending from silica undersaturated feldspathoidal to low-silica rhyolitic compositions. Raton-Clayton lavas also exhibit the subduction-like trace element signature, but their ages and location clearly indicates that they are rift related. Many of the Raton-Clayton lavas show evidence that open system processes played a role in their evolution. This field allowed us access to very young volcanic material that had undergone minimal weathering. This field also gave us the opportunity to look at a wide variety of rock compositions, where the previous two localities contained only one major composition.

Dr. Don F. Parker has been my advisor throughout the research and writing of this dissertation. He has assisted with sample analysis performed at Baylor University and with the editing of this document and the three manuscripts it contains. Minghua Ren assisted me with the initial electron microprobe work and performed additional

microprobe work for the second and third manuscripts. David Edlin was my field assistant during the summer of 2008 and wrote his senior thesis on Sierra Grande from the Raton-Clayton volcanic field.

CHAPTER TWO

Petrogenesis of the McDermott Formation Trachyandesite, San Juan Basin, Colorado and New Mexico

This chapter published as: Wegert, D., and Parker, D.F., 2011, Petrogenesis of the McDermott Formation Trachyandesite, San Juan basin, Colorado and New Mexico: Rocky Mountain Geology, v. 46, n. 2, p. 183-196

ABSTRACT

Lahar deposits within the Late Cretaceous McDermott Formation (Maastrichtian) contain abundant trachyandesite volcanic clasts with a fairly narrow range of whole rock composition. The outcrop pattern and thickness variations of the McDermott Formation suggest a source located in the general area of the present-day La Plata Mountains. Major and trace element trends indicate a possible petrogenetic relationship between the McDermott trachyandesite and La Plata Mountains intrusive rocks. Incompatible trace element compositions show subduction signatures in the trachyandesite and La Plata intrusive rocks, as well as in lower crustal xenoliths from the nearby Navajo volcanic field. Trace element patterns of Proterozoic units from the adjacent San Juan uplift rule out involvement of these upper crustal units in McDermott petrogenesis. Near zero εNd_t (-1.94 and 0.47) values rule out a crustal source for these magmas as crustal values typically range from -6 to -18. Ba/La vs. Nb/La plots and εNd_t data suggest a subduction modified continental lithospheric mantle source for these rocks. This lithospheric mantle may have acquired its orogenic trace element signature during formation of the Proterozoic Yavapai terrane, which underlies the region.

INTRODUCTION

The McDermott Formation is a volcaniclastic sedimentary unit that crops out along the northwestern margin of the San Juan Basin in New Mexico and Colorado (Figures 1 and 2) (Reeside, 1924). Lahar deposits comprise most of the unit and contain abundant trachyandesitic boulders. The McDermott Formation is thickest in the northwest part of the basin and thins to the southeast (Reeside, 1924). McDermott samples exhibit incompatible trace element patterns similar to those of typical arc magmas, yet there is little additional evidence to suggest that the McDermott Formation is related to concurrent subduction. Similar subduction-like geochemical signatures in younger Colorado Plateau rocks that are clearly not related to concurrent subduction, have been attributed to a metasomatized lithospheric mantle source (Fitton et al., 1988). However, little to no work has been done up to this point to characterize the McDermott Formation or to determine its source.

The objectives of this study are to characterize the petrography, chemistry and petrogenesis of McDermott trachyandesite, to determine likely sources for the incompatible trace element patterns seen in this unit, and to place this magmatism in a regional context. We investigate a possible relationship between the McDermott Formation and contemporaneous intrusive units of the La Plata Mountains. We also evaluate several potential magma contaminants and discuss possible sources for the McDermott Formation magmas.

This study is part of a larger project studying the source of subduction-like trace element signatures in magmas in and around the Rio Grande Rift. This study focuses on these signatures in pre-rift volcanic rocks. Future work will look at the volcanic rocks of

the Raton-Clayton volcanic field in New Mexico and Colorado as examples of rift-related mantle melts.

GEOLOGIC SETTING

General Geology

The Laramide Orogeny in Colorado began in the late Cretaceous as basement uplifts divided the Sevier foreland basin into smaller, isolated basins (Dickinson et al., 1988). Laramide volcanism has been attributed to shallow angle subduction of the Farallon plate (Lipman et al., 1972; Dickinson and Snyder, 1978). Other studies have suggested that early Laramide tectonism caused downwarping of lithospheric material, and subsequent isostatic uplift allowed decompression melting to occur (Mutschler et al., 1987). A newer hypothesis is that the subduction of an oceanic plateau caused the shift of the Laramide volcanism inward (Gutscher et al., 2000).

The Proterozoic crust of Colorado is largely composed of arc terranes accreted onto the Wyoming craton (Karlstrom et al., 2004). These terranes are divided into two provinces: the Yavapai province is a juvenile accreted-arc terrane with 1.8-1.7 Ga ages, and the Mazatzal province is comprised of 1.7-1.6 Ga supracrustal rocks. A transition zone of deformation between these two terranes is the result of Mazatzal suturing that affected Yavapai rock units along the suture boundary (Shaw and Karlstrom, 1999; Magnani et al., 2004; Karlstrom et al., 2004). This transition zone has remained a zone of weakness within the crust and has been exploited as a pathway for magmatism and as a shear zone (Mutschler et al., 1987; Karlstrom et al., 2004; McCoy et al., 2005). Additionally, the underlying mantle lithosphere has likely been modified by fluids

escaping from subducting slabs during the Proterozoic, and possibly also during late Phanerozoic subduction along the western edge of North America.

Magmatic activity in the southern part of the Laramide orogen occurred ca. 75-37 Ma along the Colorado Mineral Belt and further south (McMillan, 2004; Chapin et al., 2004). Late Cretaceous to Eocene magmatic activity throughout central and southern New Mexico was caused by the Farallon plate interacting with asthenospheric mantle under a Jurassic rift zone (McMillan, 2004). Similarities in major and trace element patterns suggest similar petrogenetic histories for all the Laramide to Eocene magmas in southwestern New Mexico (McMillan, 2004).

Younger Laramide magmatic activity in southwestern Montana and northwestern Wyoming exploited Proterozoic crustal weaknesses (Meen and Eggler, 1987; Harlan et al., 1996; Feeley and Cosca, 2003). Volcanism followed two northwest-southeast trending belts. The western belt contains mostly K-poor compositions and the eastern belt has K-rich compositions (Feeley and Cosca, 2003; Harlan et al., 1996). This change in potassium content was attributed by previous workers to variations in the differentiation processes affecting the magmas (Feeley and Cosca, 2003).

Colorado Mineral Belt

Laramide magmatism in Colorado occurred ca. 75 - 42 Ma and was localized along the Colorado Mineral Belt (COMB) (Mutschler et al., 1987). The COMB is a ~200 km long, linear arrangement of Laramide igneous bodies running northeast-southwest from near Denver, Colorado, to the Four Corners area (Figure 1) (McCoy et al., 2005). The COMB and other northeast-southwest trending lineaments seem to roughly parallel the Proterozoic suture zones (Shaw and Karlstrom, 1999; Chapin et al., 2004; Karlstrom

et al., 2004; Magnani et al., 2004). The COMB lies along the northern boundary of the Yavapai-Mazatzal transition zone (Karlstrom and Humphreys, 1998). The La Plata Mountains, and the Allard stock, discussed below, lie near the southwestern end of the COMB (Figure 2) (Wilson and Sims, 2002).

The COMB igneous intrusions are generally calc-alkaline in the central portion of the belt, while alkaline compositions are more prevalent at the ends (Mutschler et al., 1987). Mafic alkaline rocks can be found at the ends of the COMB and are likely lithospheric mantle melts (Mutschler, et al. 1987). These igneous bodies are well known for their mineral deposits, which are sources for economically important elements including Ag, Au, Pb, Zc, Mo, and W (McCoy et al., 2005).

La Plata Mountains

The La Plata Mountains are a dissected dome that contains Laramide-age stocks, sills and laccoliths that intruded and disturbed Pennsylvanian to Cretaceous sedimentary units (Eckel et al., 1949; Werle et al., 1984). The La Plata intrusive rocks may represent the plumbing beneath a Laramide volcanic edifice that has since eroded (Lipman et al., 1972). K-Ar dating of the La Plata intrusive rocks yielded ages of ca. 68 Ma (Cunningham et al., 1994). There are two main groups of igneous rocks found in the La Platas. The first group contains rocks that are intermediate in composition between diorite and monzonite and are highly porphyritic (Werle et al., 1984; Eckel et al., 1949). This group contains the oldest of the La Plata intrusive rocks and forms numerous stocks, sills, and dikes that intruded through sedimentary rock layers (Eckel et al., 1949). The second group contains rocks with syenite to monzonite compositions that are not porphyritic, are highly altered, and form five stocks and associated dikes that cut across

sedimentary units (Werle et al., 1984; Eckel et al., 1949). The Allard Stock is one of these five stocks in the central part of the La Plata Mountains (Figure 2) (Werle et al., 1984). These non-porphyritic rocks show evidence of having assimilated country rock during emplacement (Eckel, 1949).

Nearby Tertiary Volcanic Fields

The relatively close Navajo and Dulce volcanic fields provide important information concerning the chemical and isotopic makeup of the mantle and crust below the Four Corners region and also below the McDermott outcrop.

Navajo Volcanic Field

The 28-19 Ma Navajo volcanic field contains two main types of volcanic centers: serpentinized ultramafic breccias and minette diatremes (Condie et al., 1999). The breccias form kimberlite-like bodies and are significantly less abundant than the minettes (Condie et al., 1999; Mattie et al., 1997). These units contain xenoliths of lower crustal and mantle rocks, but mantle xenoliths are rare in the minettes (Mattie et al., 1997). Condie and Selverstone (1999) calculated an average composition for the lower crust beneath the Navajo volcanic field from Navajo xenoliths.

Dulce Volcanic Field

The Dulce volcanic field (27-24 Ma) is comprised of a dike swarm that crops out near the town of Dulce, New Mexico erupted 27-24 Ma (Chapin et al., 2004). The mafic rock forming these dikes is reportedly derived from melting of metasomatized lithospheric mantle (Gibson, et al., 1993). These mantle derived-basalts were used in geochemical modelling in an attempt to estimate the crustal contribution to the McDermott Formation magmas.

McDermott Formation

The McDermott Formation overlies the Kirkland Shale and is overlain by the Animas Formation in the San Juan basin (Figure 3). The McDermott Formation is composed of sandstone, shale and conglomerate layers with the latter containing numerous large clasts of volcanic material. Much of the conglomerate occurs in lahar deposits that were emplaced during the tectonic uplift, as evidenced by the tilt of the McDermott Formation being more than the overlying Animas and less than the underlying Kirkland Shale (Figure 3). This suggests that McDermott deposition occurred during the strongest phase of Laramide tectonism. The McDermott Formation is reported to be Upper Cretaceous (Maastrichtian stage) based on fossils found within the unit (Reeside, 1924). The unit varies from as much as 400 feet (~122m) thick in southwest Colorado to as little as 30 feet (~9m) thick near the San Juan River (Reeside, 1924). This suggests that the source area is probably near the northwest part of the San Juan basin.

ANALYTICAL METHODS

Thin section, major and trace element geochemical (ICP-OES, -MS, and XRF) and isotope geochemical analyses were conducted to investigate potential sources for the McDermott Formation clasts. Samples were crushed on a stainless steel plate and then powdered in a precontaminated SPEX tungsten-carbide shatterbox. Six grams of the resulting powder were mixed with 1 gram of powdered Bakelite and pressed into a pellet for wavelength-dispersive XRF analysis. Additional powder was sent to Activation Laboratories for ICP-OES and -MS analysis. Eleven samples from three different sections of the McDermott Formation, chosen for apparent variability, and four samples

of intrusive rocks from the La Plata Mountains were collected and analyzed. Precambrian upper crustal units (Twilight Gneiss and Baker's Bridge Granite) of the nearby San Juan uplift were collected and analyzed as potential assimilants. Published analyses of the Allard stock (Werle et al., 1984) and an average of lower crustal xenoliths from the Four Corners area (Condie and Selverstone, 1999) were used to supplement our analyses. A significant number of published Allard stock analyses were excluded due to extensive alteration during mineralization.

RESULTS

Hand Sample and Thin Section

Thin section analysis established that the McDermott Formation samples contain phenocrysts of plagioclase, opaques, ± clinopyroxene, and ± amphibole. All samples show significant sericitization of the plagioclase phenocrysts. Sample 060672 McD contained xenocrysts of polycrystalline quartz and microcline. Amphibole phenocrysts have been highly weathered, leaving little more than fragments and rectangular void spaces. The La Plata Mountains samples contained amphibole, opaques, sericitized plagioclase, ± biotite, and ± clinopyroxene.

Major Element Geochemistry

There is little chemical variability among eight samples from the McDermott Formation (Table 1). Figure 4 is a TAS Classification diagram of the McDermott Formation, Allard stock, and La Plata Mountains samples (Le Bas et al., 1986). Nine of the eleven McDermott Formation samples fall within the trachyandesite field, seven of which are benmoreites and the other two latites. One McDermott Formation sample falls

in the andesite field and another falls in the basaltic trachyandesite field and is technically a mugearite. Our La Plata Mountains intrusive rock samples show more variation, falling in the basaltic trachyandesite, trachyandesite, and andesite fields, specifically one benmoreite, one shoshonite, one mugearite, and one andesite. Allard stock samples (enriched in K_2O by potassium metasomatism) fall within the basaltic trachyandesite, trachyandesite, and trachyte fields and include latites, shoshonites, and trachytes.

The McDermott Formation samples generally fall in the middle of the Allard stock range in major and trace element compositions and exhibit only minor variability (Figure 5). The McDermott samples show a trend of increasing K_2O while silica remains relatively unchanged. This is likely due to some K-metasomatism of the McDermott Formation samples, though not to the extent of some Allard stock samples.

Trace Element Geochemistry

McDermott Formation samples, as well as samples from the La Plata Mountains, and the average Four Corners lower crustal xenolith composition, have a subduction signature in mantle normalized incompatible trace element concentrations (Figure 6). One McDermott Formation sample (060672 McD) is megascopically contaminated with quartz and microcline and has Ba concentration four times higher than other McDermott samples. It was not included in from the graphs of Figure 6. Subduction related magmas are typically characterized by relatively high Large Ion Lithophile Element (LILE) concentrations (e.g., Ba) and low High Field Strength Element (HFSE) concentrations (e.g., Nb and Ta) as well as being enriched in the Light Rare-Earth Elements (LREE) compared to the Heavy Rare-Earth Elements (HREE) (Davidson, 1996). The LILE enrichment is believed to be the result of fluids escaping from the subducted slab because

LREE and LILE are more fluid mobile (Davidson, 1996). The depletion in HFSE is attributed to their retention by some phase in the asthenospheric mantle.

The average composition of Four Corners lower crustal xenoliths (Condie and Selverstone, 1999) shows a trace element pattern similar to those of the McDermott Formation and La Plata samples, but with lower concentrations (Figure 6). Also shown are the concentrations of three samples of Twilight Gneiss and one of Baker's Bridge Granite, both of which are prominent in exposures of Proterozoic basement rocks in the nearby San Juan uplift (Figure 2). The different patterns rule out significant involvement of upper crustal rocks such as Twilight Gneiss and Baker's Bridge Granite in McDermott Formation petrogenesis, especially the negative spikes for Sr, P, and Ti that are absent in McDermott plots.

The McDermott, La Plata, and Four Corners crustal average show similar trends in rare-earth element (REE) concentrations normalized to chondrite values. They have generally higher concentrations of the light REEs compared to the heavy REEs (Figure 7).

Ba/La vs. Nb/La ratio plots may be used to distinguish probable source regions for magmas (Figure 8) (Menzies et al., 1991). The Type I field represents ocean island basalt (OIB) asthenospheric mantle, Type II subduction-modified continental lithosphere and Type III OIB-modified continental lithosphere. Figure 8 shows that the McDermott trachyandesite and La Plata intrusive rocks plot in the Type II field. Also shown are analyses of Proterozoic crustal rocks, our La Plata intrusive rocks, lower crustal xenoliths from the Navajo volcanic field, and mantle derived mafic rocks from the Navajo and Dulce volcanic fields (Gibson et al., 1993; Condie et al., 1999). All of these analyses plot

in the Type II field with the exception of one mafic rock from the Navajo volcanic field (Gibson et al., 1993).

Isotope Geochemistry

Two McDermott Formation samples selected for variability were analyzed for Nd isotopes and yielded εNd_t values of -1.937 and 0.465 assuming a late Maastrichtian age (70.6 Ma). These McDermott εNd_t values are similar to values reported for mantle-derived mafic magmas from the Navajo (1.42 and -1.23) and Dulce (-3.61, -3.37, and -2.87) volcanic fields (Gibson et al., 1993). εNd_t values for Proterozoic basement rocks are typically strongly negative (e.g. -5 to -20; Condie et al., 1999; Parker et al., 2005). Asthenospheric mantle sources typically have εNd_t values around +5 or higher, while Rio Grande Rift lithospheric mantle has values around 0 to +4 (Perry et al., 1988). Lower crustal material shows εNd_t values of -6 to -18 from xenoliths (Condie et al., 1999). Perry et al. (1993) reported εNd values of -14 for crustal rocks, -6 to -8 for rhyolite magmas and 0 for basaltic magmas from the San Juan volcanic field.

The McDermott Formation εNd_t values were used in calculating the Neodymium Crustal Index (NCI). The NCI represents the amount of Nd derived from crustal material, with a value of 1 indicating that all the Nd is derived from crustal sources and 0 indicating all the Nd is derived from a mantle source (DePaolo et al., 1992). We assume a range of -12 to -18 for potential crustal contaminants (Condie et al., 1999). NCI values for the McDermott samples were calculated using the εNd_t ranges for asthenospheric and lithospheric mantle listed above. Asthenospheric mantle values yield NCI values between 0.2 and 0.5, while lithospheric values yield values between 0.0 and 0.37.

DISCUSSION

McDermott, Allard stock, and other La Plata samples fall along similar trends in major element diagrams. Incompatible trace element concentrations (Figure 6) and rare-earth element concentrations (Figure 7) also suggest a genetic relationship between the La Plata Mountains intrusive rocks and the McDermott Formation samples.

Batch melting calculations using Condie and Selverstone's (1999) average lower crustal composition indicate that the McDermott volcanic clasts could be formed through as little as 40 percent partial melting of lower crustal material. However, the large difference between the lower crustal εNd values (-6 to -18) and the McDermott Formation εNd values (-1.937 and 0.465) suggests that the McDermott magmas were not lower crustal melts. Ba/La vs. Nb/La plots indicate a subduction-modified continental lithospheric source for the McDermott trachyandesite and La Plata intrusive rocks (Figure 8). εNd_t McDermott values fall at the end of the Mantle Array near the boundary with continental compositions, suggesting a lithospheric mantle source for these magmas (Rollinson, 1993). NCI calculations suggest that while asthenospheric mantle is a potential source, a lithospheric mantle source is more plausible because the greater degree of crustal assimilation suggested for the asthenospheric mantle would greatly increase the εNd_t of the McDermott. Most likely, McDermott magmas were produced by fractional crystallization of lithospheric mantle-derived parental basalt, modified by assimilation of a significant amount of crustal material.

SUMMARY AND CONCLUSIONS

Incompatible trace element patterns suggest a petrogenetic relationship between the Allard stock, La Plata intrusive rocks, and the McDermott Formation. The McDermott deposits were not derived from any intrusive units now exposed at the level of erosion. Instead, the La Plata Mountains intrusive rocks may represent the plumbing system under the volcano(s) from which the McDermott Formation lahars were derived. εNd_t values of McDermott Formation trachyandesite rule out pure upper crustal and lower crustal sources for the McDermott intermediate volcanic rocks. The McDermott Formation magmas were likely formed by partial melting of a lithospheric mantle source, which was contaminated by a small to moderate amount of crustal material.

ACKNOWLEDGEMENTS

We thank Baylor University and the Baylor Geology Department for providing the funding necessary to complete this project. We also thank Baylor Geology's 2006 petrology class for assistance with sample preparation.

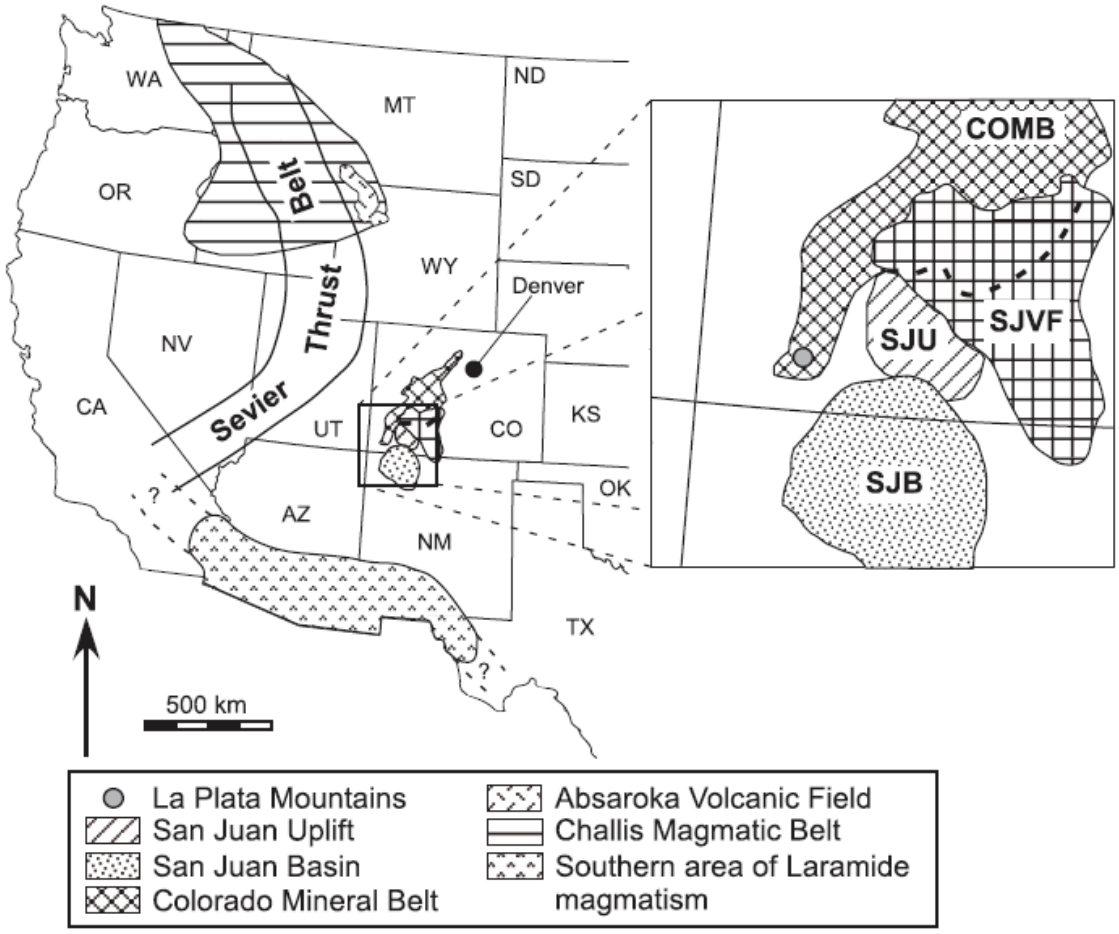

Figure 2.1. Location diagram showing some major tectonic and magmatic features of the western United States (based on Dickinson et al., 1988; Wilson and Sims, 2003; Feeley and Cosca, 2003; Cowan and Bruhn, 1992; Miller et al., 1992; Mutschler et al., 1987).

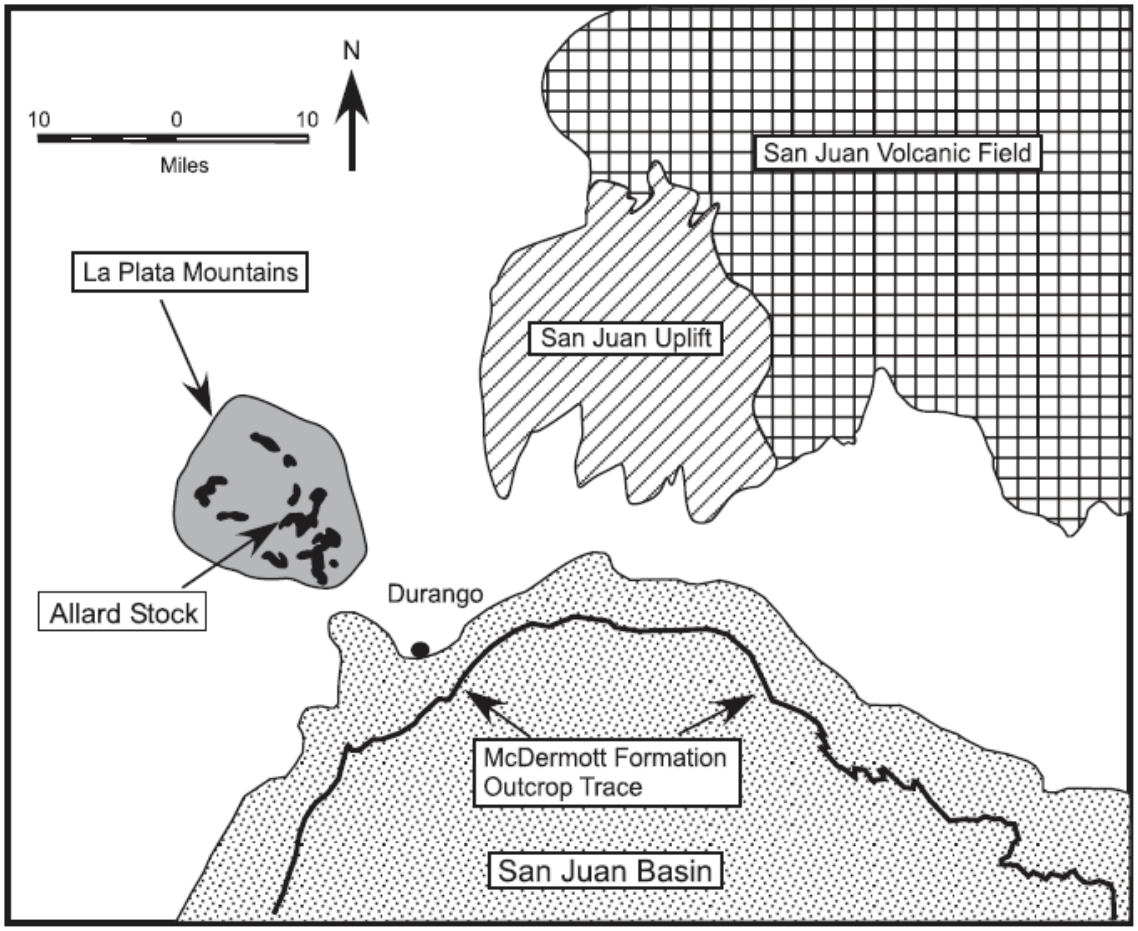

Figure 2.2. Generalized map of the Durango area showing the extent of the McDermott Formation, the La Plata Mountains (intrusive rock units shown in black; created from Tweto, 1979).

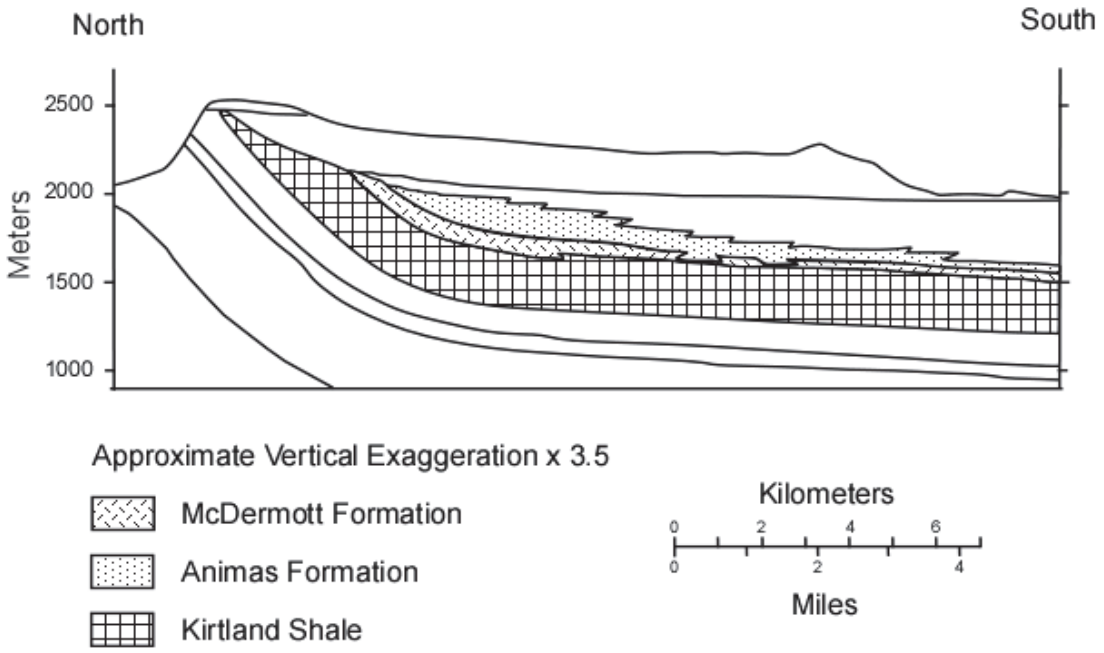

Figure 2.3. Generalized geologic cross section showing the major units present in the study area (from Condon, 1990 after Baltz et al., 1966)

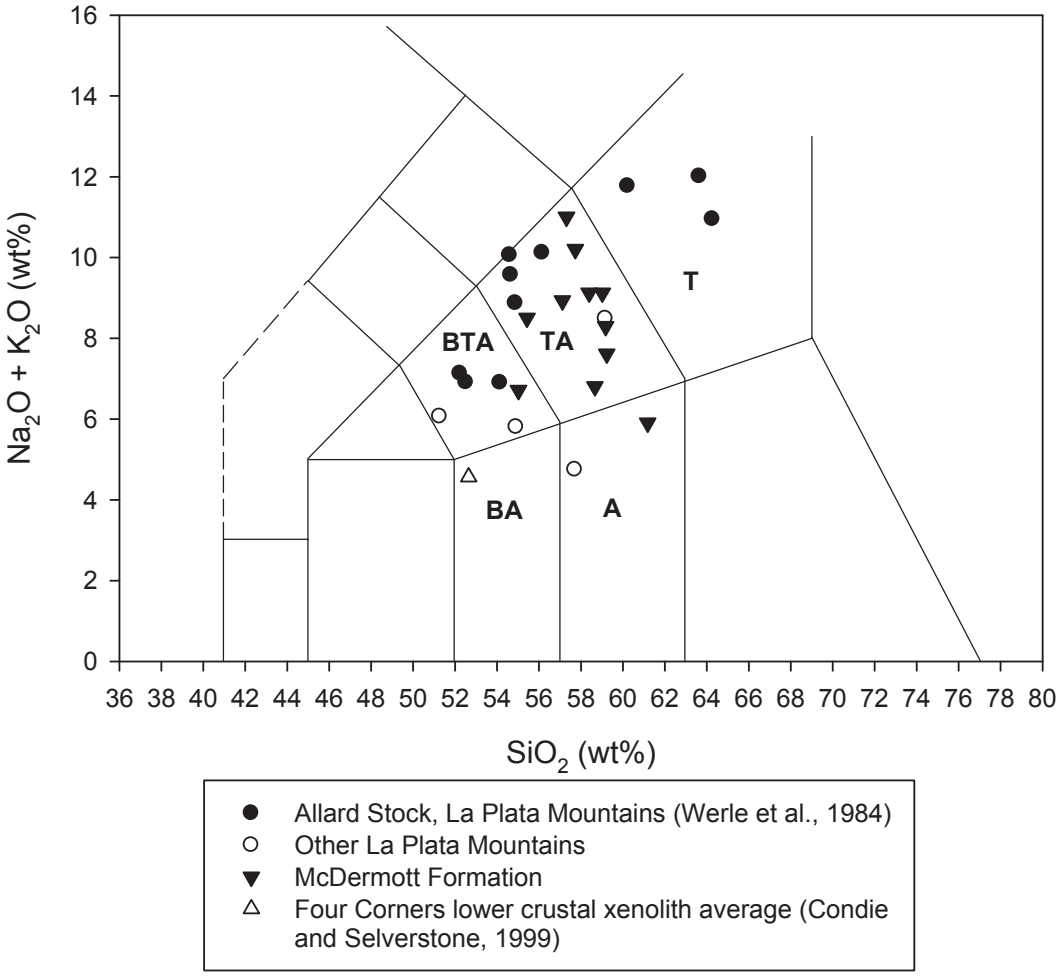

Figure 2.4. TAS classification diagram for the McDermott Formation, La Plata Mountains intrusive rocks, Allard stock, and the average composition of lower crustal xenoliths from the Navajo volcanic field (Le Bas et al., 1986; Werle et al., 1984; Condie and Selverstone, 1999). BTA is the basaltic trachyandesite field, TA is the trachyandesite field, BA is the basaltic andesite, A is the andesite field, and T is the trachyte field.

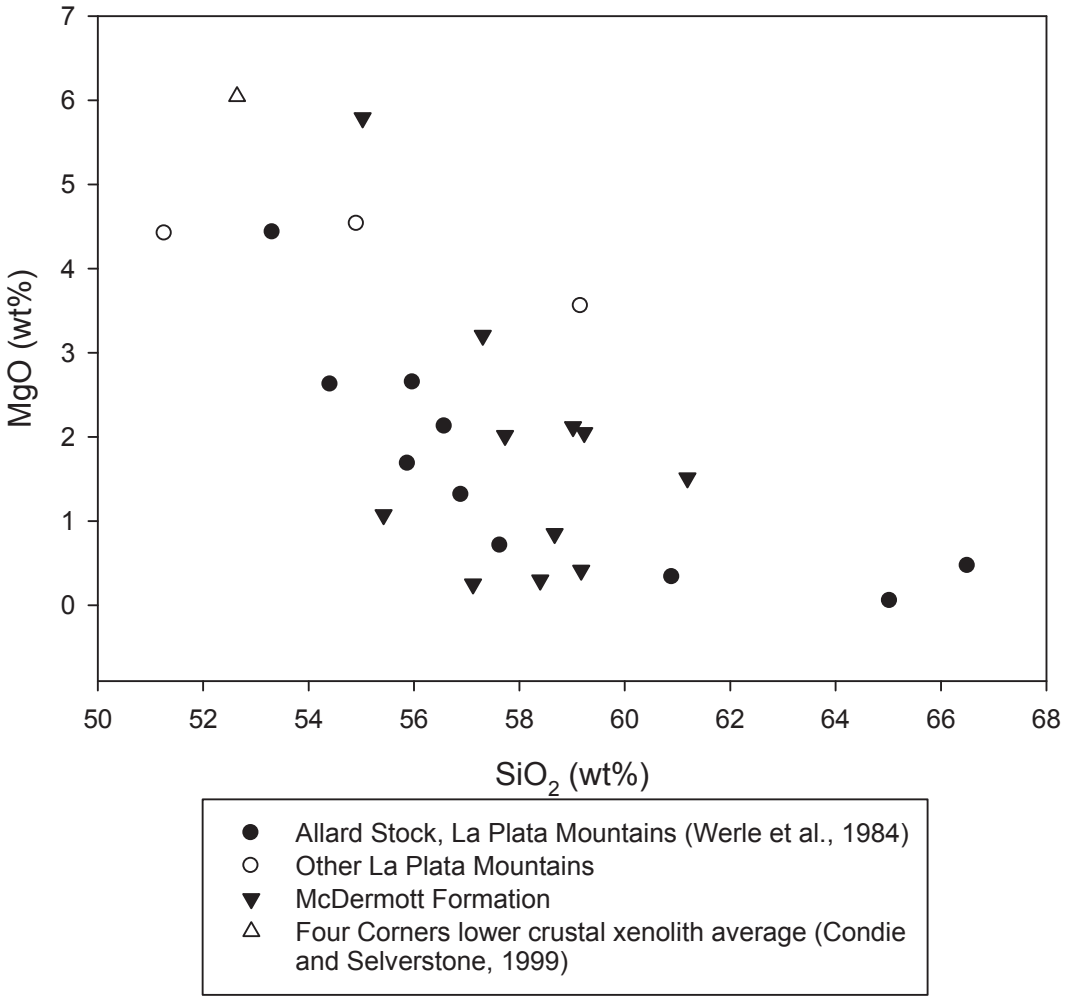

Figure 2.5. SiO_2 vs. MgO diagram. The McDermott Formation samples tend to fall within the range of La Plata intrusives and Allard stock compositions (Werle et al., 1984).

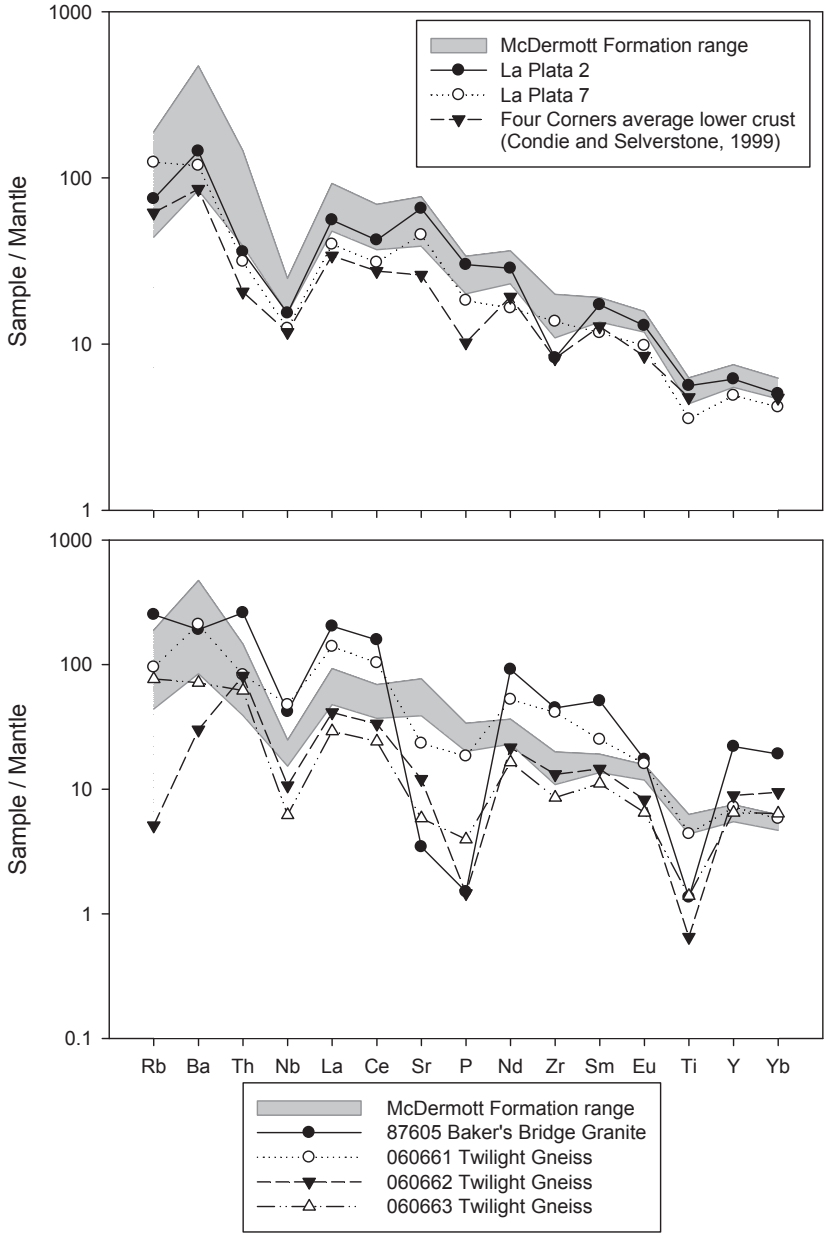

Figure 2.6. (a) Spider diagram showing the similarities between incompatible trace element concentrations of McDermott trachyandesite, La Plata intrusives, and the Four Corners lower crustal xenolith average (Condie and Selverstone, 1999). (b) Spider diagram showing the trends for the Twilight Gneiss and Baker's Bridge Granite in relation to the McDermott Formation. Compositions in both plots are normalized to primitive mantle values of McDonough and Sun (1995).

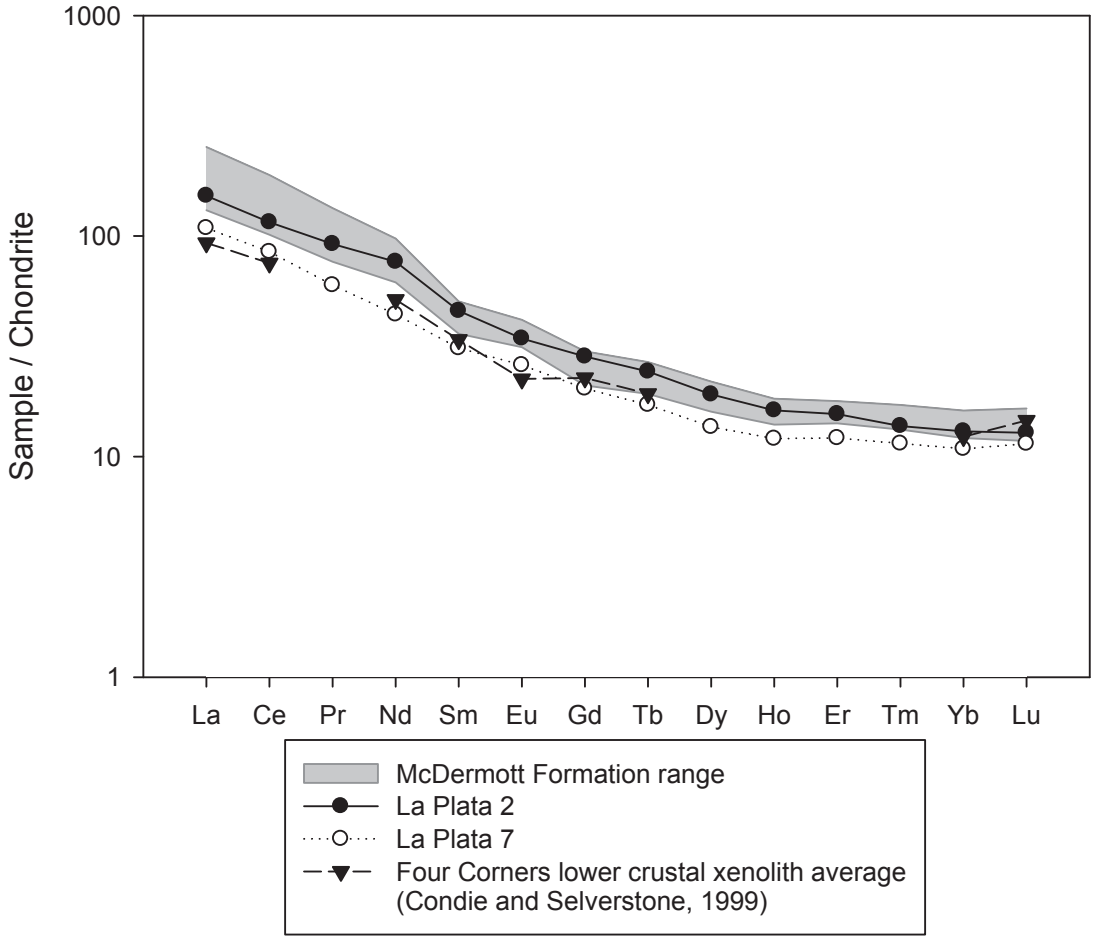

Figure 2.7. Rare-Earth Element diagrams of the McDermott trachyandesite, La Plata intrusives, and Four Corners xenoliths average (Condie and Selverstone, 1999). All three groups show a greater increase in the concentration of the Light REEs relative to the Heavy REEs. This pattern is likely due to the presence of garnet, which preferentially retains HREE in the source rock. These compositions are normalized to chondrite values of Wakita et al. (1971).

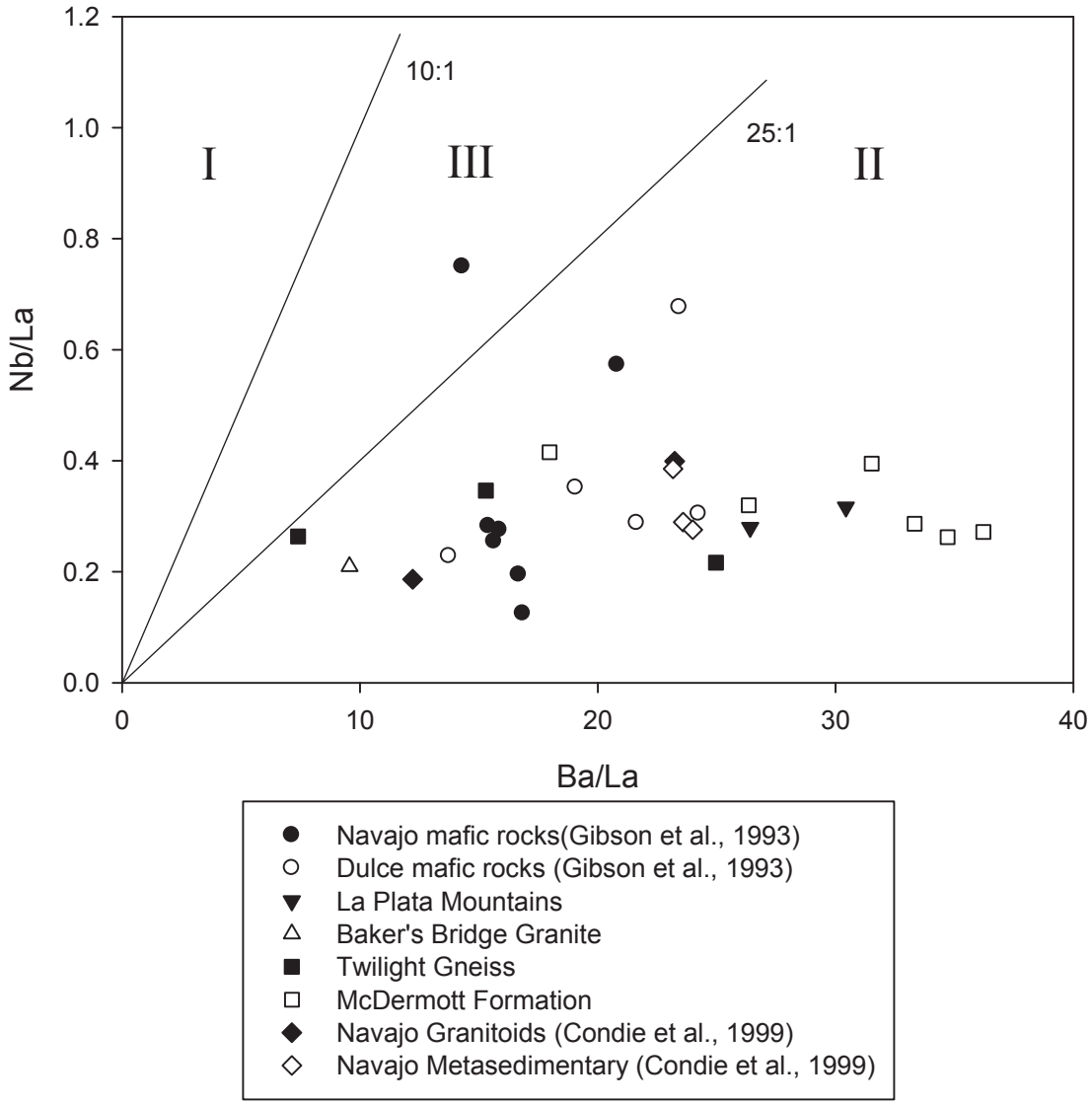

Figure 2.8. Ba/La vs. Nb/La trace element diagram. The La Plata intrusive rocks and the McDermott trachyandesite plot in the Type II (subduction-modified continental lithosphere) field of Menzies et al. (1991). The Type I field represents OIB asthenospheric mantle and Type III represents OIB-modified continental lithosphere.

Table 2.1. Major, trace, and isotope analyses of eight McDermott (McD), four La Plata, Baker's Bridge Granite (BBG), and the three Twilight Gneiss (TG) analyses normalized to 100% anhydrous. XRF analyses are in bold and ICP analyses in normal font. The TAS classification for the McDermott and La Plata samples are listed at the bottom. Analyses 1-4: Intrusive rocks collected along the La Plata River. Analyses 5-6 and 13-15: UTM 13S 0239915 4119078. Analyses 7 and 8: UTM 13S 0249550 4128300. Analyses 9 and 10: UTM 13S 0245706 4123220. Analysis 11 and 12: Outcrop above analyses 9 and 10 location. Analyses 16: Sample from Baker's Bridge. Analyses 17-18: UTM 13S 0257345 4172817.

	1	2	3	4	5	6	7	8
	La Plata 2	La Plata 7	La Plata 3	La Plata 5	060673 McD	060674 McD	060651McD	060652McD
SiO_2	50.38	58.08	**55.41**	**52.59**	57.2	53.65	58.24	55.57
TiO_2	1.101	0.693	**0.82**	**1.01**	0.842	0.881	0.982	0.947
Al_2O_3	16.68	16.25	**17.76**	**16.24**	18.96	19.48	16.16	16.5
FeO	9.76	6.26	**6.00**	**6.88**	6.44	7.50	7.57	7.85
MnO	0.17	0.11	**0.07**	**0.17**	0.082	0.199	0.153	0.107
MgO	4.34	3.49	**8.72**	**4.34**	0.4	1.04	2.09	1.94
CaO	9.28	4.58	**2.46**	**8.30**	4.24	5.42	4.03	3.11
Na_2O	4.01	5.45	**2.77**	**3.02**	6.03	4.82	7.48	4.68
K_2O	1.95	2.88	**1.79**	**2.54**	1.99	3.41	1.52	5.14
P_2O_5	0.61	0.37	**0.22**	**0.68**	0.48	0.4	0.46	0.42
LOI	0.35	0.7			1.62	1.63	0.708	1.359
Total	99.59	99.56	**96.69**	**96.54**	98.94	99.17	99.39	97.62

Table 2.1. Continued.

	1	2	3	4	5	6	7	8
	La Plata 2	La Plata 7	La Plata 3	La Plata 5	060673 McD	060674 McD	060651McD	060652McD
Ba	935	770	**287**	**768**	1146	1378	550	3004
Rb	44	73	**91**	**65**	37	51	26	109
Sr	1277	887	**122**	**996**	1077	880	762	1474
Zr	85	141	**277**	**84**	177	129	113	123
Hf	2.2	3.3			4.7	3.7	3.2	3.4
Y	25.9	20.7	**27**	**24**	23.1	25.1	24.4	24.2
Nb	9.9	8	**24**	**15**	13.9	10.4	12.7	9.7
Th	2.79	2.45	**11**	**3**	6.09	3.04	4.25	4.25
Zn	80	60			70	120	90	90
V	294	146			130	141	167	198
Ni	30	60	**51**	**12**	< 20	< 20	< 20	< 20
La	35.4	25.3			43.5	39.7	30.6	34.2
Ce	69.3	50.9			89.5	76.2	61.2	64.6
Pr	8.57	5.58			10.5	9.38	7.17	7.41
Nd	35	20.2			39.6	36.2	28.4	29.3
Sm	6.86	4.66			6.79	6.98	5.44	5.52
Eu	1.95	1.48			1.92	2.37	1.80	1.75
Gd	5.73	4.1			5.32	5.53	4.27	4.42
Tb	0.89	0.63			0.79	0.86	0.71	0.74
Dy	4.76	3.4			4.22	4.81	4.01	4.29
Ho	0.9	0.67			0.81	0.91	0.78	0.83
Er	2.53	1.97			2.41	2.62	2.31	2.46
Tm	0.344	0.287			0.357	0.378	0.337	0.363
Yb	2.17	1.81			2.22	2.41	2.17	2.36
Lu	0.319	0.285			0.316	0.37	0.327	0.367
eNd						-1.937	0.465	
TAS	Mugearite	Benmoreite	Andesite	Shoshonite	Benmoreite	Latite	Benmoreite	Latite

Table 2.1. Continued.

	9 060671McD	10 060672McD	11 060952McD	12 060953McD	13 070841McD	14 070842McD	15 070843McD	16 87605 BBG	17 060661 TG
SiO_2	57.26	54.56	56.97	55.00	**54.87**	**53.42**	**61.96**	71.52	62.9
TiO_2	0.931	1.064	0.892	1.202	**0.78**	**1.05**	**0.60**	0.261	0.853
Al_2O_3	16.79	17.38	19.77	19.59	**18.47**	**16.59**	**15.88**	12.53	15.07
FeO	5.98	8.60	6.27	6.77	**5.06**	**7.20**	**5.63**	2.48	5.53
MnO	0.158	0.111	0.125	0.209	**0.15**	**0.22**	**0.32**	0.035	0.099
MgO	1.98	0.79	0.29	0.24	**3.07**	**5.62**	**1.53**	0.32	1.48
CaO	5.69	3.72	3.82	4.01	**2.35**	**6.02**	**8.87**	0.7	3.69
Na_2O	5.22	5.03	6.51	6.34	**8.94**	**4.91**	**4.51**	3.04	4.26
K_2O	2.14	1.3	2.39	2.26	**1.60**	**1.61**	**1.47**	5.87	3.38
P_2O_5	0.53	0.44	0.52	0.67	**0.47**	**0.45**	**0.49**	0.03	0.37
LOI	1.478	4.517	1.469	1.622				1.74	1.1
Total	98.15	97.52	99.03	97.91	**95.74**	**97.09**	**101.26**	98.78	99.28

Table 2.1. Continued.

	9	10	11	12	13	14	15	16	17
	060671McD	060672McD	060952McD	060953McD	070841McD	070842McD	070843McD	87605 BBG	060661 TG
Ba	1293	13160	2122	1166	**1435**	**1030**	**1175**	1234	1357
Rb	43	18	44	39	**15**	**26**	**18**	148	56
Sr	917	1012	1084	1140	**500**	**994**	**837**	67	455
Zr	141	112	204	174	**161**	**107**	**146**	462	424
Hf	3.8	3.1	5.3	4.9				12.4	9.4
Y	31.2	28.9	25	29	**24**	**22**	**21**	92.7	30.3
Nb	11.1	10.4	15.9	14.6	**13**	**10**	**11**	27	30.7
Th	4.48	4.13	11.3	5	**6**	**4**	**4**	20.3	6.44
Zn	60	60	60	60				70	120
V	164	111	102	195				< 5	63
Ni	< 20	< 20	< 20	< 20	**10**	**6**	**14**	< 20	20
La	38.8	29.4	58.6	37.0				129	88.7
Ce	81.9	64.5	113	79.5				259	169
Pr	9.69	7.32	12.4	9.56				31.3	18.8
Nd	38.9	30.6	44.4	37.8				112	64.2
Sm	7.48	6.21	7.47	7.31				20.3	9.96
Eu	2.11	1.93	1.87	2.33				2.61	2.41
Gd	5.96	5.09	5.35	5.8				17	7.2
Tb	0.97	0.86	0.84	0.93				2.94	1.07
Dy	5.37	4.89	4.43	5.13				16.5	5.54
Ho	1	0.92	0.81	0.97				3.16	1
Er	2.86	2.62	2.3	2.78				9.42	2.86
Tm	0.422	0.379	0.330	0.394				1.35	0.394
Yb	2.66	2.37	2.01	2.50				8.27	2.51
Lu	0.406	0.333	0.292	0.369				1.19	0.372
eNd									
TAS	Benmoreite	Benmoreite	Benmoreite	Benmoreite	Benmoreite	Mugearite	Andesite		

Table 2.1. Continued.

	18	19
	060662 TG	060663 TG
SiO_2	76.88	70.43
TiO_2	0.129	0.272
Al_2O_3	12.29	13.39
FeO	1.58	4.06
MnO	0.018	0.073
MgO	0.23	1.91
CaO	2.37	1.73
Na_2O	5.75	3.96
K_2O	0.33	2.21
P_2O_5	0.03	0.08
LOI	0.77	1.33
Total	100.5	99.84

Table 2.1. Continued.

	18 060662 TG	19 060663 TG
Ba	194	462
Rb	3	45
Sr	235	114
Zr	135	88
Hf	3.9	2.5
Y	37.5	27.3
Nb	6.9	4
Th	6.31	4.82
Zn	< 30	60
V	< 5	23
Ni	< 20	< 20
La	26.2	18.5
Ce	54.9	39.7
Pr	6.67	5.1
Nd	26.4	20.1
Sm	5.79	4.42
Eu	1.24	0.98
Gd	5.36	4.06
Tb	0.99	0.74
Dy	5.99	4.32
Ho	1.25	0.88
Er	3.9	2.76
Tm	0.614	0.422
Yb	4.08	2.76
Lu	0.632	0.426
eNd		
TAS		

REFERENCES CITED

Baltz, E.H., Ash, S.R., and Anderson, R.Y., 1966, History of nomenclature and stratigraphy of rocks adjacent to the Cretaceous-Tertiary boundary, western San Juan Basin, New Mexico: United States Geological Survey Professional Paper, p. D1-D23.

Chapin, C.E., Wilks, M., and McIntosh, W.C., 2004, Space-time patterns of Late Cretaceous to present magmatism in New Mexico-comparison with Andean volcanism and potential for future volcanism: New Mexico Bureau of Geology and Mineral Resources Bulletin 160, p. 13-40.

Condie, K.C., Latysh, N., Van Schmus, W.R., Kozuch, M., and Selverstone, J., 1999, Geochemistry, Nd and Sr isotopes, and U/Pb zircon ages of granitoid and metasedimentary xenoliths from the Navajo Volcanic Field, Four Corners area, southwestern United States: Chemical Geology, v. 156, p. 95-133.

Condie, K.C., and Selverstone, J., 1999, The crust of the Colorado Plateau: new views of an old arc: Journal of Geology, v. 107, p. 387-397.

Condon, S.M., 1990, Geologic and structure contour map of the Southern Ute Indian Reservation and adjacent areas, southwestern Colorado and northwest New Mexico: United States Geological Survey Miscellaneous Investigations Series Map I-1958, 1:100,000 scale.

Cowan, D.S., and Bruhn, R.L., 1992. Late Jurassic to early Late Cretaceous geology of the U.S. Cordillera, i*n* Burchfiel, B.C., Lipman, P.W., and Zoback, M.L., (*eds.*), The Cordilleran Orogen: Conterminous U.S.: Boulder, Colorado, Geological Society of America, The Geology of North America, v. G-3, p. 169-203.

Cunningham, C.G., Naeser, C.W., Marvin, R.F., Luedke, R.G., and Wallace, A.R., 1994, Ages of selected intrusive rocks and associated ore deposits in the Colorado Mineral Belt: U.S. Geological Survey Bulletin 2109, 31 p.

Davidson, J.P., 1996, Deciphering mantle and crustal signatures in subduction zone magmatism. *in* Bebout, G.E., Scholl, D.W., Kirby, S.H., Platt, J.P., (*eds*.), Subduction: Top to Bottom. American Geophysical Union Monograph 96, p. 251-262.

De Paolo, D.J., Perry, F.V., and Baldridge, W.S., 1992, Crustal versus mantle sources of granitic magmas: A two parameter model based on Nd isotopic studies: Royal Society of Edinburgh Transactions: Earth Sciences, v. 83, p. 439-446.

Dickinson, W.R., Klute, M.A., Hayes, M.J., Janecke, S.U., Lundin, E.R., McKittrick, M.A., and Olivares, M.D., 1988, Paleogeographic and paleotectonic setting of Laramide sedimentary basins in the central Rocky Mountain region: Geological Society of America Bulletin, v. 100, p. 1023-1039.

Dickinson, W.R., and Snyder, W.S., 1978, Plate tectonics of the Laramide orogeny: Geological Society of America, Memoir 151, p. 355-366.

Eckel, E.B., Williams, J.S., and Galbraith, F.W., 1949, Geology and ore deposits of the La Plata district, Colorado, with sections by G.M. Schwartz, D.J. Varnes, and E.N. Goddard: U.S. Geological Survey Professional Paper 219, 179 p.

Feeley T.C., and Cosca, M.A., 2003, Time vs. composition trends of magmatism at Sunlight volcano, Absaroka volcanic province, Wyoming: Geological Society of America Bulletin, v. 115, p. 714-728.

Fitton, J.G., James, D., Kempton, P.D., Ormerod, D.S., and Leeman, W.P., 1988, The role of lithospheric mantle in the generation of late Cenozoic basic magmas in the western United States: Journal of Petrology, Special Lithosphere Issue, p. 331-349

Gibson, S.A., Thompson, R.N., Leat, P.T., Morrison, M.A., Hendry, G.L., Dickin, A.P., and Mitchell, J.G., 1993, Ultrapotassic Magmas along the flanks of the Oligo-Miocene Rio Grande Rift, USA: Monitors of the zone of lithospheric mantle extension and thinning beneath a continental rift: Journal of Petrology v. 34, p. 187-228.

Gutscher, M.-A., Spakman, W., Bijwaard, H., and Engdahl, E.R., 2000, Geodynamics of flat subduction: Seismicity and tomographic constraints from the Andean margin: Tectonics, v. 19, p. 814-833

Harlan, S.S., Snee, L.W., and Geissman, J.W., 1996, $^{40}Ar/^{39}Ar$ geochronology and paleomanetism of Independence volcano, Absaroka volcanic supergroup, Beartooth Mountains, Montana: Canadian Journal of Earth Science, v. 33, p. 1648-1654.

Karlstrom, K.E., Amato, J.M., Williams, M.L., Heizler, M., Shaw, C.A., Read, A.S., and Bauer, P., 2004, Proterozoic tectonic evolution of the New Mexico region: A synthesis, *In* Mack, G.H., and Giles, K.A., (*eds*.), The Geology of New Mexico: A Geologic History: New Mexico Geological Society Special Publication 11, p. 1-34.

Karlstrom, K.E., and Humphreys, E.D., 1998, Persistent influence of Proterozoic accretionary boundaries in the tectonic evolution of southwestern North America: interaction of cratonic grain and mantle modification events: Rocky Mountain Geology, v. 33, p. 161-179.

Le Bas, M.J., Le Maitre, R.W., Streckeisen, A., and Zanettin, B., 1986, A chemical classification of volcanic rocks based on the total alkali-silica diagram: Journal of Petrology v. 27, p. 745-750.

Lipman, P.W., Prostka, H.J., and Christiansen, R.L., 1972, Cenozoic volcanism and plate-tectonic evolution of the Western United States. I. Early and Middle Cenozoic: Philosophical Transactions of the Royal Society of London, v. 271, p. 217-248.

Magnani, M.B., Miller, K.C., Levander, A., and Karlstrom, K., 2004, The Yavapai-Mazatzal boundary: a long-lived tectonic element in the lithosphere of southwestern North America: Geological Society of America Bulletin, v. 116, p. 1137-1142.

Mattie, P.D., Condie, K.C., Selverstone, J., and Kyle, P.R., 1997, Origin of the continental crust in the Colorado Plateau: Geochemical evidence from mafic xenoliths from the Navajo Volcanic Field, southwestern USA: Geochimica et Cosmochimica Acta, v. 61, p. 2007-2021.

McCoy, A.M., Karlstrom, K.E., Shaw, C.A., Williams, M.L., 2005. The Proterozoic Ancestry of the Colorado Mineral Belt: 1.4 Ga shear zone system in central Colorado, *in* Keller, G.R., (*ed.*), The Rocky Mountain Region: An Evolving Lithosphere: American Geophysical Union Geophysical Monograph Series 154, p. 71-90.

McDonough, W.F., and Sun, S.S., 1995, The composition of the Earth. Chemical Geology 120, p. 223-253.

McMillan, N.J., 2004, Magmatic record of Laramide subduction and the trasnition to Tertiary extension: upper Cretaceous through Eocene igneous rocks of New Mexico, *In* Mack, G.H., and Giles, K.A., (*eds*.), The Geology of New Mexico: A Geologic History: New Mexico Geological Society Special Publication 11, p. 249-270.

Meen, J.K., and Eggler, D.H., 1987, Petrology and geochemistry of the Cretaceous Independence volcanic suite, Absaroka Mountains, Montana: clues to the composition of the Archean sub-Montanan mantle: Geological Society of America Bulletin, v. 98, p. 238-247.

Menzies, M.A., Kyle, P.R., Jones, M., and Ingram, G., 1991, Enriched and depleted source components for tholeiitic and alkaline lavas from Zuni-Bandera, New Mexico: Inferences about intraplate processes and stratified lithosphere: Journal of Geophysical Research, v. 96, p. 13645-13671.

Miller, D.M., Nilsen, T.H., and Bilodeau, W.L., 1992, Late Cretaceous to early Eocene geologic evolution of the U.S. Cordillera, *in* Burchfiel, B.C., Lipman, P.W., and Zoback, M.L., (*eds.*), The Cordilleran Orogen: Conterminous U.S.: Boulder, Colorado, Geological Society of America, The Geology of North America v. G-3, p. 205-260.

Mutschler, F.E., Larson, E.E., and Bruce, R.M., 1987. Laramide and younger magmatism in Colorado – new petrologic and tectonic variations on old themes, *in* Drexler, J.W., and Larson, E.E., (*eds*.), Cenozoic volcanism in the southern Rocky Mountains updated: a tribute to Rudy C. Epis – Part I: Colorado School of Mines Quarterly v. 82, p. 1-47.

Parker, D.F., Ghosh, A., Price, C.W., Rinard, B.D., Cullers, R.L., and Ren, M., 2005. Origin of rhyolite by crustal melting and the nature of parental magmas in the Oligocene Conejos Formation, San Juan Mountains, Colorado, USA: Journal of Volcanology and Geophysical Research, v. 139, p. 185-210

Perry, F.V., Baldridge, W.S., and DePaolo, D.J., 1988. Chemical and isotopic evidence for lithosphere thinning beneath the Rio Grande rift. Nature, 332: 432-434

Perry, F.V., DePaolo, D.J., and Baldridge, W.S., 1993. Neodymium isotopic evidence for decreasing crustal contributions to Cenozoic ignimbrites of the western United States: Implications for the thermal evolution of the Cordilleran crust, Geological Society of America Bulletin, v. 105, p. 872-882

Reeside, J.B. Jr., 1924, Upper Cretaceous and Tertiary formations of the western part of the San Juan Basin Colorado and New Mexico: United States Geological Survey, Professional Paper 134, p. 1-70.

Rollinson, H.R., 1993. Using geochemical data; evaluation, presentation, interpretation: Longman Scientific and Technical, Harlow, United Kingdom, 352 p.

Shaw, C.A., and Karlstrom, K.E., 1999, The Yavapai-Mazatzal crustal boundary in the southern Rocky Mountains: Rocky Mountain Geology, v. 34, p. 37-52.

Tweto, O., 1979, Geologic map of Colorado: United States Geological Survey, 1:500,000 scale.

Wakita, H., Rey, P., and Schmitt, R.A., 1971, Abundances of the 14 rare earth elements and 12 other rare elements in Apollo 12 samples: five igneous and one breccia rocks and four soils: Proceedings Second Lunar Science Conference, Geochimica et Cosmochimica Acta, Supplement 2, p. 1319-1325.

Werle, J.L., Ikramuddin, M, and Mutschler, F.E., 1984, Allard stock, La Plata Mountains Colorado – an alkaline rock-hosted porphyry copper – precious metal deposit: Canadian Journal of Earth Science v. 21, p. 630-641.

Wilson, A.B., and Sims, P.K., 2003, Colorado mineral belt revisited – an analysis of new data: U.S. Geological Survey Open-File Report 03-046, 7 p.

CHAPTER THREE

The Nathrop Domes, Nathrop, Colorado, U.S.A.: Geochemistry and Petrogenesis of a Topaz Rhyolite

This chapter published as: Wegert, D., Parker, D.F., and Ren, M., 2013, The Nathrop Domes, Colorado: geochemistry and petrogenesis of a topaz rhyolite: Rocky Mountain Geology, v. 48, n. 1, p. 1-14

ABSTRACT

The four Nathrop Domes (~30 Ma) are located near Buena Vista, Colorado, within the Arkansas Valley Graben segment of the Rio Grande Rift. The domes are largely composed of sparsely to moderately porphyritic, flow-banded rhyolite, with local vitrophyric margins. Phenocrysts include sanidine, plagioclase, quartz, biotite, and Fe–Ti oxides. Bright red Mn-garnet locally occurs in vapor-phase cavities. Two-feldspar and two-oxide temperatures assuming 1 kb pressure were, respectively, 670°C and 653°C. All four domes erupted rhyolite of essentially identical major-element chemistry, although with substantial trace-element variations, high incompatible trace-element contents (Rb up to 364 ppm; Nb up to 67 ppm), and extreme depletion of Ba, Sr, P, Eu, and Ti. These depletions are consistent with fractionation of observed phenocrysts. A rare-earth element diagram shows parallelism of the rhyolite plots, with sloping light REE values, flat heavy REE values, and a prominent, negative Eu anomaly. The narrow range of major-element compositions within the Nathrop Domes' rhyolites precludes any fractionation modeling amongst them. Nonetheless, their elevated Rb/Sr ratios (as great as 75–120) strongly suggest that these magmas have undergone extensive fractional crystallization.

Neodymium isotope analysis shows εNdt values of -10.1 for a Bald Mountain sample and -13.9 from the Precambrian granite sample (t = 29 Ma). The similarity of the εNdt of the Bald Mountain rhyolite and the Precambrian granite suggests that the Nathrop rhyolite magmas were initially formed through partial melting of Precambrian rocks. Neodymium Crustal Index (NCI) calculations were performed using the Precambrian granite to estimate the contribution of crustal sources, assuming lithospheric mantle contributions of basalt with εNd of 0 to 4, or asthenospheric mantle contributions with εNd of 5 or greater. The resulting calculations indicate NCI values of 0.727 to 0.789, assuming lithospheric mantle, and 0.799 assuming an asthenospheric mantle contribution with εNd = 5. Thus, 72.7 to 79.9 percent of the Nd present in the Nathrop rhyolite sample is likely from crustal sources, depending upon what type of mantle contribution was involved. The Nathrop rhyolites may represent the earliest phase of magmatism associated with the northern segments of the Rio Grande Rift.

INTRODUCTION

The Nathrop Domes are a group of four rhyolite domes located along the eastern edge of the Arkansas Valley Graben south of Buena Vista in central Colorado, near the village of Nathrop (Fig. 1). Just to the east lies the Mosquito Range, which is underlain by Precambrian crust (Tweto and Sims, 1963; Bickford and Boardman, 1984). The four domes are composed of borderline peraluminous to metaluminous rhyolite ("topaz rhyolite"), the origin of which is usually attributed to small amounts of partial melting of continental crust, probably lower crustal granulites (Christiansen et al., 1986; Mutschler et al., 1987).

Topaz-bearing rhyolites are characterized by high concentrations of incompatible elements and fluorine. They are also typically associated with occurrences of economically valuable lithophile elements such as uranium and lithium. These "topaz rhyolites" are fairly widespread across the western United States (Burt et al., 1982; Christiansen, et al., 1986). The majority of topaz rhyolites in the western U.S. are found associated with extensional tectonic environments, primarily the Basin and Range Province and the Rio Grande Rift. They also appear to be restricted to areas underlain by the Proterozoic craton (Burt et al., 1982; Christiansen et al., 1986). The age (~30 Ma) of the domes and their geologic setting along the Arkansas Valley Graben suggest that they may represent some of the oldest magmatic products of the Rio Grande Rift.

Our project uses geochemical and isotopic analyses to test the hypothesis that the Nathrop rhyolites were formed as a result of partial melting of crustal material during rift initiation. Major- and trace-element analyses, combined with isotopic analyses, are used to constrain possible sources for the Nathrop Domes magmas and to examine possible lines of magmatic descent.

GEOLOGIC SETTING

Rio Grande Rift

The Rio Grande Rift extends from central Colorado through New Mexico, into western Texas and northern Mexico where it merges with the Basin and Range Province (Chapin, 1971; Baldridge et al., 1984). The amount of extension varies with the southern portion of the rift being roughly 2.5-times wider than the northern section (Chapin, 1979). The rift is divided into four primary rift basins, the northernmost being the Upper

Arkansas Basin (Fig. 1; Chapin and Cather, 1994). Crustal extension is reported to have occurred in two phases: the basins were initially formed by low-angle faulting; this was followed by rifting dominated by higher-angle faulting (Gibson et al., 1993; Baldridge et al., 1995). As part of an ancient subduction zone, the mantle in this region would have undergone metasomatism. Highly alkalic magmas occurring on the flanks of the Rio Grande Rift have been attributed to partial melting of such metasomatized lithospheric mantle (Perry et al., 1987; Gibson et al., 1993).

Extension is reported to have thinned the crust from approximately 50 km under the Great Plains to 30–35 km beneath the southern portion of the rift (Perry et al., 1987; Gibson et al., 1992; Gilbert, 2012). The northern portion of the rift, having undergone less extension, has crust approximately 5 km thicker (Perry et al., 1987). Previous studies have also noted a thinning of the lithosphere to as little 70 km thick beneath the central portion of the rift (Gibson et al., 1992).

Precambrian Basement

The basement beneath the rift in northern New Mexico and southern Colorado belongs to the Yavapai terrane, which is 1.69 to 1.78 billion years old (Perry et al., 1987; Shaw and Karlstrom, 1999). It is considered to be an arc terrane that accreted onto the Wyoming Craton about 1.7 Ga (Karlstrom and Humphreys, 1998; Shaw and Karlstrom, 1999). The Nathrop Domes were erupted through and overlie Precambrian intrusive igneous rocks (Van Alstine, 1969; Christiansen et al., 1986). We refer to the local rock as granite, though it has been classified as a gneissic quartz monzonite by some authors (Van Alstine, 1969; Burt et al., 1982; Christiansen et al., 1986); it was mapped as a

granodiorite by Keller et al. (2004). We observed the granitic basement rock to locally exhibit weak foliation within the study area.

Central Colorado Volcanic Field

The Nathrop Domes lie on the western edge of the Thirtynine Mile Volcanic Complex (Fig. 1) (Wobus et al., 1990), and both fall within the larger Central Colorado Volcanic Field of McIntosh and Chapin (2004). The Central Colorado Volcanic Field included 10 or more volcanic centers, separated now by erosion and faulting during the Neogene, the largest remnant being the Thirtynine Mile Volcanic Complex (McIntosh and Chapin, 2004). Exposures of Wall Mountain Tuff can be found along the eastern portion of the Nathrop Domes area near Bald Mountain (McIntosh and Chapin, 2004; Keller et al., 2004). The majority of the volcanic rocks of the Central Colorado Volcanic Field were erupted between 36 and 27 Ma (McIntosh and Chapin, 2004), with Nathrop Domes' lavas falling near the end of this eruptive sequence at 29–30 Ma (Van Alstine, 1969; McIntosh and Chapin, 2004; McIntosh and Chapin, 2007).

Nathrop Domes

The four major domes of the Nathrop Domes are (from smallest to largest) Dorothy Hill (DH) (a.k.a. Nathrop Butte), Ruby Mountain (RM), Sugar Loaf Mountain (SLM), and Bald Mountain (BM) (Fig. 1; Keller et al., 2004; Christiansen et al., 1986; Schooler, 1982). These rhyolites exhibit flow banding and contain numerous vesicles and lithophysae. Exposures of tuff and vitrophyre occur along the eastern side of Ruby Mountain, and vitrophyre was also noted on the eastern sides of Sugar Loaf and Bald mountains.

Van Alstine (1969) reported K–Ar ages of 28.0 ± 0.8 from Ruby Mountain obsidian, 29.1 ± 0.9 from Sugar Loaf rhyolite, and 29.3 ± 1.5 Ma from rhyolite from Dorothy Hill (?). Additional age dates reported by McIntosh and Chapin (2004) include two for Bald Mountain (28.8 ± 0.21 and 30.4 ± 0.08 Ma) and one for Sugar Loaf (30.1 ± 0.08 Ma). McIntosh and Chapin (2007) recalculated these ages using the updated Fish Canyon Tuff sanidine age, which shifts the age range to 30.65–29.1 Ma. These ages roughly coincide with other high-silica intrusions in the Arkansas Valley Graben, which may mark the beginning of rifting (Chapin and Cather, 1994; Tweto, 1979). Geologic mapping suggests that the Nathrop Domes cross-cut several faults, indicating that dome emplacement postdates the onset of rift-related faulting (Fig. 1) (Keller et al., 2004).

METHODS

Major- and trace-element geochemical analysis was conducted by Activation Laboratories Ltd. (Actlabs), Ancaster, Ontario, Canada, using fusion ICP and ICP–MS on seven samples from the Nathrop Domes and one of Precambrian granite (Table 1). Samples were crushed on a steel plate and then powdered in a tungsten carbide shatterbox. The detection limit for major-element oxides was 0.01 wt. % or better; trace-element detection limits ranged from 30 to as small as 0.002 ppm (Table 1). One sample of topaz rhyolite and one sample of the Precambrian granite were selected for Nd isotope analysis (Table 1), also performed by Actlabs. The isotope samples were dissolved in HF, HNO_3, and $HClO_4$, the rare-earth elements were separated through cation-exchange techniques, and, finally, the Sm and Nd were separated through extraction

chromatography. These analyses were then used to calculate the εNd_t for the two samples and were used in neodymium crustal index calculations (DePaolo et al., 1992).

Electron microprobe analyses of polished sections and mounted grains from several rock types were conducted at the University of Texas at El Paso using a CAMECA® SX-50 electron microprobe. These included vitrophyre from Bald Mountain (sample 070731), granophyre from Sugar Loaf Mountain (sample 070736), and two vapor-phase garnet crystals from Ruby Mountain. Phenocrysts analyzed include feldspar, magnetite, Mn-ilmenite, and biotite (Tables 2 and 3, Fig. 2).

PETROGRAPHY

Topaz rhyolite from the Nathrop Domes is typically flow banded, holocrystalline, and aphanitic, although Sugar Loaf Mountain contains up to 30 volume percent phenocrysts. Phenocrysts include sanidine, plagioclase, and quartz, and smaller amounts of biotite and Fe–Ti oxides. Vitrophyre occurs along the margins of the domes with the same phenocryst assemblage as granophyre. Quartz, feldspar, and garnet are common in lithophysae within the Ruby Mountain samples. Topaz has been reported by previous authors (Van Alstine, 1969); however, no samples containing identifiable topaz were found during the course of our investigation.

GEOCHEMISTRY

Geothermometry

Two-feldspar temperature calculations were conducted following the procedure of Putirka (2008), and two-oxide temperatures were calculated using QUILF (Andersen et

al., 1993). The two-feldspar data, from samples of Sugar Loaf Mountain rhyolite and Bald Mountain vitrophyre, returned crystallization temperatures about 670°C ± 30° (assuming 1 kb pressure). The two-oxide data, from the Sugar Loaf Mountain rhyolite, returned a temperature of 653°C ± 48°. Mg/Mn-equilibrium calculations following Bacon and Hirschmann (1988) were conducted for the magnetite-Mn ilmenite pair used in the above temperature calculation. The log (Mg/Mn) values for ilmenite and magnetite were both -1.5, which fall on the same trend that Bacon and Hirschmann (1988) found based on magnetite-ilmenite pairs known to be in equilibrium.

Whole-Rock Chemistry

All four domes erupted rhyolite of essentially identical major-element composition, although with substantial trace-element variation (Table 1), and they plot within the within-plate granite field on a Y–Nb vs. Rb diagram (Fig. 3). All samples of the Nathrop Domes rhyolites (Fig. 4) are high silica (~76–78 wt. %), are borderline peraluminous to metaluminous, and have low FeO (~0.55 wt.%). These rhyolites meet most of the criteria to be called A-type rhyolites; however, the Nb, Zr, Ce, and Y concentrations are lower than those expected for an A-type rhyolite, and the FeO_{total}/MgO and (Na_2O+K_2O)/CaO ratios are borderline (Whalen et al., 1987).

Trace-element compositions indicate that these rhyolites are highly fractionated with large incompatible trace-element contents (e.g., Rb up to 364 ppm; Nb up to 67 ppm) and extreme depletion of Ba, Sr, P, Eu, and Ti in mantle-normalized trace-element diagrams ("spider diagrams") (Fig. 5). These depletions are consistent with fractionation of observed phenocrysts (Ba in sanidine; Sr and Eu in feldspar; Ti in Fe–Ti oxides; P in apatite). A rare-earth element diagram shows parallelism of the rhyolite plots, with

sloping light REE values, flat heavy REE values, and prominent, negative Eu anomalies (Fig. 6). The narrow range of major-element compositions within the Nathrop Domes rhyolites precludes any precise fractionation modeling amongst them. Nonetheless, their elevated Rb/Sr ratios (as great as 75–120) strongly suggest that these magmas have undergone extensive fractional crystallization (Halliday et al. 1991). A rough calculation, assuming Raleigh fractionation and a bulk-distribution coefficient of 0.15 for Rb, yielded an estimated 25-percent fractionation between samples 070652 RB and 070736 SLM. We do not argue for genetic relations between the rhyolite samples, only that similar fractionation processes produced similar trends in Figures 5 and 6.

The granite plot in Figure 5 is parallel to the rhyolite plots with higher sample/mantle ratios, except for the left side of the diagram, where the rhyolite plots fall above the granite for Nb, Th, and Rb, and fall below the granite for Ba. The rhyolite plots show well-developed negative Ba anomalies. The granite appears to exhibit a typical subduction geochemical signature, involving a Ba peak and a Nb trough (Davidson, 1996), features lacking in the rhyolite plots (Fig. 5). We attempted modeling the rhyolite magmas as descendants of a melt similar to that of the Precambrian granite, but this modeling failed. If an anatectic melt was the parental magma to the Nathrop rhyolite, it was probably generated from different crustal rocks at greater depth.

Isotope Chemistry

Neodymium isotope analysis shows εNdt values of -10.1 for a Bald Mountain sample and -13.9 from the Precambrian granite sample (t = 29 Ma) (Table 1). The Precambrian value corresponds well with εNd values of -14 for crustal rocks in Colorado reported in Perry et al. (1993), but the rhyolite value is more negative than those of

rhyolites from the nearby San Juan Volcanic Field (-6 to -8; Perry et al., 1993). The similarity of the εNdt of the Bald Mountain rhyolite and the Precambrian granite suggests, however, that the Nathrop Domes rhyolite magmas were formed, at least in large part, through partial melting of Precambrian-age rock, but not the locally exposed Precambrian granite.

Neodymium crustal index (NCI) calculations were performed using the Precambrian granite to estimate the contribution of crustal sources (DePaolo et al., 1992). This calculation uses the εNd of the sample, crust, and mantle to estimate the amount of Nd derived from a crustal source (DePaolo et al., 1992). These calculations were performed assuming lithospheric mantle contributions of basalt with εNd of 0 to 4, or asthenospheric mantle contributions with εNd of 5 or greater (Perry et al., 1993). The resulting calculations indicate NCI values of 0.727 to 0.789, assuming lithospheric mantle, and 0.799, assuming an asthenospheric mantle contribution with εNd = 5 (Perry et al., 1987). Thus, 72.7 to 79.9 percent of the Nd present in the Nathrop Domes sample is likely from crustal sources, depending upon what type of mantle contribution was involved. This conclusion is supported by a $^{87}Sr/^{86}Sr$ ratio reported by Christiansen et al. (1986) of 0.714 ± 0.0060, assuming an age of 29.3 Ma for the Nathrop Domes. The high Sr isotope ratio, εNd values, and the NCI calculations clearly indicate that the major source for the magma was crustal.

DISCUSSION

The above analysis suggests that heat from intrusion of basalt into the crust may have caused partial melting of the crust, thereby creating the ancestral magmas that

differentiated to form the Nathrop Domes. Regionally, such basalt was concurrently available as part of the Thirtynine Mile Volcanic Complex (Wobus et al., 1990; McIntosh and Chapin, 2004). Although a treatment of the Thirtynine Mile Volcanic Complex is beyond the scope of our paper, a relationship between anatectic rhyolite similar to the Nathrop Domes rhyolite is suggested by a plot of K/Rb vs. Rb, where mixing of rhyolite with basaltic magmas could generate the concave plot exhibited in Figure 7. The parental hybrid magma was not likely a basalt, but a more felsic composition with a low K/Rb ratio and Rb concentration that could have evolved through fractional crystallization to produce the Nathrop Domes rhyolites. Modeling indicates that simple fractionation is not sufficient to account for the variability in trace elements within the Nathrop Domes rhyolites. These differences are likely the result of different degrees of partial melting of the lower crust, different amounts of assimilation, or different compositions of source rocks.

Topaz rhyolites are known to be enriched in a variety of trace elements such as Rb, Cs, Li, U, Th, Nb, Ta, Sn, W, Mo, and Be (Burt et al., 1982). This suggests a significant amount of fractionation has occurred in order to increase the concentration of these elements in the Nathrop Domes rhyolites. Topaz rhyolites are interesting due to their unique mineralogy, and several are found near major, economically valuable, mineral deposits. Their proximity to deposits like those at the Climax mine in Colorado and Spor Mountain in Utah has created further interest in studying these highly evolved volcanic rocks as more and more evidence suggests spatial and genetic links (Burt, et al., 1982). The Chalk Mountain topaz rhyolite, found in the Mosquito Range near the northern end of the Arkansas Valley Graben, has been suggested to have been the upper

portion of the Climax deposit that was downfaulted (Burt et al., 1982). While there is no direct evidence for any economically important mineral deposits associated with the Nathrop Domes, the association of other topaz rhyolites to such deposits suggests that the existence of such deposits in the Nathrop area is plausible.

The geochemical and isotopic data suggest that these rhyolites were formed through partial melting of lower crustal material, but including a mantle component. These rhyolites are evidence for the accumulation of basaltic magma in the lower crust, which provided sufficient heat for partial melting of the lower crust. Field relations show that the rhyolites post-date several faults in the area, suggesting that the faults provided the pathway for the magma to ascend, and the domes, therefore, may mark early magmatism in the Arkansas Valley Graben segment of the Rio Grande Rift.

CONCLUSIONS

Our Nd isotopic analyses and a previously published Sr isotopic analysis suggest a predominantly crustal source for the Nathrop Domes topaz rhyolite. The Nathrop Domes parental magmas were likely formed through partial melting of crustal rocks, possibly mixed with smaller amounts of mantle-derived basalt. The anatectic magmas then underwent significant crystal fractionation during ascent and, eventually, erupted as highly-evolved, low-temperature descendents of the initial crustal melts. Heat for crustal melting was likely from mafic magmas injected into the crust as part of the initial development of the Rio Grande Rift.

ACKNOWLEDGMENTS

We thank Baylor University and Baylor Department of Geology for providing the funding necessary to complete this project. We would also like to thank Eric Christiansen, Nancy McMillan, Donald Burt, and Art Snoke for their constructive reviews of this manuscript.

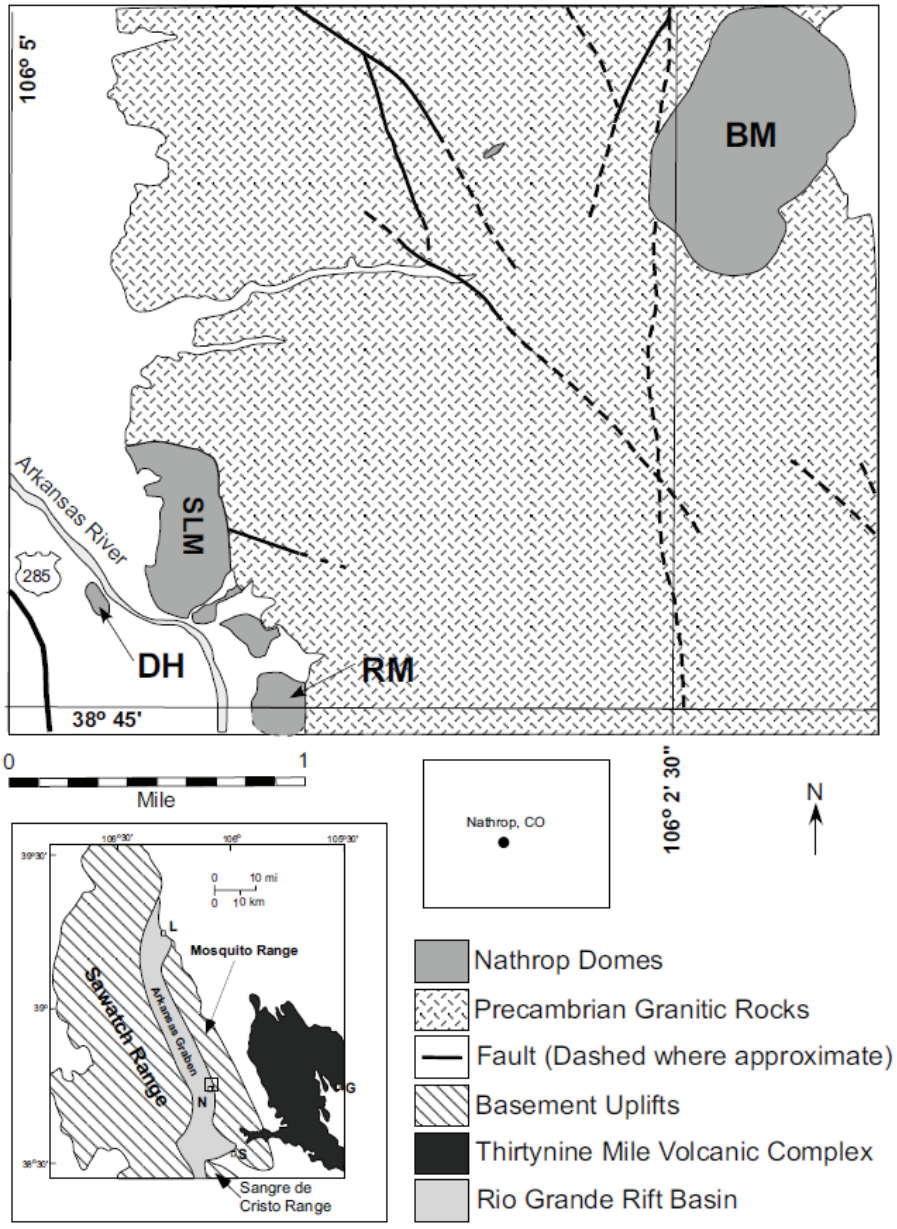

Figure 3.1. Generalized map of the Nathrop Domes (modified from Keller et al., 2004; inset modified from McIntosh and Chapin, 2004). Each of the four named edifices is reported to have a separate vent (Christiansen et al., 1986, and references therein). BM, SLM, and RM are, respectively, Bald, Sugar Loaf, and Ruby mountains, and DH is Dorothy Hill. Generalized location map showing the major uplifts, the Arkansas Valley Graben, and the Thirtynine Mile Volcanic Complex (modified from McIntosh and Chapin, 2004). The black box on the inset map indicates the study area. From bottom up, S is Salida, N is Nathrop, G is Guffey, and L is Leadville.

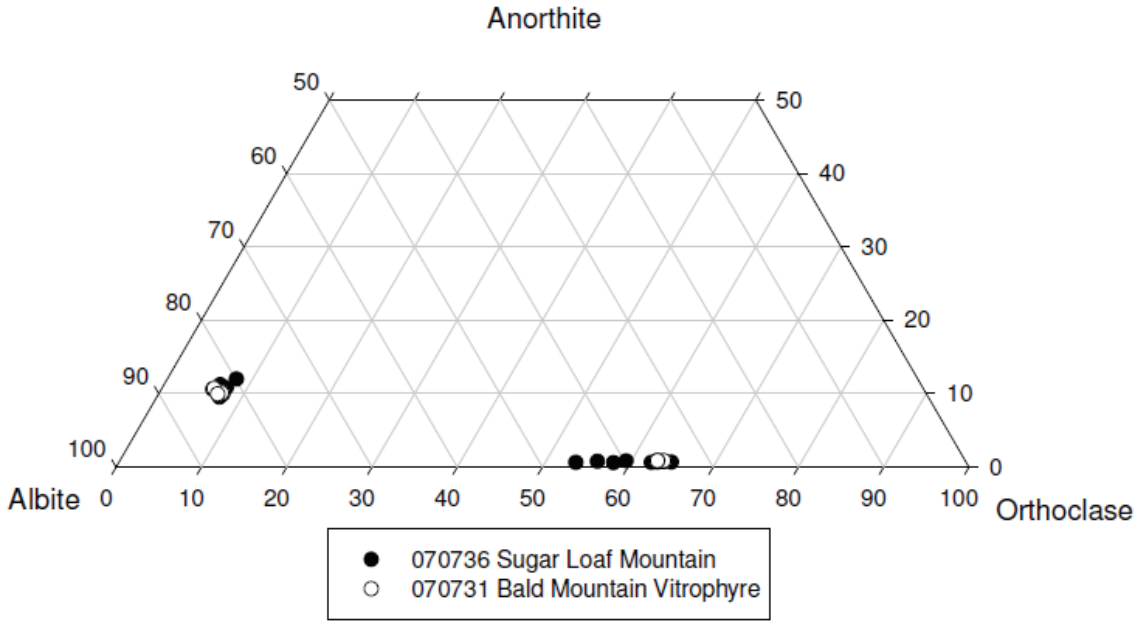

Figure 3.2. Feldspar composition ternary showing the compositions of feldspars from Bald Mountain vitrophyre and Sugar Loaf Mountain rhyolite.

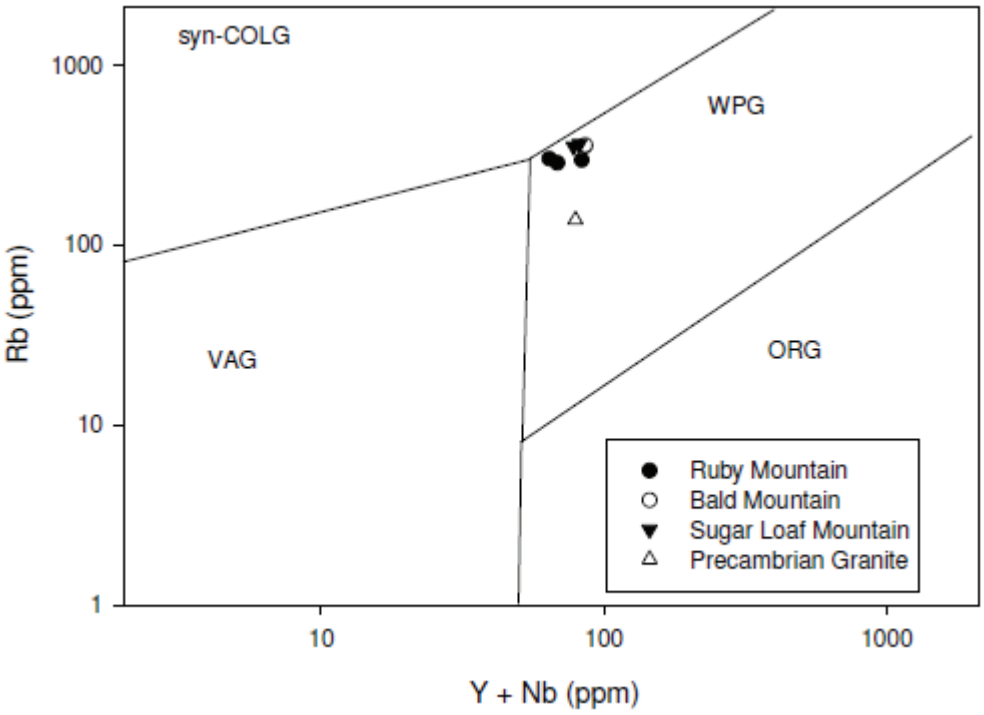

Figure 3.3. Y+Nb vs. Rb plot after Pearce et al. (1984). The Nathrop Domes rhyolites fall within the within-plate granites field (WPG). Other fields are syn-colisional granites (syn-COLG), volcanic arc granites (VAG), and ocean-ridge granites (ORG).

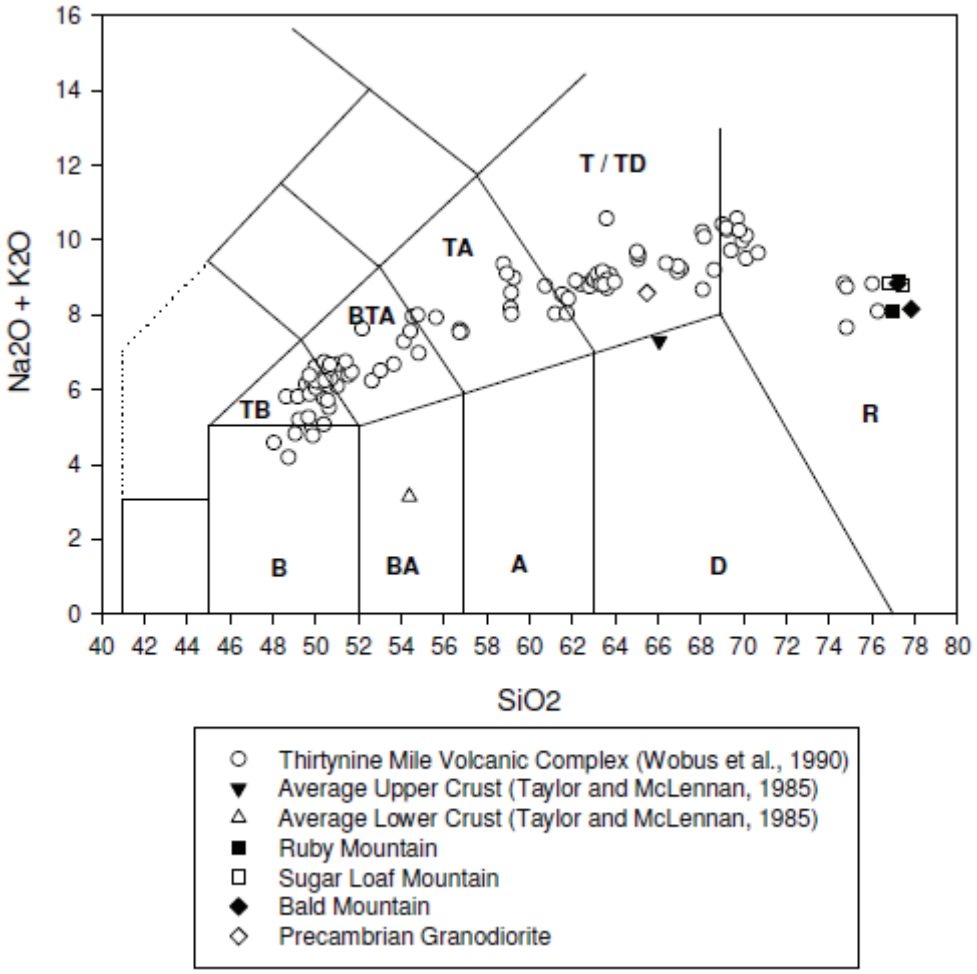

Figure 3.4. TAS diagram (Le Bas et al., 1986) showing analyses from the Thirtynine Mile Volcanic Complex (Wobus et al., 1990) and our analyses from the Nathrop Domes. The labeled fields are basalt (B), basaltic andesite (BA), andesite (A), dacite (D), rhyolite (R), trachybasalt (TB), basaltic trachyandesite (BTA), trachyandesite (TA), and trachyte / trachydacite (T / TD).

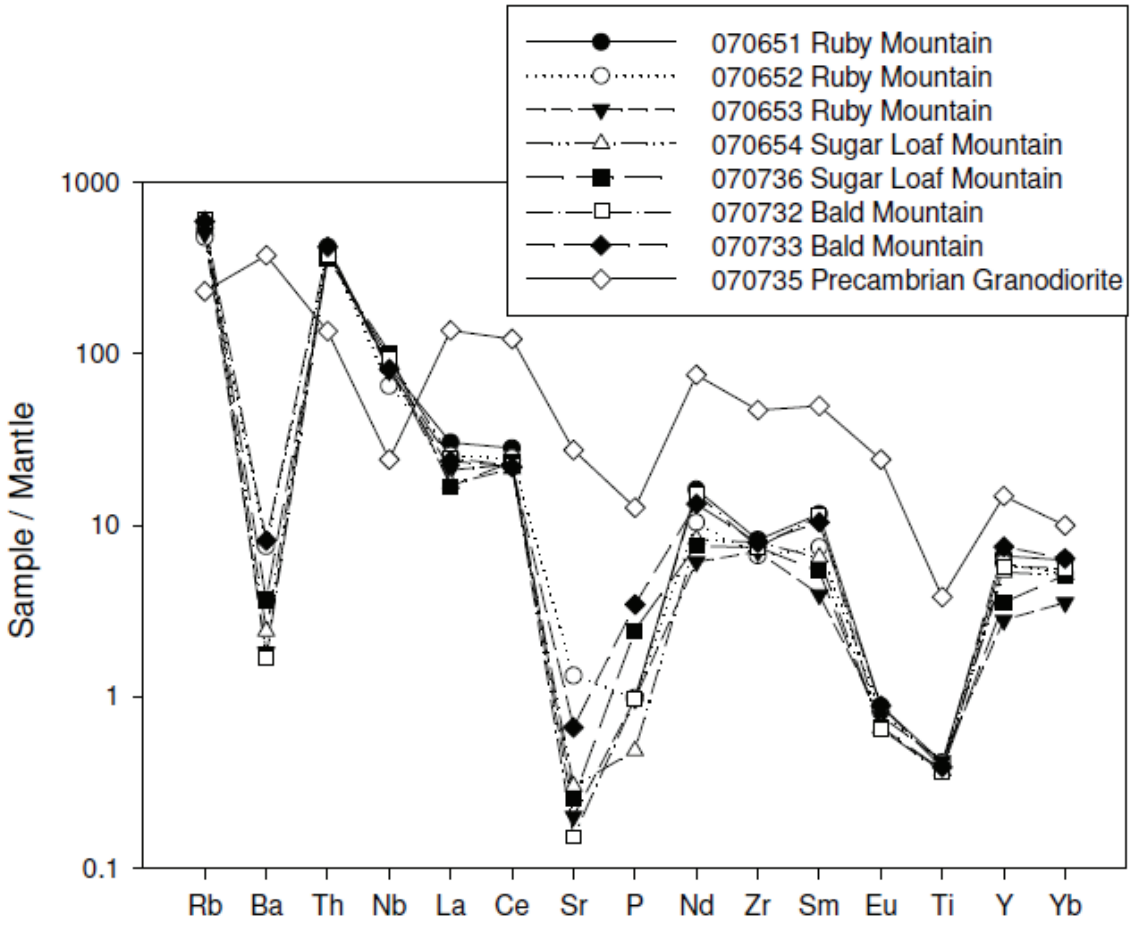

Figure 3.5. Mantle normalized variation diagram (McDonough and Sun, 1995) of samples from Ruby, Sugar Loaf, and Bald mountains plus a sample of the local Precambrian host granite. The host granite exhibits a typical subduction signature of Ba enrichment and Nb depletion (Davidson, 1996). The Nathrop Domes rhyolites are enriched, relative to the granite, in Rb, Th, and Nb, but relatively depleted in all others.

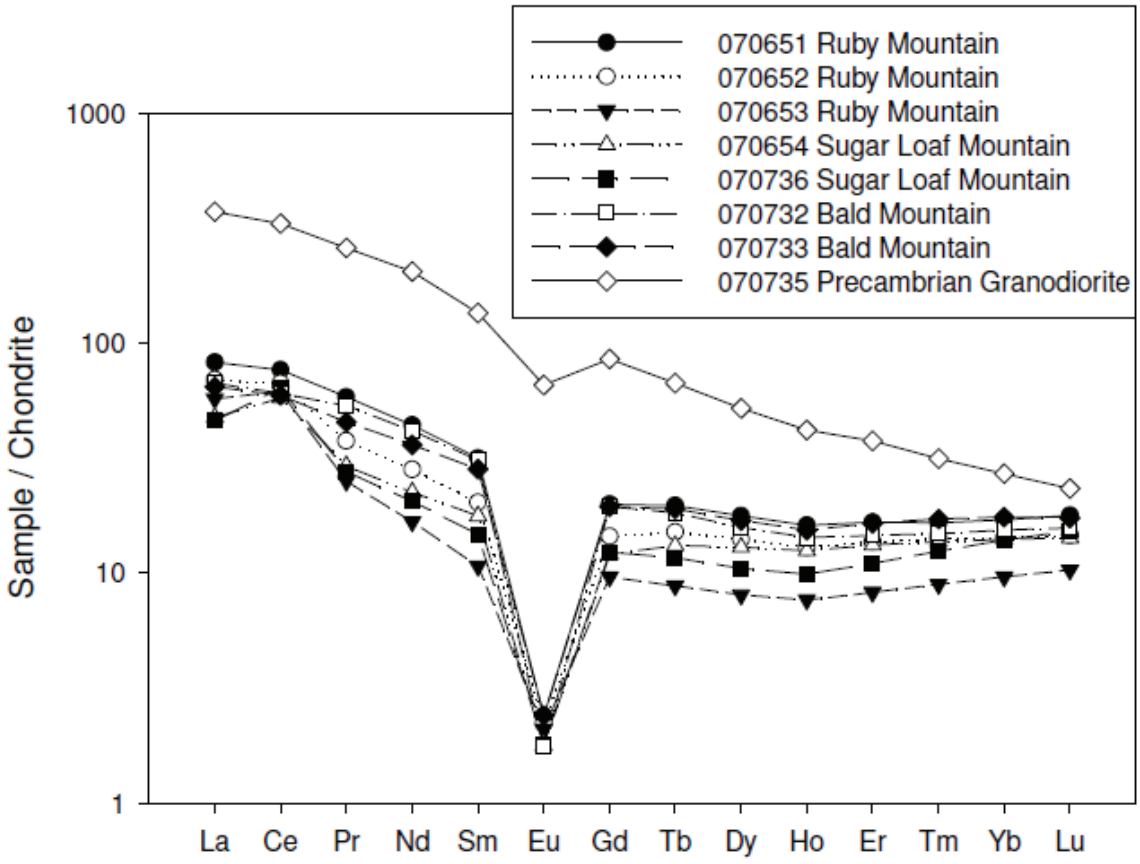

Figure 3.6. REE diagram of samples from Ruby, Sugar Loaf, and Bald Mountain domes as well as the Precambrian host rock. The lower heavy REE concentration can be attributed to their retention in the source rock or fractionation of minerals such as apatite. Sample values normalized to chondrite according to Wakita et al. (1971).

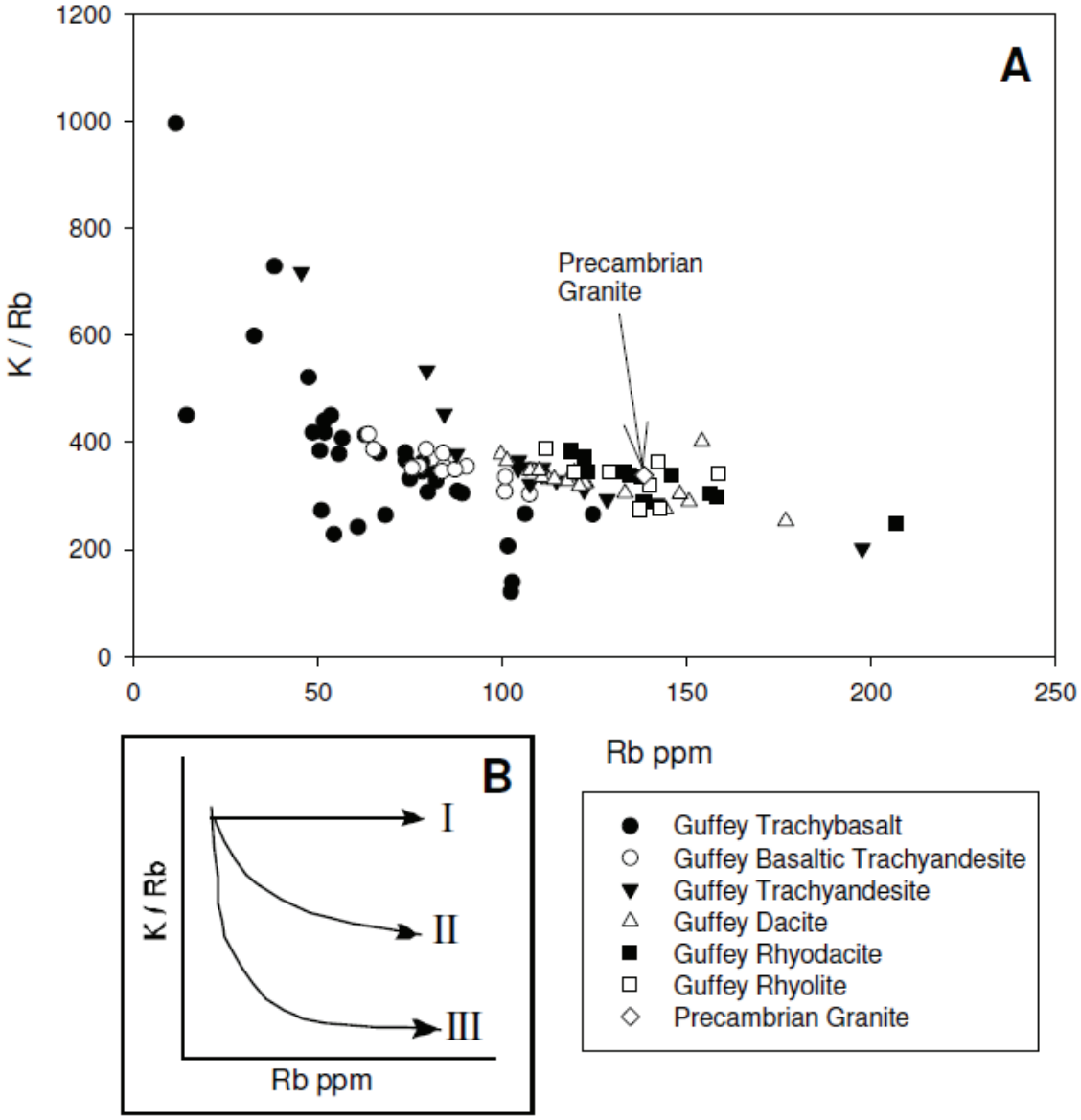

Figure 3.7. A) K/Rb vs. Rb plot. This plot shows the Guffey volcano samples from the Thirtynine Mile Volcanic Complex (Wobus et al., 1990) and the Precambrian granite. The curve of the trend toward the Precambrian granite suggests that assimilation of crustal material similar to the Precambrian granite may have played a part in the evolution of the Thirtynine Mile Volcanic Complex magmas (Parker et al., 2005). B) K/Rb vs. Rb general trends. Trend I illustrates pure fractionation of the magma, and trend III illustrates pure crustal assimilation. The K/Rb ratio should not be lowered by fractional crystallization, as both elements are incompatible in mafic magmas. Trend II shows combined assimilation and fractional crystallization. (Parker et al., 2005)

Table 3.1. Whole-rock geochemical analyses of Nathrop Domes samples and Precambrian granite.

	070651 RM	070652 RM	070653 RM	070654 SLM	070736 SLM	070732 BM	070733 BM	070735 PCG	Detection Limit
SiO_2	76.96	76.12	77.55	78.00	76.56	76.97	76.86	65.25	0.01
TiO_2	0.08	0.08	0.08	0.07	0.07	0.07	0.08	0.75	0.001
Al_2O_3	12.58	11.88	12.89	12.83	13.00	12.85	12.08	15.99	0.01
FeO*	0.55	0.55	0.54	0.49	0.49	0.51	0.55	3.87	0.01
MnO	0.10	0.10	0.09	0.10	0.11	0.09	0.11	0.07	0.001
MgO	0.05	0.07	0.06	0.07	0.06	0.04	0.09	1.31	0.01
CaO	0.45	2.04	0.33	0.30	0.49	0.32	0.86	3.59	0.01
Na_2O	4.28	3.66	4.10	4.06	4.22	4.19	3.90	2.94	0.01
K_2O	4.57	4.35	4.77	4.81	4.61	4.63	4.16	5.62	0.01
P_2O_5	0.02	0.02	0.02	0.01	0.05	0.02	0.07	0.26	0.01
LOI	1.09	1.38	0.40	0.17	0.40	0.41	0.76	0.62	
Total	100.73	100.25	100.83	100.91	100.06	100.10	99.52	100.27	
Sc	4	3	3	5	5	5	5	12	1
Be	6	7	6	8	8	8	8	3	1
V	b.d.	b.d.	b.d.	b.d.	5	6	b.d.	58	5
Cr	b.d.	b.d.	b.d.	b.d.	b.d.	b.d.	b.d.	b.d.	20
Ni	b.d.	b.d.	b.d.	b.d.	b.d.	b.d.	b.d.	b.d.	20
Cu	b.d.	b.d.	b.d.	b.d.	b.d.	b.d.	b.d.	20	10
Zn	30	30	40	40	40	50	30	80	30
Ga	22	19	22	23	24	24	22	21	1
Ge	2.2	1.7	2.1	2.1	2.2	2.5	1.9	1.4	0.5
As	b.d.	b.d.	b.d.	b.d.	b.d.	5	b.d.	b.d.	5
Rb	296	283	303	357	364	358	350	138	1

Table 3.1. Continued.

	070651 RM	070652 RM	070653 RM	070654 SLM	070736 SLM	070732 BM	070733 BM	070735 PCG	Detection Limit
Sr	0	26	4	6	5	3	13	542	2
Y	28.3	25.6	12	23	15.1	24.5	31.8	63.3	0.5
Zr	86	69	74	84	78	78	82	490	1
Nb	54.9	42.1	52.4	55.7	66.7	61.3	52.8	15.8	0.2
Mo	4	b.d.	b.d.	b.d.	b.d.	2	2	b.d.	2
Ag	b.d.	b.d.	b.d.	b.d.	b.d.	b.d.	b.d.	b.d.	0.5
In	b.d.	b.d.	b.d.	b.d.	b.d.	b.d.	b.d.	b.d.	0.1
Sn	3	2	3	4	4	4	3	2	1
Sb	b.d.	6.6	b.d.	4.1	b.d.	b.d.	0.9	3.7	0.2
Cs	6.8	4.9	4.8	7.3	7.5	6.8	7.2	1.8	0.1
Ba	b.d.	49	12	16	24	11	53	2463	3
La	19.6	16.3	13.7	11.4	10.9	15.9	15.2	88.3	0.05
Ce	46.9	40.8	38.1	35.9	39.2	37.2	36.1	203	0.05
Pr	5.42	3.46	2.35	2.75	2.57	4.98	4.18	24.1	0.01
Nd	20.1	12.8	7.69	10.4	9.4	19.1	16.4	93.6	0.05
Sm	4.69	2.98	1.6	2.65	2.18	4.6	4.16	20	0.01
Eu	0.135	0.124	0.119	0.101	0.102	0.099	0.134	3.7	0.005
Gd	3.97	2.85	1.93	2.43	2.45	3.89	3.84	17	0.01
Tb	0.71	0.54	0.32	0.48	0.42	0.66	0.68	2.42	0.01
Dy	4.36	3.42	1.99	3.22	2.57	3.88	4.12	12.8	0.01
Ho	0.88	0.7	0.42	0.69	0.54	0.78	0.83	2.29	0.01
Er	2.66	2.17	1.33	2.14	1.76	2.33	2.61	6.01	0.01
Tm	0.409	0.346	0.222	0.342	0.307	0.367	0.42	0.777	0.005
Yb	2.75	2.27	1.56	2.28	2.24	2.47	2.79	4.36	0.01
Lu	0.438	0.356	0.256	0.353	0.374	0.387	0.423	0.574	0.002

Table 3.1. Continued.

	070651 RM	070652 RM	070653 RM	070654 SLM	070736 SLM	070732 BM	070733 BM	070735 PCG	Detection Limit
Hf	4.5	3.5	4.4	4.7	4.9	4.7	4.2	11.6	0.1
Ta	6.79	3.72	5.14	5.2	6.26	6.43	4.82	2.01	0.01
Tl	1.28	1.5	1.67	2.1	1.8	2.16	1.7	0.87	0.05
Pb	22	41	28	39	25	41	33	36	5
Bi	0.8	b.d.	b.d.	0.3	0.5	0.5	b.d.	0.2	0.1
Th	33.3	32.4	32.1	31.4	28.5	29.8	33	10.7	0.05
U	14.7	5.87	6.33	9.67	8.86	11.5	8.95	1.81	0.01
La/Yb_N	4.84	4.88	5.97	3.40	3.31	4.37	3.70	13.76	
$^{147}Sm/^{144}Nd$							0.1577	0.1198	± 0.5%
$^{143}Nd/^{144}Nd$							0.5121	0.5119	
εNd_t							-10.1	-13.9	

RM = Ruby Mountain; SLM = Sugar Loaf Mountain; BM = Bald Mountain; PCG = Precambrian granodiorite

FeO* = total Fe as FeO; LOI = Loss on Ignition

b.d. = below detection limit

Detection Limit reported in percent for major and minor elements and in ppm for trace elements

$^{143}Nd/^{144}Nd$ ratios are relative to the JNd-1 standard

Table 3.2. Selected electron microprobe analyses of plagioclase and K-feldspar from Nathrop Domes samples. 070731 BM is a vitrophyre sample from Bald Mountain. 070736 SLM is a rhyolite sample from Sugar Loaf Mountain.

	070731 BM							070736 SLM				
	K-feld #9	K-feld #12	K-feld #20	K-feld #24	Plag #42	Plag #43	Plag #45	K-feld #7	K-feld #10	K-feld #31	K-feld #35	K-feld #50
SiO_2	65.38	65.15	64.82	65.28	65.54	65.49	65.27	65.71	65.54	65.38	65.49	66.19
TiO_2	0.00	0.03	0.00	0.06	0.04	0.02	0.01	0.00	0.00	0.07	0.09	0.08
Al_2O_3	18.82	18.96	18.84	18.77	21.18	21.52	21.22	18.72	18.82	18.92	19.08	19.00
FeO	0.26	0.18	0.23	0.21	0.22	0.25	0.22	0.19	0.17	0.23	0.16	0.21
MnO	0.04	0.00	0.05	0.01	0.05	0.02	0.04	0.00	0.00	0.02	0.04	0.05
CaO	0.17	0.17	0.17	0.16	2.14	2.21	2.07	0.13	0.13	0.13	0.13	0.15
Na_2O	3.89	3.87	3.90	3.81	9.69	9.49	9.59	4.10	3.94	4.12	5.29	4.93
K_2O	10.35	10.61	10.36	10.12	1.31	1.07	1.21	10.56	11.25	10.92	9.42	9.73
Total	98.91	98.96	98.38	98.41	100.17	100.06	99.62	99.41	99.84	99.79	99.71	100.33
An	0.87	0.84	0.84	0.84	10.09	10.68	9.91	0.62	0.65	0.64	0.60	0.74
Ab	36.03	35.34	36.06	36.09	82.58	83.18	83.16	36.89	34.55	36.22	45.78	43.18
Or	63.10	63.81	63.10	63.07	7.33	6.14	6.93	62.49	64.81	63.14	53.62	56.08

Table 3.2. Continued.

	070736 SLM												
	K-feld #52	K-feld #65	K-feld #66	Plag #2	Plag #3	Plag #40	Plag #41	Plag #62	Plag #63	Plag #69	Plag #71	Plag #73	Plag #80
SiO_2	65.16	65.37	65.39	65.22	65.33	65.46	65.15	63.99	64.82	64.65	65.02	65.26	64.66
TiO_2	0.06	0.08	0.12	0.02	0.00	0.11	0.05	0.06	0.03	0.06	0.08	0.08	0.06
Al_2O_3	18.99	18.84	18.89	21.29	21.25	21.19	21.27	21.48	21.20	21.37	21.27	21.14	21.42
FeO	0.22	0.19	0.17	0.19	0.23	0.20	0.20	0.19	0.24	0.28	0.20	0.20	0.18
MnO	0.05	0.01	0.00	0.03	0.01	0.01	0.03	0.06	0.04	0.06	0.05	0.04	0.06
CaO	0.15	0.17	0.12	2.30	2.20	2.01	2.08	2.51	2.16	2.30	2.14	2.09	2.22
Na_2O	4.04	4.57	4.74	9.33	9.59	9.71	9.57	9.24	9.61	9.61	9.41	9.67	9.33
K_2O	11.09	10.37	10.11	1.14	1.05	1.31	1.33	1.43	1.22	1.18	1.28	1.24	1.31
Total	99.76	99.59	99.54	99.52	99.67	99.98	99.67	98.95	99.31	99.50	99.44	99.72	99.24
An	0.71	0.81	0.56	11.18	10.57	9.51	9.91	11.97	10.28	10.90	10.32	9.93	10.75
Ab	35.39	39.78	41.38	82.19	83.41	83.14	82.54	79.92	82.81	82.46	82.33	83.05	81.72
Or	63.90	59.41	58.06	6.62	6.02	7.36	7.55	8.11	6.91	6.64	7.35	7.02	7.52

Table 3.3. Selected electron microprobe analyses of phenocryst minerals from Nathrop Domes samples. 070731 BM is a vitrophyre sample from Bald Mountain. 070736 SLM is a rhyolite sample from Sugar Loaf Mountain. 070737 RM is a garnet from Ruby Mountain.

	070731 BM			070737 RM
	Biotite	Biotite		Garnet
	#25	#34		#14
SiO_2	34.93	35.97		35.04
TiO_2	3.36	3.02		0.38
Al_2O_3	12.08	12.55		20.54
Cr_2O_3	0.14	0.14		0.06
FeO	21.15	20.12		12.95
MnO	1.62	1.22		31.74
MgO	12.88	12.56		0.34
CaO	0.12	0.17		0.36
Na_2O	0.51	0.51		
K_2O	7.74	7.69		0.00
Total	94.53	93.95		101.41
			Pyr	1.32
			Alm	28.06
			Gro	0.99
			Spe	69.63
Formula	24 Oxygens		Formula	24 Oxygens
Si	5.486	5.619	Si	5.778
Ti	0.397	0.355	Ti	0.047
Al	2.235	2.310	Al	3.991
Fe^{2+}	2.777	2.628	Fe	1.786
Mn	0.215	0.161	Mn	4.432
Mg	3.016	2.925	Mg	0.084
Ca	0.021	0.028	Ca	0.063
Na	0.155	0.154		
K	1.550	1.532		
Total	15.852	15.712	Total	16.181

Table 3.3. Continued

	070736 SLM			
	Magnetite #43	Magnetite #21	Ilmenite #23	Ilmenite #26
SiO2	0.00	0.00	0.00	0.00
TiO2	3.18	2.60	44.63	45.92
Al2O3	2.19	1.49	0.00	0.00
Cr2O3	0.20	0.23	0.24	0.25
FeO	78.43	86.09	37.34	37.43
MnO	8.06	4.55	16.57	15.41
MgO	0.28	0.22	0.62	0.60
Total	92.34	95.18	99.40	99.61
Fe_2O_3	59.14	63.25	16.77	14.25
FeO	25.21	29.18	22.25	24.61
Rev. Total	98.06	101.27	100.84	100.79
Formula	4 Oxygens		3 Oxygens	
Si	0.000	0.000	0.000	0.000
Ti	0.092	0.073	0.842	0.866
Al	0.099	0.066	0.000	0.000
Fe^{3+}	1.716	1.788	0.317	0.269
Fe^{2+}	0.813	0.917	0.467	0.516
Mn	0.263	0.145	0.352	0.327
Mg	0.016	0.012	0.023	0.022
Total	2.999	3.001	2.001	2.000

REFERENCES CITED

Andersen, D. J., Lindsley, D. H., Davidson, P. M., 1993, QUILF: A PASCAL program to assess equilibria among Fe–Mg–Mn–Ti oxides, pyroxenes, olivine, and quartz: Computers and Geosciences, v. 19, p. 1333–1350.

Bacon, C. R., and Hirschmann, M. M., 1988, Mg/Mn partitioning as a test for equilibrium between coexisting Fe–Ti oxides: American Mineralogist, v. 73, p. 57–61.

Baldridge, W. S., Olsen, K. H., and Callender, J. F., 1984, Rio Grande Rift: Problems and perspectives, *in* Baldridge, W. S., Dickerson, P. W., Riecker, R. E., and Zidek, J., eds., Rio Grande Rift: Northern New Mexico: New Mexico Geological Society Thirty-fifth Annual Field Conference, Guidebook, v. 35, p. 1–12.

Baldridge, W. S., Keller, G. R., Haak, V., Wendlandt, E., Jiracek, G. R., and Olsen, K. H., 1995, The Rio Grande Rift, *in* Olsen, K. H., ed., Continental rifts: Evolution, structure, and tectonics: Developments in Geotectonics, v. 25, Amsterdam, Elsevier, p. 233–275.

Bickford, M. E., and Boardman, S. J., 1984, A Proterozoic volcano–plutonic terrane, Gunnison and Salida areas, Colorado: The Journal of Geology, v. 92, p. 657–666.

Burt, D. M., Sheridan, M. F., Bikun, J. V., and Christiansen, E. H., 1982, Topaz rhyolites—Distribution, origin, and significance for exploration: Economic Geology, v. 77, p. 1818–1836.

Chapin, C. E., 1971, The Rio Grande Rift, Part I: Modifications and additions, *in* James, H. L., ed., Guidebook of the San Luis Basin, Colorado: New Mexico Geological Society, Twenty-second Annual Field Conference, Guidebook, v. 22, p. 191–201.

Chapin, C. E., 1979, Evolution of the Rio Grande Rift—A summary, *in* Riecker, R. E. ed., Rio Grande Rift: Tectonics and magmatism: Washington, D.C., American Geophysical Union, p. 1–5.

Chapin, C. E., and Cather, S. M., 1994, Tectonic setting of the axial basins of the northern and central Rio Grande Rift, *in* Keller, G. R., and Cather, S. M., eds., Basins of the Rio Grande Rift: Structure, stratigraphy, and tectonic setting: Boulder, Colorado, Geological Society of America Special Paper 291, p. 5–25.

Christiansen, E. H., Sheridan, M. F., and Burt, D. M., 1986, The geology and geochemistry of Cenozoic topaz rhyolites from the western United States: Geological Society of America Special Paper 205, 82 p.

Davidson, J. P., 1996, Deciphering mantle and crustal signatures in subduction zone magmatism, *in* Bebout, G. E., Scholl, D. W., Kirby, S. H., and Platt, J. P., eds., Subduction: Top to bottom: American Geophysical Union Monograph Series, v. 96, p. 251–262.

DePaolo, D. J., Perry, F. V., and Baldridge, W. S., 1992, Crustal versus mantle sources of granitic magmas: A two-parameter model based on Nd isotopic studies: Royal Society of Edinburgh Transactions: Earth Sciences, v. 83, p. 439–446.

Gibson, S. A., Thompson, R. N., Leat, P. T., Dickin, A. P., Morrison, M. A., Hendry, G. L., and Mitchell, J. G., 1992, Asthenosphere-derived magmatism in the Rio Grande Rift, western USA: Implications for continental break-up, *in* Storey, B. C., Alabaster, T., and Pankhurst, R. J., eds., Magmatism and the causes of continental break-up: Geological Society Special Publication, v. 68, p. 61–89.

Gibson, S. A., Thompson, R. N., Leat, P. T., Morrison, M. A., Hendry, G. L., Dickin, A. P., and Mitchell, J. G., 1993, Ultrapotassic magmas along the flanks of the Oligo–Miocene Rio Grande Rift, USA: Monitors of the zone of lithospheric mantle extension and thinning beneath a continental rift: Journal of Petrology, v. 34, p. 187–228.

Gilbert, H., 2012. Crustal structure and signatures of recent tectonism as influenced by ancient terranes in the western United States: Geosphere, v. 8, p. 141–157.

Halliday, A. N., Davidson, J. P., Hildreth, W., and Holden, P., 1991, Modelling the petrogenesis of high Rb/Sr silicic magmas: Chemical Geology, v. 92, p. 107–114.

Karlstrom, K. E., and Humphreys, E. D., 1998, Persistent influence of Proterozoic accretionary boundaries in the tectonic evolution of southwestern North America: Interaction of cratonic grain and mantle modification events: Rocky Mountain Geology, v. 33, p. 161–179.

Keller, J. W., McCalpin, J. P., and Lowry, B. W., 2004, Geologic map of the Buena Vista east quadrangle, Chaffee County, Colorado: Colorado Geological Survey Open-File Report OF04-04.

Le Bas, M. J., Le Maitre, R. W., Streckeisen, A., and Zanettin, B., 1986, A chemical classification of volcanic rocks based on the total alkali-silica diagram: Journal of Petrology, v. 27, p. 745–750.

McDonough, W. F., and Sun, S. S., 1995, The composition of the Earth: Chemical Geology, v. 120, p. 223–253.

McIntosh, W. C., and Chapin, C. E., 2004, Geochronology of the central Colorado volcanic field: New Mexico Bureau of Geology and Mineral Resources, Bulletin 160, p. 205–237.

McIntosh, W. C., and Chapin, C. E., 2007, Geochronology of the early southern Rocky Mountain volcanic field, *in* The Volcanoes of Colorado: A Colorado Scientific Society Symposium Honoring Thomas A. Steven: Greeley, Colorado, University of Northern Colorado, p. 13–14.

Mutschler, F. E., Larson, E. E., and Bruce, R. M., 1987, Laramide and younger magmatism in Colorado—New petrologic and tectonic variations on old themes, *in* Drexler, J. W., and Larson, E. E., eds., Cenozoic volcanism in the southern Rocky Mountains updated: A tribute to Rudy C. Epis—Part I: Colorado School of Mines Quarterly, v. 82, p. 1–47.

Parker, D. F., Ghosh, A., Price, C. W., Rinard, B. D., Cullers, R. L., and Ren, M., 2005, Origin of rhyolite by crustal melting and the nature of parental magmas in the Oligocene Conejos Formation, east–central San Juan Mountains, Colorado, USA: Journal of Volcanology and Geothermal Research, v. 139, p. 185–210.

Pearce, J. A., Harris, N. B. W., and Tindle, A. G., 1984, Trace element discrimination diagrams for the tectonic interpretation of granitic rocks: Journal of Petrology, v. 25, p. 956–983.

Perry, F. V., Baldridge, W. S., and DePaolo, D. J., 1987, Role of asthenosphere and lithosphere in the genesis of late Cenozoic basaltic rocks from the Rio Grande Rift and adjacent regions of the southwestern United States: Journal of Geophysical Research, v. 92, p. 9193–9213.

Perry, F. V., DePaolo, D. J., and Baldridge, W. S., 1993, Neodymium isotopic evidence for decreasing crustal contributions to Cenozoic ignimbrites of the western United States: Implications for the thermal evolution of the Cordilleran crust: Geological Society of America Bulletin, v. 105, p. 872–882.

Putirka, K. D., 2008, Thermometers and barometers for volcanic systems: Reviews in Mineralogy and Geochemistry, v. 69, p. 61–120.

Schooler, R. A., 1982, Interpretation of rock and vapor phase relations in the Ruby Mountain Volcanic Complex, Chaffee County, Colorado [Master's thesis]: Bowling Green, Ohio, Bowling Green State University, 104 p.

Shaw, C. A., and Karlstrom, K. E., 1999, The Yavapai–Mazatzal crustal boundary in the southern Rocky Mountains: Rocky Mountain Geology, v. 34, p. 37–52.

Taylor, S. R., and McLennan, S. M., 1985, The Continental Crust: Its composition and evolution. Blackwell, Oxford, 312 p.

Tweto, O., 1979, The Rio Grande Rift system in Colorado, *in* Riecker, R. E., ed., Rio Grande Rift: Tectonics and magmatism: Washington, D.C., American Geophysical Union, p. 33–56.

Tweto, O., and Sims, P. K., 1963, Precambrian ancestry of the Colorado mineral belt: Geological Society of America Bulletin, v. 74, p. 991–1014.

Van Alstine, R. E., 1969, Geology and mineral deposits of the Poncha Springs NE quadrangle, Chaffee County, Colorado, with a section on fluorspar mines and prospects: U.S. Geological Survey Professional Paper 626, 52 p.

Wakita, H., Rey, P., and Schmitt, R. A., 1971, Abundances of the 14 rare-earth elements and 12 other rare elements in Apollo 12 samples: Five igneous and one breccia rocks and four soils: Proceedings of the Second Lunar Science Conference, v. 2, p. 1319–1329.

Whalen, J. B., Currie, K. L., and Chappell, B. W., 1987, A-type granites: Geochemical characteristics, discrimination and petrogenesis: Contributions to Mineralogy and Petrology, v. 95, p. 407–419.

Wobus, R. A., and 11 others, 1990, Geochemistry of high-potassium rocks from the mid-Tertiary Guffey volcanic center, Thirtynine Mile Volcanic Field, central Colorado: Geology, v. 18, p. 642–645.

CHAPTER FOUR

Magma Series of the Raton-Clayton Volcanic Field, New Mexico

ABSTRACT

Six magma series occur within the late Miocene to Quaternary Raton-Clayton volcanic field. Widely-distributed members of both the tholeiitic and the alkaline basalt series range in composition from true basalt through trachybasalt and basaltic trachyandesite to trachyandesite. A less widely distributed strongly alkaline basalt series rocks include basanite and nephelinite. A xenocrystic basalt series characterizes the circa 100,000 yr Capulin lavas, whereas two-pyroxene andesite forms the nearby Sierra Grande composite volcano. The sixth series consists of dacite and rhyolite of domes in the western part of the field. Magmas within each series evolved through assimilation-fractional crystallization processes.

Calculated depths of segregation of Raton-Clayton basalts indicate that strongly alkaline basaltic rocks originated at depths of 217-140 km with temperatures of segregation of 1741 to 1630 ^{o}C. Alkaline and subalkaline basalts yield calculated depths of segregation ranging from ~120-50 km, with segregation temperatures of 1612-1378 ^{o}C. εNd values for all samples indicate derivation from lithosphere, with strongly alkaline basalt series rocks and some Capulin lava having the most positive values (up to 1.53), whereas all of the other series have negative εNd, the most strongly negative being an alkaline basalt with -3.16.

The Jemez Lineament has been shown to coincide with the ancient Proterozoic boundary between the Mazatzal and Yavapai terranes, which have been interpreted as arc

complexes accreted onto the southern margin of the Archean Wyoming Province. The Raton-Clayton magmas inherited their subduction zone characteristics from lithospheric mantle fertilized during these Proterozoic orogenies.

INTRODUCTION

The Raton-Clayton volcanic field (RCVF; 10 to 0.5 Ma) lies on the eastern end of the Jemez Lineament (JL), which is a northeast to southwest line of volcanic centers transecting the generally north-south trending Rio Grande Rift (RGR; Figure 1) (Aubele and Crumpler, 2001; Stormer, 1987; Dungan et al., 1989). Magmatism in this field is clearly rift-related, however, many samples exhibit subduction-like patterns in incompatible trace element diagrams, as do many other non-subduction related igneous rocks of the western United States (Fitton et al., 1988; Davis et al., 1995). In this regard, especially conspicuous is a large composite volcano, Sierra Grande of the RCVF, in what is mostly a bimodal basalt-dacite field. Also of note is the young (<100,000 year old) cinder cone and flow complex of Capulin Mountain.

This project attempts to answer two main questions: what processes were involved in the formation and evolution of the Raton-Clayton magmas, and what is the source for the subduction-like trace element signature in these rift-related volcanic rocks? As subduction ended more than 20 Ma ago, there are only two likely sources for the subduction signature found in the RCVF magmas: assimilation of crustal rocks with this signature by mantle melts, or the melts themselves containing a primary signature due to subduction-related metasomatism of the mantle.

REGIONAL GEOLOGY

Rio Grande Rift

The RGR has been defined in different ways by different workers. Most define it as a continental rift comprised of four basins (the Arkansas, San Luis, Espanola, and Albuquerque) extending from central Colorado to northern Mexico, which forms the eastern boundary of the Basin and Range Province (Figure 1) (Kluth and Schaftenaar, 1994; Gibson et al., 1992; Baldridge, 2004; Baldridge et al., 1995; Chapin and Cather, 1994; Chapin, 1971). Some workers have also included the Trans-Pecos region of southwestern Texas as a southern annex of the RGR (Barker, 1979; Parker and McMillan, 2007).

The basins of the RGR underwent two phases of extension: an initial low angle faulting phase followed by high angle faulting (Baldridge et al., 1991; Kluth and Schaftenaar, 1994). The amount of extension varies with the southern portion of the rift being roughly 2.5 times wider than the northern section (Chapin, 1979).

Seismic studies suggest that the crust has thinned to approximately 30-35 km beneath the southern RGR, while the crust under the Great Plains averages around 50 km thick (Perry et al., 1987; Gibson et al., 1992; Gilbert, 2012). Crustal thinning in the northern section of the RGR is approximately 5 km less than in the southern section (Perry et al., 1987). The crust underlying the RCVF is approximately 44 km thick (Gilbert, 2012). Some previous studies suggested that upwelling has brought asthenospheric material to depths of 35 to 50 km along parts of the rift (Sinno et al., 1986; Perry et al., 1987; Mutschler et al., 1987). The boundary between the asthenosphere and lithosphere appears to be located between 70 and 100 km depth

beneath the RGR and along the flanks (Gibson et al., 1992; Gibson et al., 1993; Yuan and Dueker, 2005), although some workers suggest depths of 200 km or more (CD ROM Working Group, 2002).

Rift volcanism was primarily found along two trends: along the Jemez Lineament (JL) and along the RGR axis (Figure 1) (Mutschler et al., 1987). An early phase of rift development involved eruption of more calc-alkaline intermediate and felsic magmas, though this changed to basaltic and rhyolitic magmas during the second phase (Gibson et al., 1993). One unusual aspect of the RGR is the relatively low amount of volcanic material erupted within the rift when compared to other rifts (Baldridge et al., 1991; Keller and Baldridge, 1999). A second is presence of subduction-like trace element patterns in these rift magmas. Previous workers have noted that highly alkalic magmas are concentrated on the rift flanks and have attributed these magmas to partial melting of metasomatized lithospheric mantle (Perry et al., 1987; Gibson et al., 1993).

Jemez Lineament

The JL is approximately 50 km wide and extends from east central Arizona to northeastern New Mexico, intersecting the RGR near where the San Luis and Espanola basins meet (CD-ROM Working Group, 2002; Yuan and Dueker, 2005; Chapin and Cather, 1994; Gibson et al., 1993). The JL coincides with the boundary between the Proterozoic Mazatzal and Yavapai provinces, which is interpreted to be an ancient suture zone (CD-ROM Working Group, 2002; Yuan and Dueker, 2005; Magnani et al., 2004; Karlstrom and Humphreys, 1998; Shaw and Karlstrom, 1999). Much of Pliocene to recent volcanism in New Mexico is located along this structural feature, rather than the central RGR (Baldridge, 2004).

Raton-Clayton Volcanic Field

Volcanic rocks of the RCVF were originally assigned to three major units: in ascending order, Raton Basalt, Clayton Basalt, and Capulin Basalt (Collins, 1949). Because the region has undergone regional uplift and concurrent erosion, the older Raton basalts typically cap high mesas, such as Raton and Johnson Mesas, whereas the Clayton basalts cap low mesas; the Capulin basalts fill current stream valleys. The Clayton basalts are associated with shield volcanoes such as Mt. Dora and with deeply eroded cinder cones, whereas the Capulin basalts are associated with young cinder cones. Additional volcanic features include the large Sierra Grande composite volcano and scattered dacite domes such as Red Mountain. (Baldwin and Muehlberger, 1959)

Classification

We generally followed the classification scheme of Stormer (1987) and subdivided the samples into a low-K basalt series (other classifications might call these "medium K"), an alkaline basalt series, a strongly alkaline basalt series, a xenocrystic basalt series, a two pyroxene andesite series, and a hornblende dacite series (Figures 2 and 3). The low-K basalt series rocks (basalt to basaltic andesite) contain olivine and occasionally plagioclase and clinopyroxene phenocrysts. The alkaline basalt series (basalt, hawaiite, potassic trachybasalt, mugearite, shoshonite and benmoreite) contains olivine and clinopyroxene phenocrysts, but none contain phenocrystic plagioclase. It contains higher concentrations of K_2O and incompatible trace elements than the low-K series. The xenocrystic basalt series (basalt, basaltic andesite, hawaiite, and mugearite) has olivine and plagioclase phenocrysts and occasionally clinopyroxene. Some large plagioclase grains have partially resorbed, xenocrystic cores and some, partially resorbed

quartz xenocrysts. Not all samples show contamination and the xenocrystic basalt series overlaps the range of the low-K series.

The fourth series is comprised of strongly alkaline basalts (basanites and nephelinites), all of which are strongly nepheline normative. These rocks contain primarily olivine phenocrysts; some also have small amounts of clinopyroxene. One main feature of this series is its general lack of plagioclase, which samples in the other series usually contain as phenocrysts or in the groundmass. The strongly alkaline rocks contain the lowest concentrations of SiO_2 and very high concentrations of incompatible trace elements relative to the other five series.

The two pyroxene andesite and the hornblende dacite series are the most silicic. The andesite series plots near the intersections of fields on the TAS diagram (Figure 2). Rocks of the andesite series contain both clinopyroxene and orthopyroxene phenocrysts with plagioclase only present in the groundmass. These also contain higher concentrations of Ba and Sr than most of the basalts. The dacite series (dacite and low-silica rhyolite) have lower Ba and Sr as well as higher Rb concentrations than the andesites. Dacites contain plagioclase and hornblende phenocrysts with rare clinopyroxene and orthopyroxene.

Ages and Field Relations

The Raton phase began around 10 Ma and continued until about 3.6 Ma, the Clayton phase is from 3.6 to 2 Ma, and finally, the Capulin phase is from 2.0 to 0.04 Ma (Aubele and Crumpler, 2001; Stroud, 1997; Stormer, 1972). Low-K basalt and alkaline basalt series lavas were erupted from the initiation of volcanism (10 Ma) to approximately 2 Ma, which corresponds to the Raton and Clayton phases (Aubele and

Crumpler, 2001). Xenocrystic basalt series lavas are exclusively young (2 - 0.4 Ma; Clayton phase) (Aubele and Crumpler, 2001). Hornblende dacites were erupted from 8 to 4 Ma, which places them in the Raton phase (Aubele and Crumpler, 2001). Stormer (1987) suggested a younger age for these lavas, placing them in the Clayton phase. The eruption of two pyroxene andesite from Sierra Grande occurred around the beginning of the Clayton phase (4 to 2 Ma; Aubele and Crumpler, 2001). The strongly alkaline basalt series was erupted from the late Clayton phase through the Capulin phase (Stormer, 1987; Aubele and Crumpler, 2001).

METHODOLOGY

Samples were collected from various points around the RCVF from public access land and from private property with permission from the land owners. We attempted to collect samples from as many different types and ages of lavas as possible. Hand specimen and thin section analysis of 48 of these samples were conducted to help select quality samples for microprobe and geochemical analysis. Microprobe analyses of eight polished sections (259 spot analyses total) were conducted at the University of Texas El Paso using a CAMECA SX-50 electron microprobe under standard analytical conditions (see extended discussion in White et al., 2005).

Geochemical analysis of all 48 samples were conducted by wavelength dispersive-XRF at Baylor University using a Rigaku Primus II WDS unit. All geochemical samples were initially crushed on a stainless steel plate and were then powdered in a pre-contaminated SPEX tungsten-carbide shatter box. A portion of the sample was mixed with powdered Bakelite in a 6:1 ratio and then pressed into a pellet for

analysis by WD-XRF. Splits of 22 samples were sent to Activation Laboratories Ltd. (Ancaster, Ontario, Canada) for major and trace element analysis using fusion ICP and ICP-MS. We combined our data with analyses from Dungan et al. (1989) and Phelps et al. (1983). XRF analyses at Baylor compare favorably with the ICP analyses from Activation Labs (see discussion in White et al., 2003).

We selected six samples for Nd isotopic analysis, also conducted by Activation Laboratories. This involved dissolution of the sample, separation of the rare-earth elements through cation exchange, and separation of Sm and Nd through extraction chromatography. Our study also incorporates published analyses from Dungan et al. (1989), Phelps et al. (1983), and Jones et al. (1974).

PETROGRAPHY

Selected electron microprobe analyses of phenocrysts from samples of all six lava types are presented in Tables 1 and 2. Plagioclase (An_{48-34}) from the low-K basalt series has rims of ternary feldspar (Figure 4). Both clinopyroxene and orthopyroxene are sometimes present with clinopyroxene being the more abundant (Figure 5; Table 2). Phenocrysts (olivine, magnetite, and rare clinopyroxene) are uncommon in both the alkaline and strongly alkaline basalt series. The groundmass of the alkaline series is comprised of plagioclase, opaques, and clinopyroxene. The strongly alkaline series contains no plagioclase, even in the groundmass.

Feldspar cores from the xenocrystic basalt series yield an average composition of $An_{29.4}$ $Ab_{63.4}$ $Or_{7.2}$, with rim compositions averaging $An_{56.0}$ $Ab_{41.2}$ $Or_{2.8}$ (Figure 4; Table 1). This reverse zoning might also be the result of contamination, as also evinced by

xenocrystic quartz. This contamination was noted by previous workers (Dungan et al., 1989; Stormer, 1987). Some orthopyroxene grains in the two pyroxene andesite series contain green to brown pleochroic cores with a clear orthopyroxene overgrowth. The core compositions are generally less magnesian than their rims ($En_{71.4}$ $Fs_{27.0}$ $Wo_{1.6}$ and $En_{82.1}$ $Fs_{15.2}$ $Wo_{2.7}$, respectively) (Figure 5; Table 2). The hornblende dacite series contains feldspars ranging from Ab_{57} to Ab_{68}.

Two-pyroxene geothermometry (after Anderson et al., 1995) suggests temperature ranges of 1068 to 885 ± 125°C from Sierra Grande latite (sample 070713) and 985 to 952 ± 28°C from Red Mountain dacite (sample 070715). Sample 080515, a low-K basaltic andesite, also contains two pyroxenes and yields temperatures around 1020 ± 307°C.

WHOLE ROCK GEOCHEMISTRY

Representative chemical analyses of RCVF rocks are given in Table 3. As discussed above, we assigned rocks to six series based on petrographic and geochemical characteristics rather than age. Basaltic rocks are generally nepheline normative, except that the strongly alkaline series is more strongly nepheline normative. Basaltic rocks become hypersthene normative as silica increases in the series and, for a few, especially in the xenocrystic series, quartz normative. The strongly alkaline series is highly nepheline normative and many have normative leucite as well. The andesite and dacite series are the only two that are entirely quartz normative.

Harker plots of oxides versus silica (Figure 6) show depletion trends for all series in CaO, MgO, MnO, and P_2O_5. FeO appears to show a double depletion trend, with the strongly alkaline series forming a separate trend from the other five series. The strongly

alkaline series shows increasing trends in Al_2O_3 and TiO_2. K_2O shows increasing trends for all series except the strongly alkaline series. Finally, the dacite series shows decreasing trends for Na_2O and Al_2O_3.

Samples from the RCVF show typical subduction signature (Davidson, 1996; Davidson et al., 1997). Large Ion Lithophile Element (LILEs; e.g. Rb, Ba, K, Sr) concentrations are significantly higher than concentrations of High Field Strength Elements (HFSEs; e.g. Nb, Zr, Ti, Hf) and Rare Earth Elements (REEs; La to Lu). Two samples from the xenocrystic basalt series exhibit a distinct Th peak, which may be the result of zircon xenocrysts that contaminated those samples. Rare-Earth Element (REE) plots (Figure 8) show nearly identical patterns for all six general lava types found in the RCVF. All show significant enrichment in light REEs relative to the heavy REEs and all exhibit a break in their slope at Sm. The strongly alkaline basalts contain higher concentrations of the REE and other incompatible elements than samples of the other series.

The K/Rb versus Rb plot appears to show separate trends for most of the series, except that the hornblende dacite plots seem to extend the two pyroxene andesite trend (Figure 9). The xenocrystic basalt series appears to form a trend with a constant K/Rb. As pure fractional crystallization of the observed phenocrysts will keep the K/Rb ratio the same, the xenocrystic basalt series may form a fractionation sequence. The other series show curved depletion trends of K/Rb vs Rb. This suggests some degree of assimilation of crustal material with low K/Rb and high Rb (Davidson et al., 1987). Assimilation of such crustal material would create a curved trend towards an assimilant composition, although some fractionation might accompany it in an assimilation-fractional

crystallization process. The wide dispersal of the six magma series and small volume of each precludes detailed modeling, as each occurrence is most likely the surficial expression of disparate magma systems that were distinct, although some may have evolved along parallel paths.

A Ba/La versus Nb/La ratio plot can be used to distinguish three mantle sources (Ocean Island Basalt Asthenospheric mantle, Subduction modified lithospheric mantle, Ocean Island Basalt modified lithospheric mantle) for basalts (Figure 10). All basalt compositions plot within the subduction-modified lithospheric mantle field, except for one low-K basalt. The timing of this subduction modification of the mantle is unknown, but previous work in the Eocene Two Buttes minette complex of Colorado suggests this modification occurred due to Proterozoic arc magmatism (Davis et al., 1996).

Possible Ancestral Magmas

We estimated ancestral magmas for primitive basalts in the RCVF through the incremental addition of equilibrium olivine to analyses until they reached equilibrium with mantle peridotite. We utilized the method of Parker et al. (2010), who followed the method of Leeman et al. (2009). Samples were selected using the following criteria: $SiO_2 \leq 52$ wt. %, MgO ≥ 6 wt. %, and Mg number ≥ 54. The calculated parental magma compositions were used to calculate pressure of magmatic segregation (Albarede, 1992) and temperature of magmatic segregation (Sugawara, 2000) (Table 7). The depth calculations were done assuming a crustal thickness of 44 km (Gilbert, 2012), crustal density of 2.85 g/cm^3, and mantle density of 3.15 g/cm^3.

Several trends become apparent from the results of these calculations. First, the strongly alkaline basalt series samples seem to have formed at great depths (217-140 km)

and high temperatures of segregation (1743-1630 ^{o}C) (Table 4; Figure 11). The alkaline basalt series samples generally fall at the other end of the spectrum with shallower depths (86-49 km) and lower temperatures of segregation (1535-1378 ^{o}C). The low-K series calculations yielded depths estimates ranging from 121-52 km, overlapping that of the alkaline series.

Isotope Geochemistry

Calculated εNd values for six samples are reported in Table 5. These data were combined with other published data to calculate the Neodymium Crustal Index (DePaolo et al., 1992; Phelps et al., 1983), which indicates the percent of the samples Nd derived from crustal sources. The strongly alkaline series has the most positive εNd values (four samples, 1 to 1.55) with one xenocrystic alkalic basalt being the only other positive value (1.39). The alkaline basalt and low-K basalt series both have low negative εNd (respectively, -3.16 and -1.78). The two pyroxene andesite and hornblende dacite series both have low negative εNd as well (respectively, -2.86 and -1.24). Published Sr isotopic initial ratios for RCVF basaltic rocks generally range from 0.7028 to 0.7040, although a few contaminated samples ranged up to 0.7083 (Jones et al., 1974). The Nd isotopic compositions place the RCVF lavas along the mantle array in and around the "Bulk Silicate Earth" field. Sr isotopic data are more widely dispersed.

Neodymium Crustal Index (NCI) calculations were conducted to estimate the amount of mantle and crustal contributions to the various magma compositions using the equation of DePaolo et al. (1992):

$$NCI = (\varepsilon Nd \text{ sample} - \varepsilon Nd \text{ mantle}) / (\varepsilon Nd \text{ crust} - \varepsilon Nd \text{ mantle})$$

Assuming εNd values of -14 for lower crustal material and +2 for lithospheric mantle, calculations resulted in NCI values ranging from 3 to 32% crustal contribution (Table 8). Asthenospheric mantle (εNd value of +5) with the same crust yields NCI values of 18 to 43% crustal contribution. If we assume that all RCVF magmas were formed from lithospheric mantle with εNd equal to the feldspathoidal basalt εNd (1.55), then the calculation yields values of 0 to 30% crustal contribution depending upon the rock type.

CONCLUSIONS

The six series of the Raton-Clayton volcanic field show anomalous geochemistry suggestive of subduction zone magmatism. This subduction signature resulted from melting of lithospheric mantle previously fertilized during the Proterozoic formation of the underlying Mazatal and Yavapai terranes. This lithospheric origin for the basaltic magmas of the six series is confirmed by trace element study and by εNd values close to bulk silicate earth. Strongly alkaline basaltic magmas originated at greater depths and higher temperatures in the lithosphere than less alkaline basalts.

Magmas within series evolved through open-system processes involving assimilation and fractional crystallization. The six series are geochemically separate and occur within widely separated lavas and intrusions, making modeling within series difficult as the composition of possible crustal assimilants is not known and many of the occurrences appear to be surficial expressions of smaller magma systems that evolved separately as small magma batches.

Acknowledgements

We would like to thank the Department of Geology at Baylor University for their support. We also would like to thank the many land owners who graciously granted us permission to collect samples from their property and the National Park Service for their permission to collect samples from Capulin Volcano National Monument.

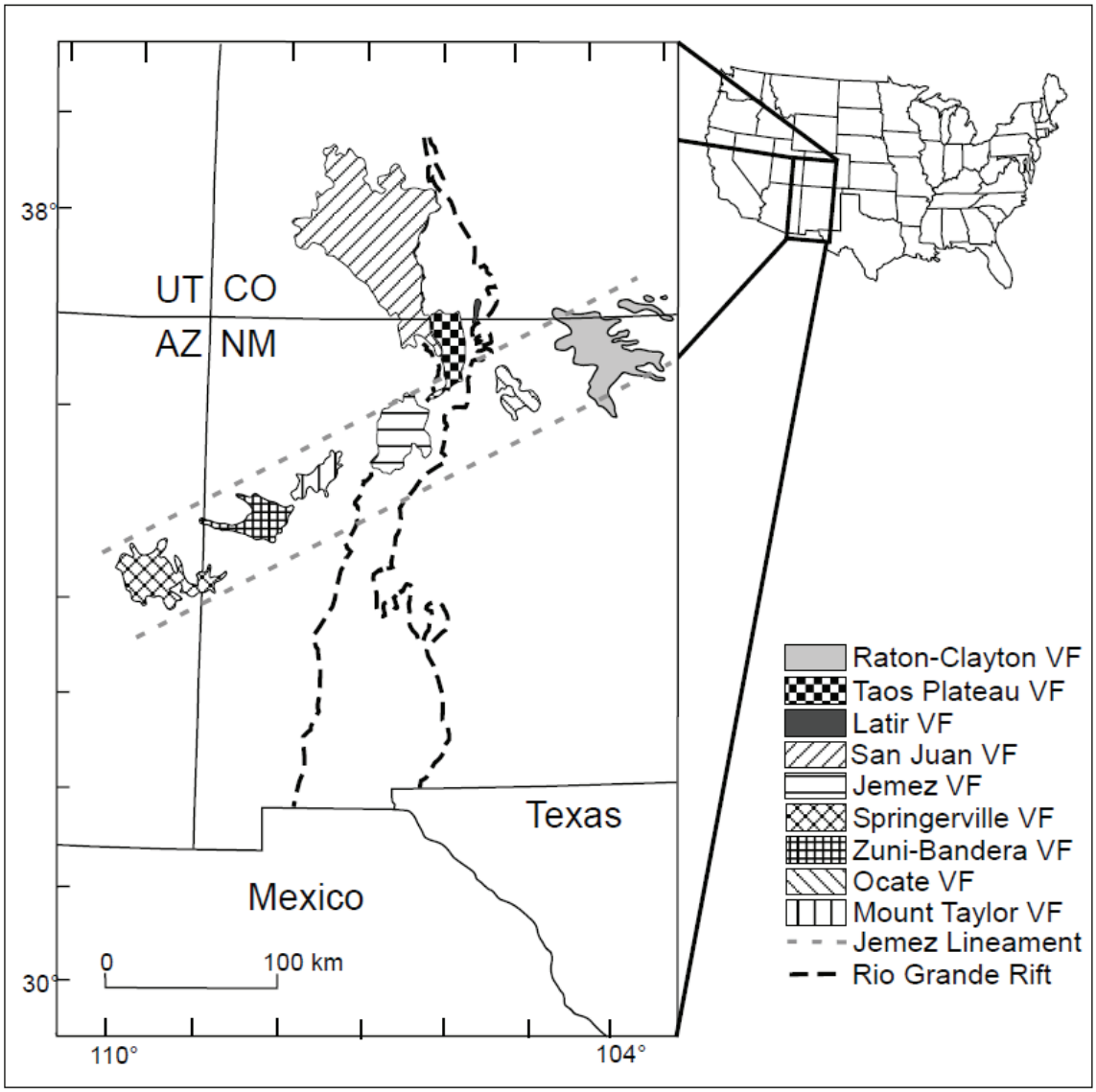

Figure 4.1. Location map showing the RCVF and other volcanic fields (VF) in relation to the Jemez Lineament and the Rio Grande Rift (modified from Baldridge, 2004 and Chapin et al., 2004).

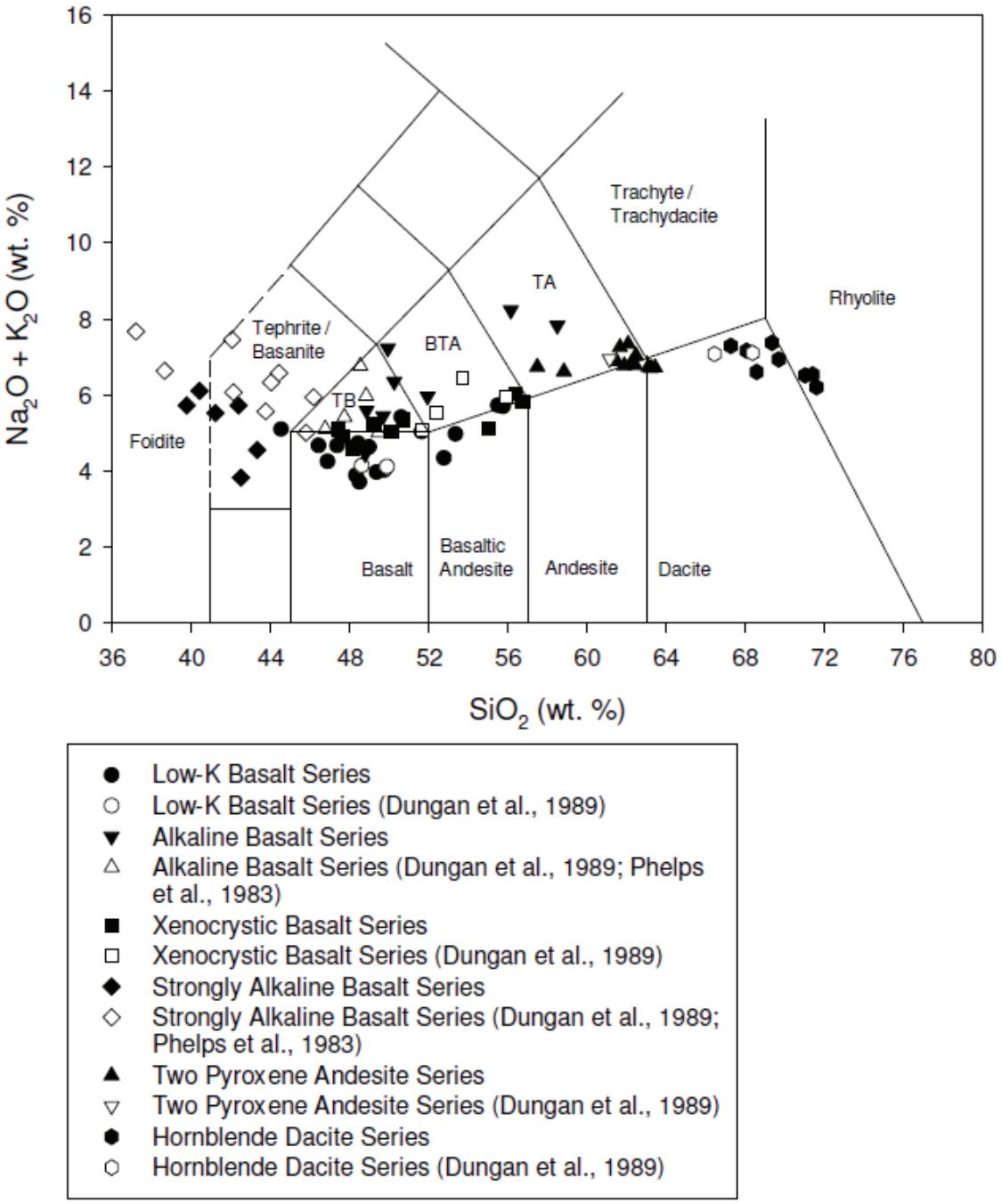

Figure 4.2. Total Alkalis versus Silica diagram (Le Bas et al., 1986) showing analyses of the six general magma series of this report for the RCVF (additional analyses from Dungan et al., 1989 and Phelps et al., 1983). TB stands for Trachybasalt, BTA for Basaltic Trachyandesite, and TA for Trachyandesite.

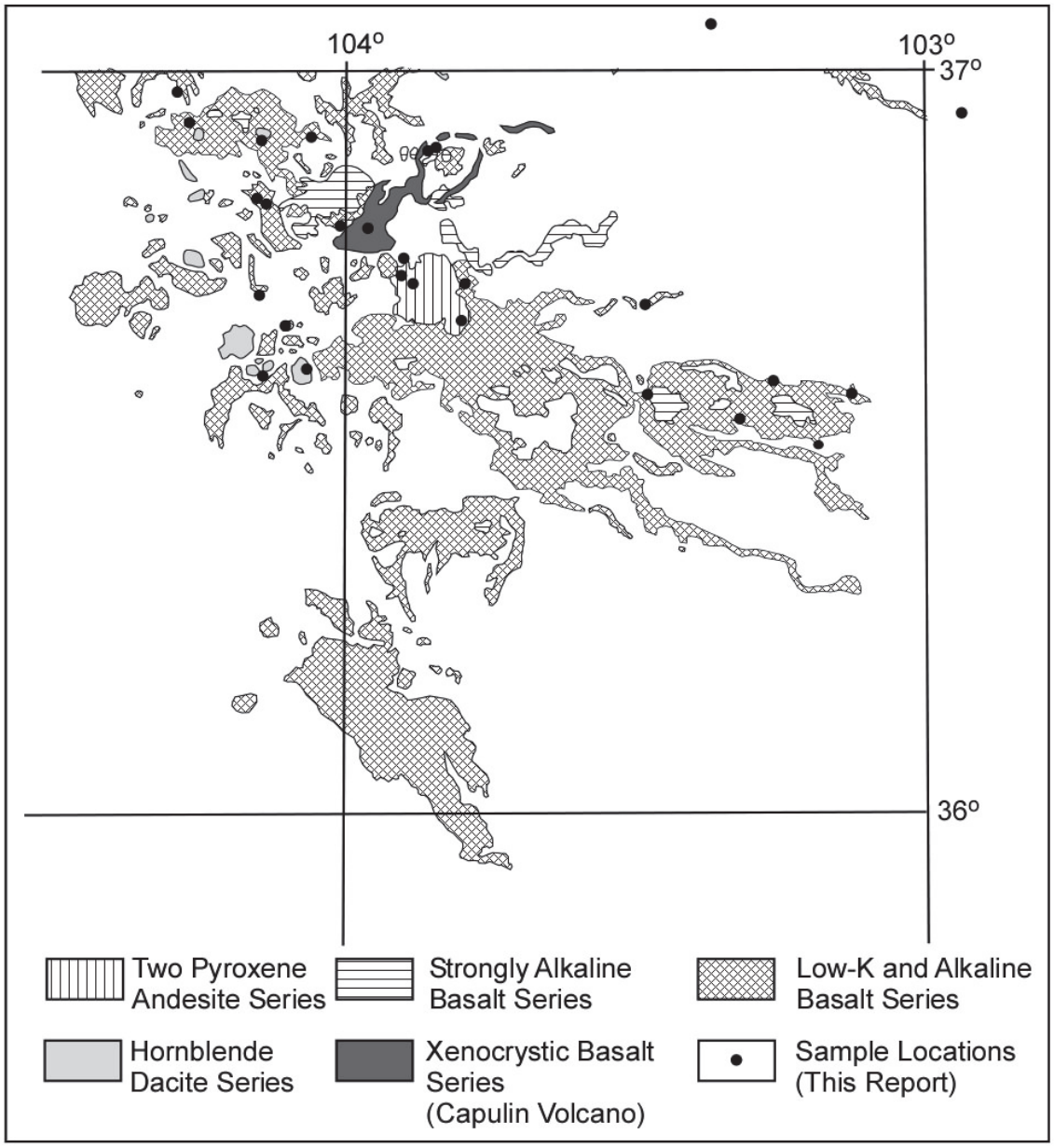

Figure 4.3. Distribution of lava types and sampling locations in the Raton-Clayton Volcanic Field (modified from Luedke and Smith, 1978).

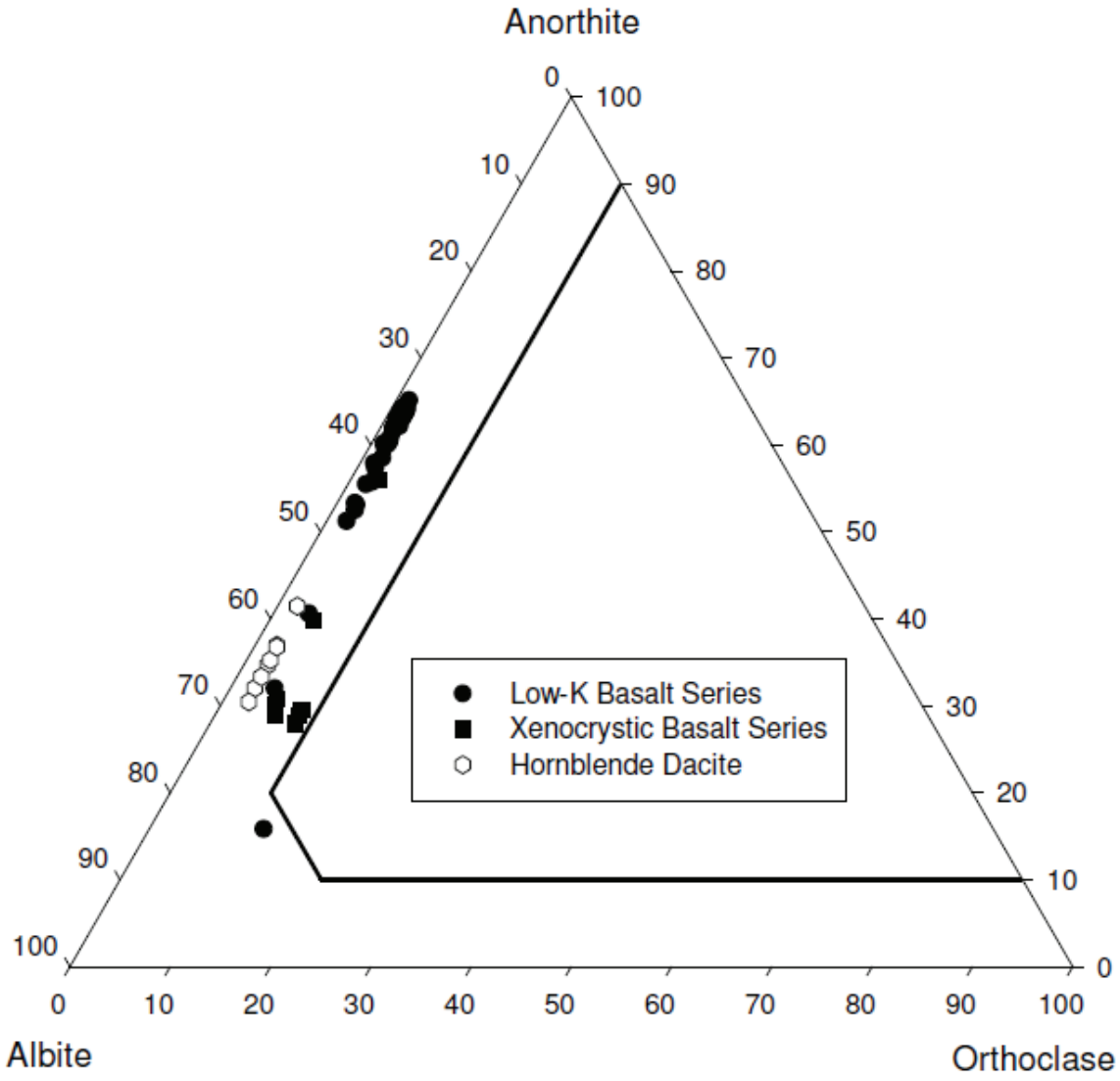

Figure 4.4. Feldspar composition ternary showing compositions of feldspar phenocrysts and xenocrysts from three of the six general lava compositions found in the RCVF.

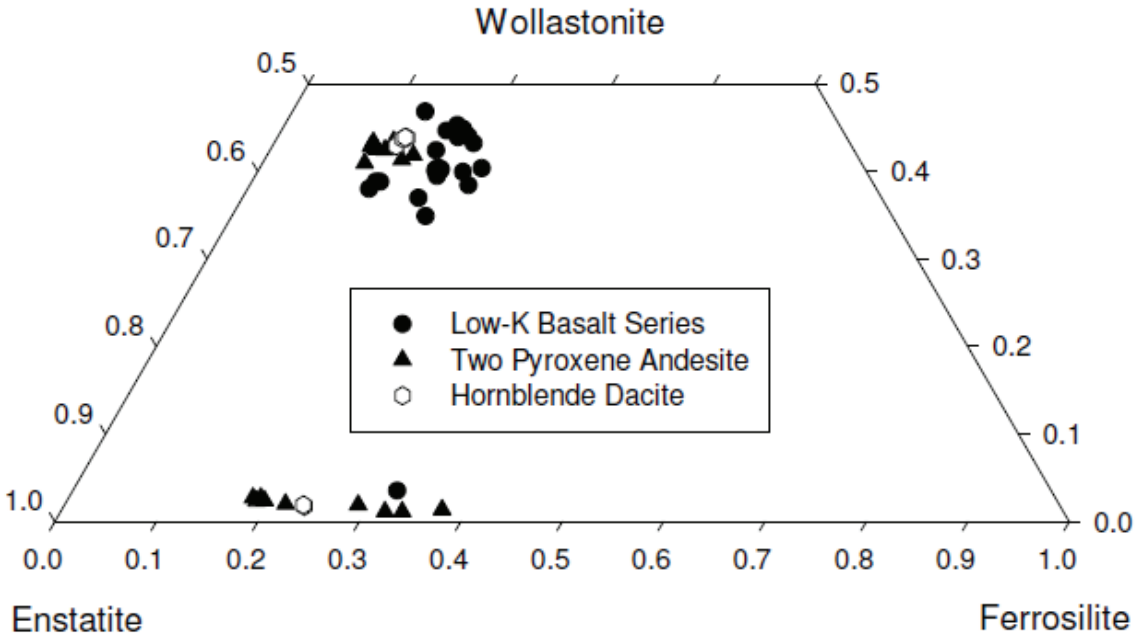

Figure 4.5. Pyroxene quadrangle showing analyses of crystals from three of the six general lava types found in the RCVF.

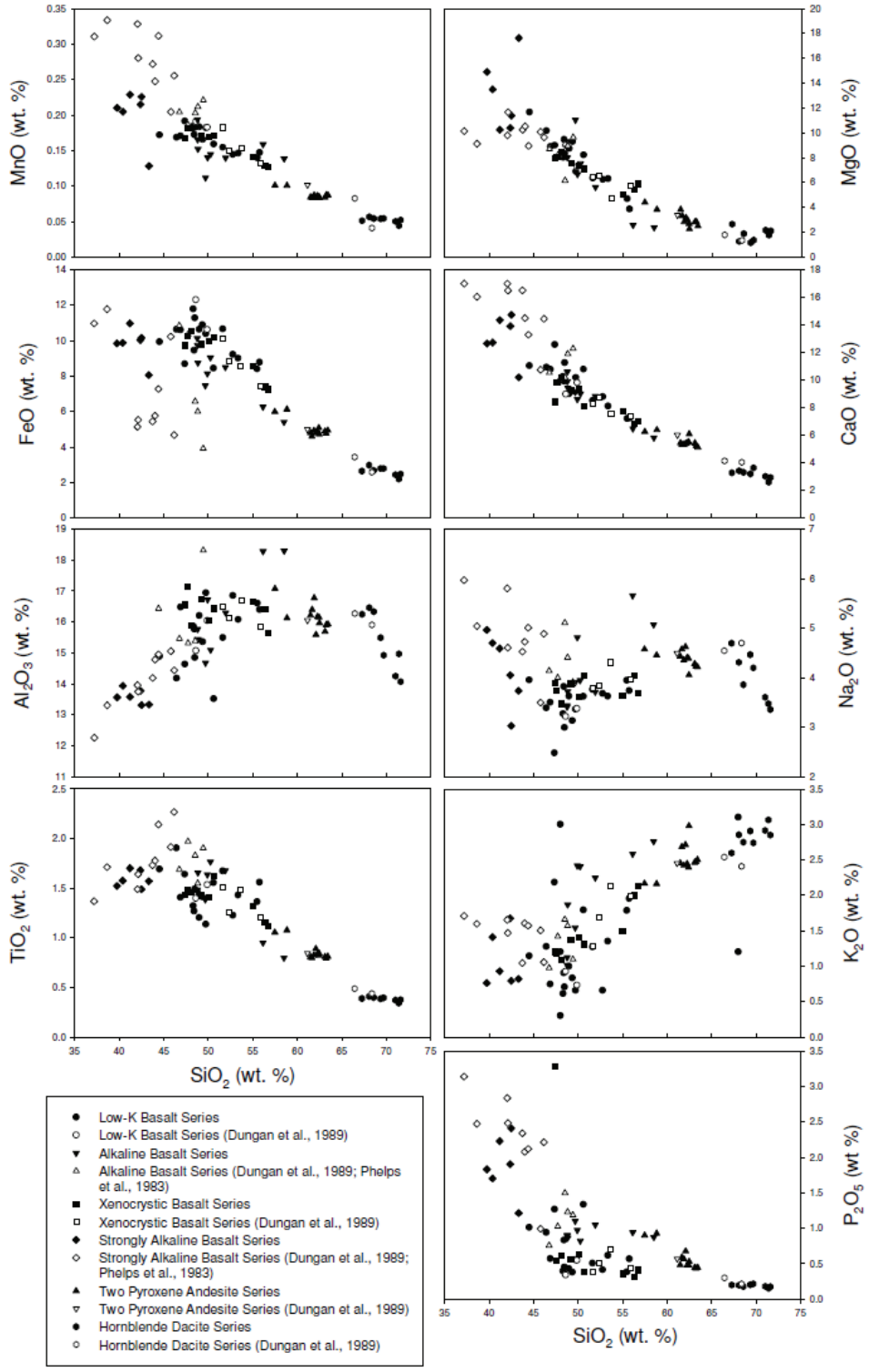

Figure 4.6. Major element Harker plots of analyses from the six general lava types found in the RCVF (includes analyses from Dungan et al., 1989 and Phelps et al., 1983).

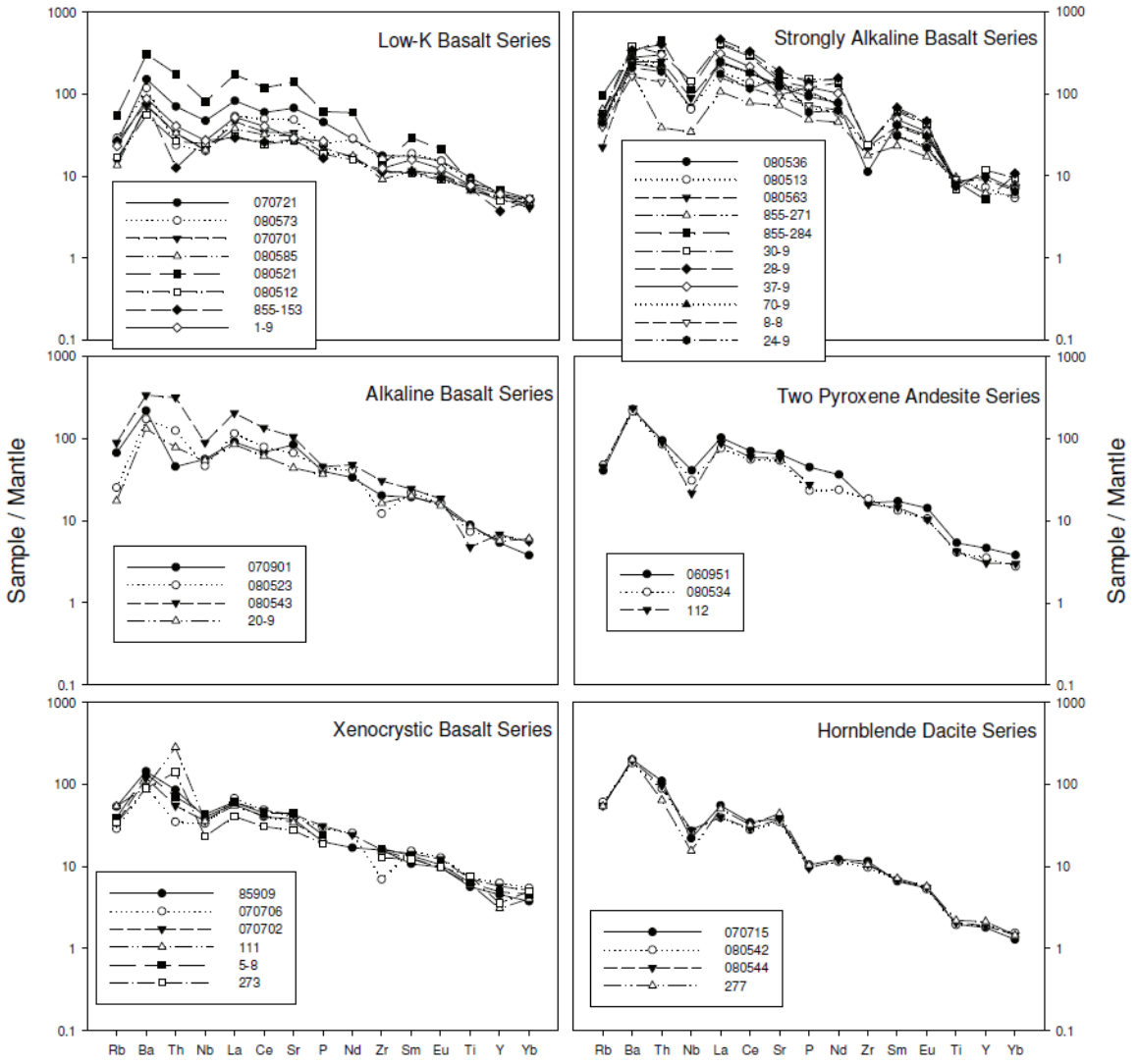

Figure 4.7. Mantle normalized variation diagram (McDonough and Sun, 1995) of analyses from each of the six general lava types from the RCVF (includes analyses from Dungan et al., 1989 and Phelps et al., 1983). Most samples exhibit subduction signatures (Ba peaks and Nb troughs), but the strongly alkaline basalts have significantly higher concentrations of these incompatible elements. The black samples are from the Low-K Basalt series, red are Alkaline Basalt series, green is the Xenocrystic Basalt series, yellow is the Strongly Alkaline Basalt series, blue represents Two Pyroxene Andesite series samples, and pink is the Hornblende Dacite series.

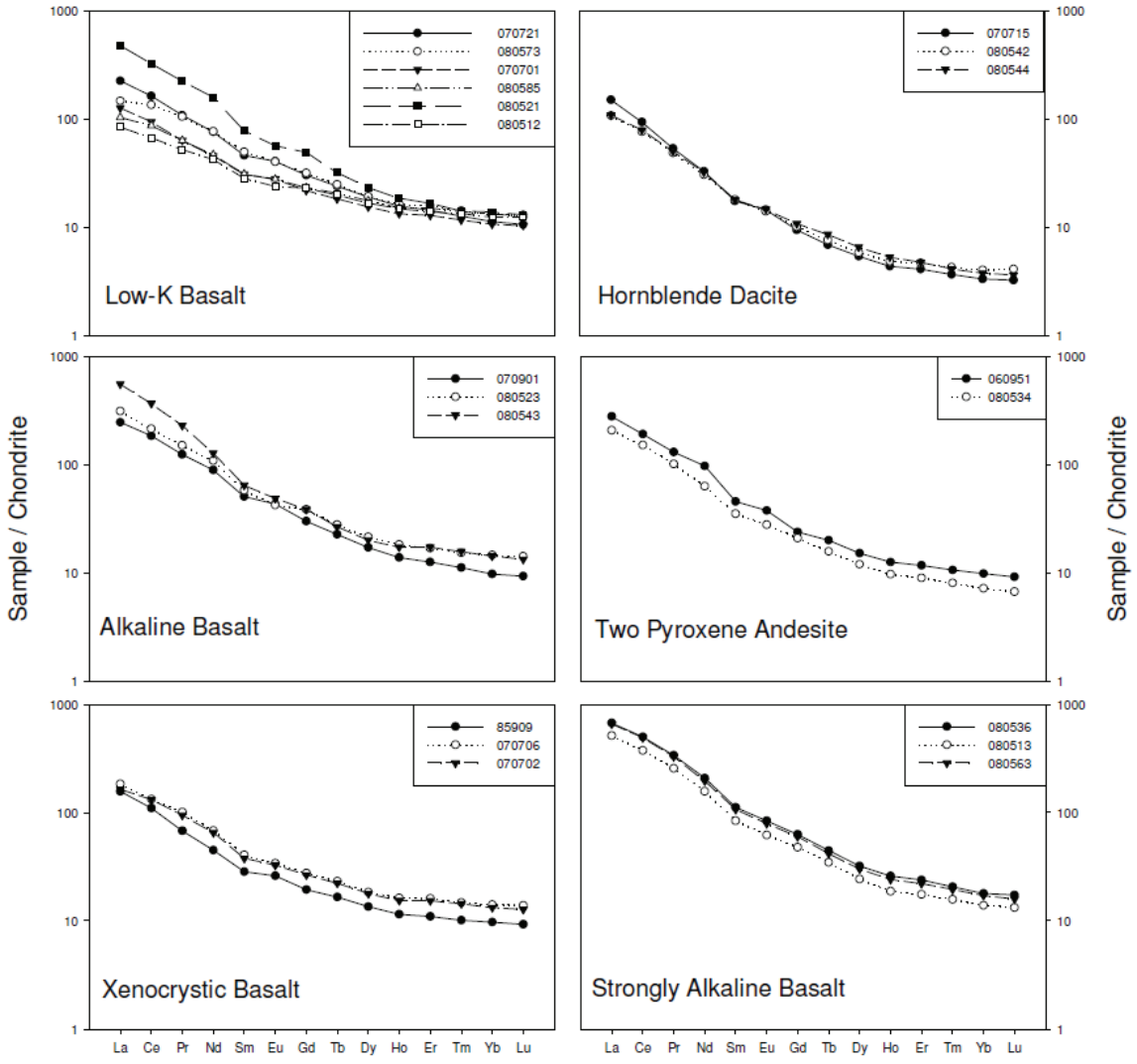

Figure 4.8. REE diagrams for the six general types of lavas found in the RCVF. Analyses are normalized to chondrite according to Wakita et al. (1971). All analyses show significant enrichment in the LREEs versus the HREEs.

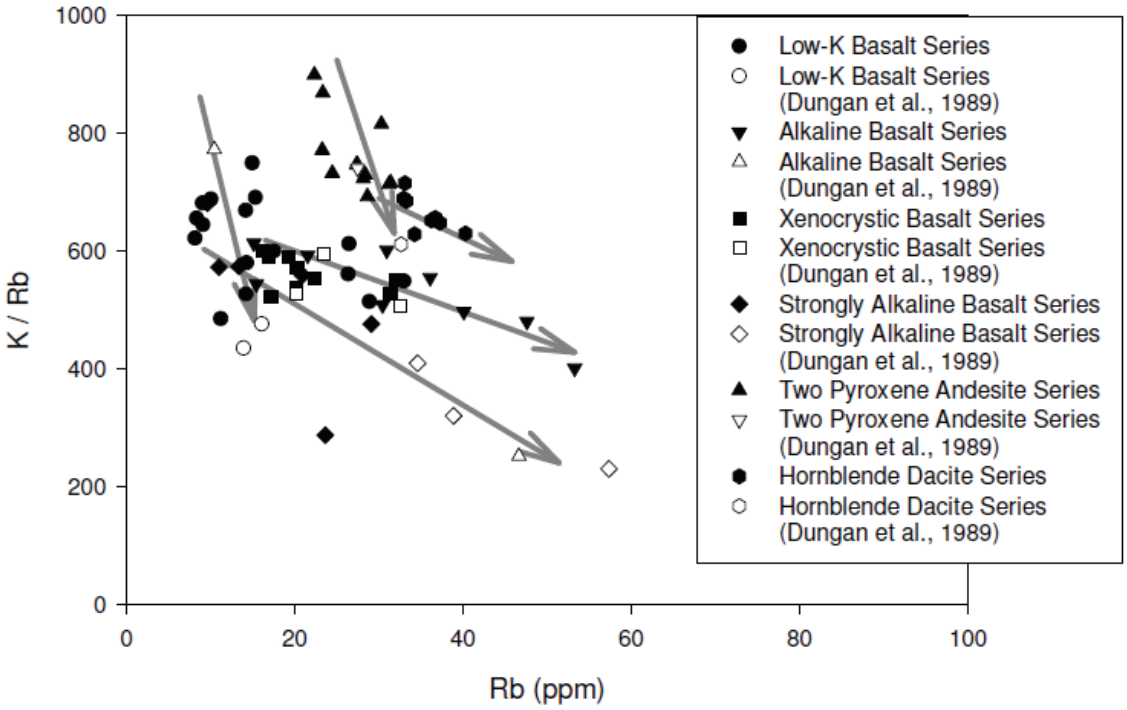

Figure 4.9. K/Rb vs Rb plot showing samples of the six general types of lavas present in the RCVF (additional analyses from Dungan et al., 1989). Arrows show general trends for each series.

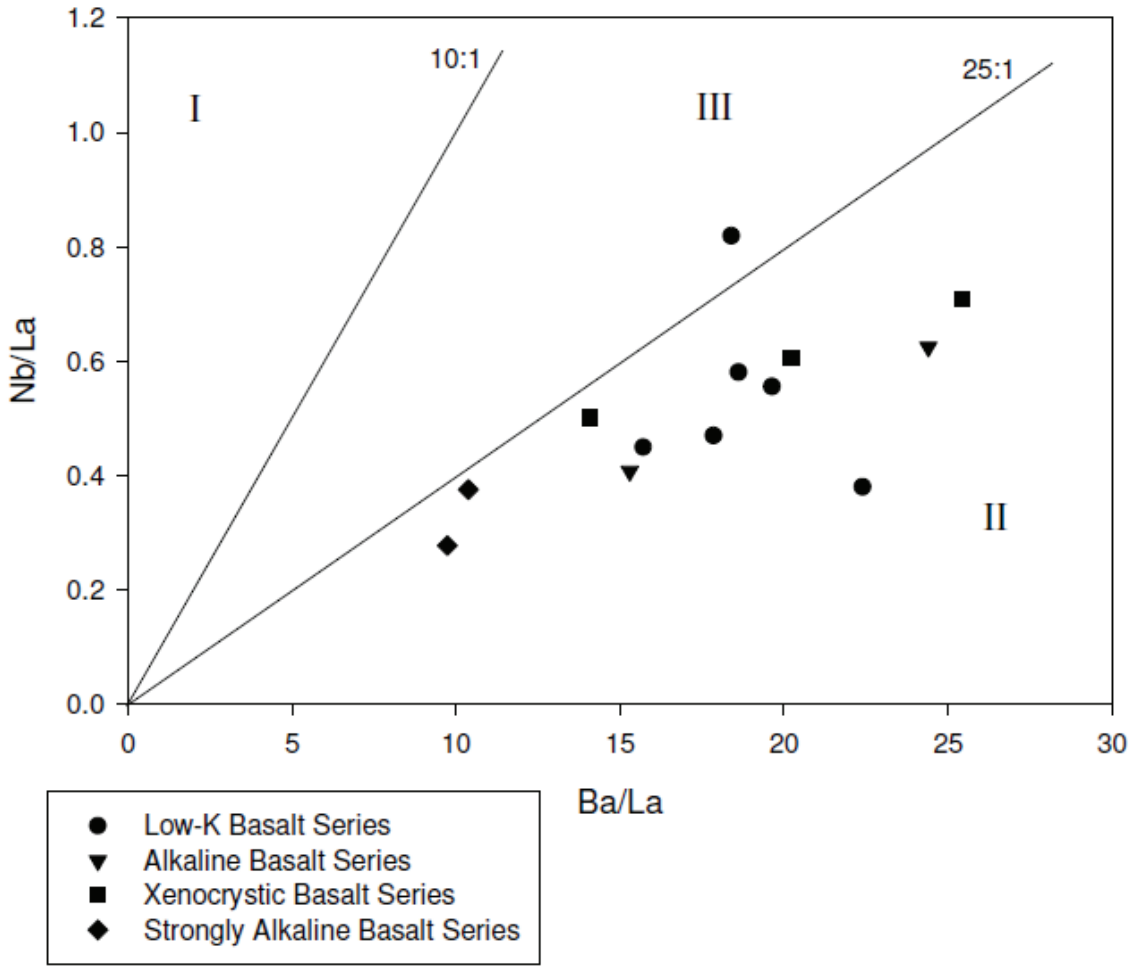

Figure 4.10. Ba/La vs. Nb/La diagram. The RCVF volcanic rocks fall primarily in the Type II field of Menzies et al. (1991), but one sample does clearly fall into the Type III field. Type I field represents OIB asthenospheric mantle, Type II represents subduction-modified continental lithosphere, and Type III represents OIB-modified continental lithosphere.

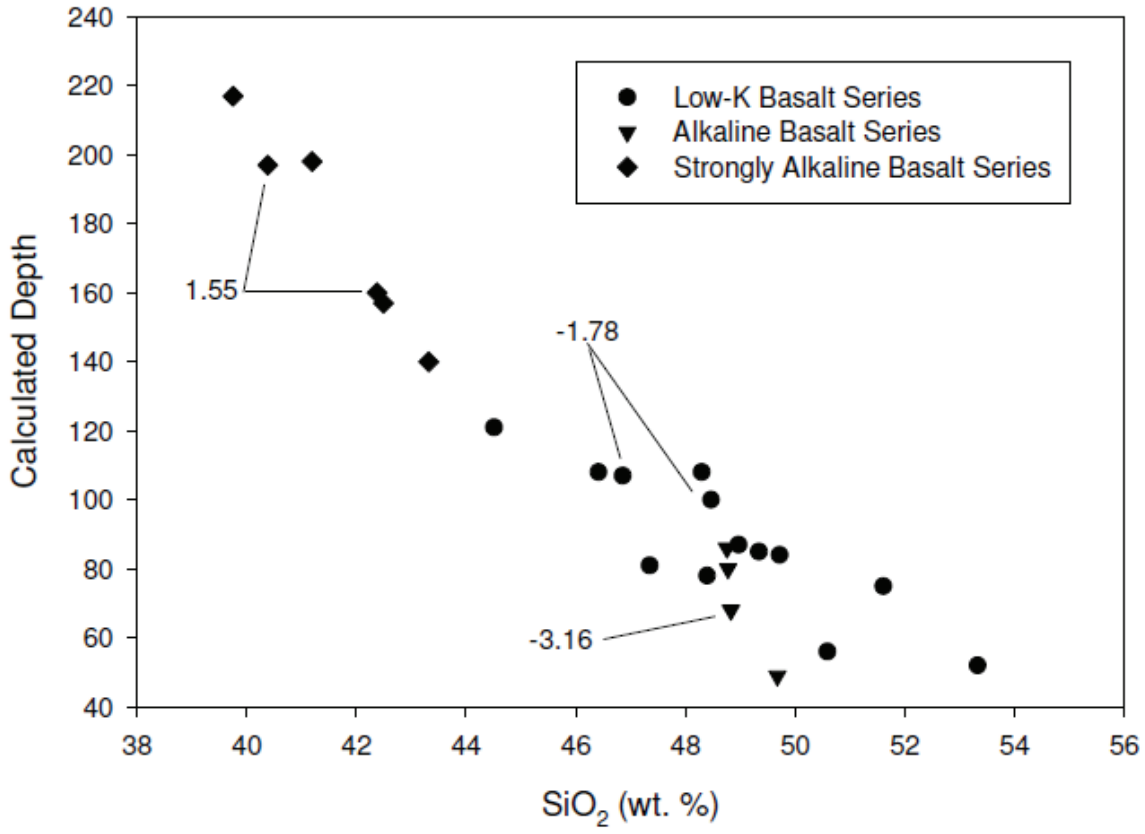

Figure 4.11. Calculated depth vs. SiO_2 plot for basalts. εNd values for analyzed samples are indicated.

Table 4.1. Selected electron microprobe analyses of plagioclase crystals from RCVF lavas.

	Low-K 070701CB				080522CB					080515CAP				
	Core	Core	Rim	Rim										
SiO_2	52.06	52.03	59.00	62.92	51.43	53.17	57.39	62.72	65.33	55.18	54.51	53.26	52.49	52.01
TiO_2	0.05	0.03	0.09	0.09	0.00	0.04	0.01	0.08	0.07	0.06	0.09	0.09	0.19	0.06
Al_2O_3	30.03	30.52	25.15	22.19	30.17	28.77	26.01	21.92	19.82	28.02	28.18	29.23	29.82	30.39
FeO	0.66	0.58	0.69	0.66	0.78	1.12	0.59	0.41	0.54	0.58	0.57	0.55	0.49	0.49
CaO	12.76	12.82	6.56	3.19	12.98	11.84	8.30	3.15	1.01	10.56	11.05	11.87	12.76	13.41
Na_2O	4.08	4.06	7.20	8.09	4.00	4.67	6.31	7.84	7.56	5.33	5.15	4.61	4.16	3.82
K_2O	0.21	0.22	0.76	1.93	0.28	0.31	0.60	2.77	5.18	0.34	0.30	0.23	0.22	0.21
Total	99.88	100.26	99.45	99.15	99.72	100.00	99.20	98.86	99.45	100.35	100.12	100.18	100.51	100.78
An	62.58	62.76	31.99	15.84	63.17	57.33	40.63	15.28	4.86	51.25	53.33	57.93	62.11	65.16
Ab	36.19	35.97	63.60	72.76	35.20	40.90	55.87	68.71	65.58	46.80	44.96	40.73	36.63	33.62
Or	1.24	1.28	4.41	11.40	1.63	1.77	3.50	16.00	29.56	1.95	1.72	1.35	1.26	1.21

	Xenocrystic 070705CAP				85909				Hornblende Dacite 070715			
	Core	Core	Rim	Rim	Core	Core	Rim	Rim	Core	Core	Rim	Rim
SiO_2	52.20	52.15	51.60	52.59	59.67	60.45	52.53	57.32	57.76	58.62	58.51	59.45
TiO_2	0.05	0.03	0.03	0.06	0.00	0.03	0.06	0.00	0.00	0.00	0.00	0.00
Al_2O_3	30.12	29.86	30.34	29.36	23.81	23.74	28.50	25.90	26.72	25.13	25.37	25.42
FeO	0.70	0.81	0.82	1.04	0.14	0.29	0.55	0.10	0.36	0.06	0.05	0.18
CaO	12.85	12.69	13.17	11.92	5.59	5.72	11.16	7.93	8.47	6.38	7.04	6.78
Na_2O	4.04	4.12	3.92	4.46	7.02	6.89	4.54	6.13	6.38	7.22	6.88	7.21
K_2O	0.24	0.21	0.21	0.32	1.42	1.40	0.47	0.73	0.33	0.40	0.39	0.41
Total	100.22	99.89	100.15	99.76	97.66	98.58	97.80	98.10	100.02	97.81	98.24	99.45
An	62.83	62.21	64.21	58.53	27.95	28.80	56.01	39.87	41.49	32.02	35.28	33.37
Ab	35.76	36.55	34.58	39.60	63.57	62.81	41.20	55.78	56.61	65.59	62.39	64.25
Or	1.41	1.24	1.21	1.87	8.48	8.39	2.78	4.35	1.90	2.39	2.33	2.39

Table 4.2. Selected electron microprobe analyses of mafic minerals from RCVF lavas.

	Olivine Low-K 070721		070701		Xenocrystic 85909		Alkaline 070714	
	Core	Rim	Core	Rim	Core	Rim	Core	Rim
SiO_2	39.72	37.70	39.16	35.71	39.15	36.11	39.01	38.79
TiO_2	0.00	0.00	0.00	0.07	0.01	0.10	0.01	0.08
Al_2O_3	0.04	0.05	0.04	0.07	0.04	0.04	0.03	0.02
FeO	15.41	24.33	16.14	34.02	16.23	29.50	16.41	18.23
MnO	0.19	0.59	0.25	0.68	0.24	0.49	0.36	0.59
MgO	45.37	37.52	44.47	28.64	43.93	33.16	43.82	42.06
CaO	0.19	0.37	0.19	0.39	0.24	0.28	0.15	0.25
Total	101.11	100.68	100.53	99.75	100.07	99.90	100.24	100.23
Fo	83.62	72.48	82.66	59.19	82.36	66.07	82.15	79.66
Fa	16.13	27.00	17.09	40.23	17.32	33.53	17.64	20.01
La	0.25	0.52	0.26	0.58	0.32	0.40	0.20	0.33

	Opaques Dacite 070715		Low-K 070721		Alkaline 070714		Xenocrystic 85909	
			Core	Rim	Core	Core	Core	Rim
SiO_2	0.00	0.00	0.00	0.00	0.00	0.00	0.00	0.28
TiO2	26.52	5.09	1.38	11.10	12.04	11.49	0.59	0.55
Al_2O_3	0.69	3.00	32.19	7.97	2.52	2.76	44.59	44.09
Cr_2O_3	0.17	0.13	20.74	7.40	1.25	1.35	13.83	12.86
FeO	65.26	84.45	34.52	63.48	74.70	74.68	24.33	21.12
MnO	0.21	0.63	0.48	0.69	0.74	0.79	0.28	0.20
MgO	0.95	1.15	10.20	5.05	4.44	4.77	14.71	15.41
NiO	0.02	0.13	0.17	0.15	0.37	0.38	0.30	0.29
CaO	0.05	0.06	0.03	0.05	0.09	0.09	0.03	0.04
Na_2O	0.02	0.02	0.01	0.00	0.00	0.00	0.01	0.00
K_2O	0.05	0.04	0.02	0.06	0.05	0.04	0.02	0.04
Total	93.92	94.71	99.75	95.96	96.20	96.35	98.70	94.89

Table 4.2. Continued.

	Clinopyroxene Andesite 070713		Dacite 070715		Low-K 070721	070701	
	Core	Rim	Core	Rim		Core	Rim
SiO_2	52.33	51.58	50.79	50.59	48.10	50.41	50.57
TiO2	0.35	0.52	0.27	0.35	1.60	1.15	1.15
Al_2O_3	1.97	2.71	2.80	3.06	4.71	1.87	1.93
Cr_2O_3	0.39	0.08	0.09	0.05	0.05	0.07	0.05
FeO	6.10	7.15	7.17	7.57	7.73	11.00	10.84
MnO	0.18	0.11	0.17	0.13	0.17	0.28	0.32
MgO	17.01	16.54	15.14	14.79	13.44	14.21	13.94
CaO	21.37	21.12	20.11	20.75	21.82	20.45	20.16
Na_2O	0.40	0.32	0.54	0.63	0.50	0.40	0.41
K_2O	0.00	0.00	0.04	0.02	0.03	0.01	0.01
Total	100.10	100.15	97.14	97.95	98.15	99.85	99.38
Wo	42.82	42.44	42.89	43.87	46.79	41.77	41.81
En	47.43	46.25	44.93	43.51	40.09	40.40	40.24
Fs	9.74	11.31	12.17	12.62	13.12	17.84	17.95

	Orthopyroxene Andesite 070713				Dacite 070715		Low-K 080515
	Core	Core	Rim	Rim	Rim	Core	
SiO_2	53.14	50.30	54.46	54.01	53.30	52.79	51.65
TiO2	0.11	0.04	0.17	0.11	0.08	0.09	0.44
Al_2O_3	1.88	4.47	1.20	1.68	1.79	1.94	2.40
Cr_2O_3	0.11	0.00	0.12	0.15	0.00	0.03	0.02
FeO	14.13	20.24	12.27	12.85	15.43	15.53	20.57
MnO	0.28	0.43	0.25	0.23	0.33	0.28	0.53
MgO	28.18	24.00	30.37	29.30	27.63	27.81	23.64
CaO	1.04	0.58	1.46	1.28	0.91	0.99	1.80
Na_2O	0.02	0.03	0.03	0.04	0.02	0.03	0.06
K_2O	0.00	0.00	0.00	0.00	0.01	0.00	0.02
Total	98.90	100.09	100.40	99.64	99.49	99.49	101.20
Wo	2.02	1.17	2.74	2.45	1.76	1.90	3.52
En	76.25	66.86	79.11	78.11	74.54	74.54	64.49
Fs	21.74	31.97	18.16	19.44	23.70	23.56	31.99

Table 4.3. Selected geochemical analyses of rocks from each of the six general lava compositions found in the RCVF.

	Low-K Basalt Series												
	070721	070721	**080573**	080573	080546	**070701**	070701	**080585**	080585	080522	080562	080582	**080512**
SiO_2	**46.42**	44.51	**51.61**	53.33	55.74	**48.47**	46.86	**48.30**	49.72	48.97	52.75	48.40	**49.34**
TiO_2	**1.90**	1.69	**1.67**	1.43	1.56	**1.49**	1.41	**1.32**	1.14	1.20	1.23	1.27	**1.41**
Al_2O_3	**14.19**	14.89	**15.50**	16.08	16.40	**14.85**	16.48	**15.86**	16.94	16.21	16.85	15.77	**15.36**
FeO	**10.63**	9.94	**10.67**	9.01	8.79	**11.28**	10.61	**11.79**	10.39	10.63	9.23	9.46	**10.90**
MnO	**0.17**	0.17	**0.15**	0.15	0.15	**0.18**	0.17	**0.18**	0.18	0.18	0.14	0.17	**0.17**
MgO	**10.16**	11.66	**6.35**	6.30	3.86	**8.32**	8.88	**8.01**	6.87	8.74	6.25	9.47	**9.29**
CaO	**10.92**	11.03	**8.51**	8.11	7.24	**11.25**	10.77	**10.25**	10.18	9.01	8.79	9.90	**9.18**
Na_2O	**3.39**	3.96	**3.76**	3.63	3.74	**3.00**	3.51	**3.27**	3.36	3.63	3.68	3.83	**3.13**
K_2O	**1.28**	1.14	**1.27**	1.35	1.95	**0.71**	0.74	**0.61**	0.66	1.00	0.66	0.90	**0.83**
P_2O_5	**0.94**	1.01	**0.51**	0.62	0.57	**0.45**	0.57	**0.40**	0.56	0.43	0.41	0.83	**0.38**
Total	**100.00**	100	**100.00**	100	100	**100.00**	100	**100.00**	100	100	100	100	**100.00**
Sm ppm						6.02							
Nd ppm						31.1							
$^{147}Sm/^{144}Nd$						0.117							
$^{143}Nd/^{144}Nd$						0.513							
+/-						2							
εNd						-1.78							

Major elements reported in weight percent. Trace elements reported in ppm.
Bold indicates an ICP-MS analysis performed by Activation Laboratories.
Italics indicates a XRF analysis performed at Baylor University.
Isotopic analysis performed by Activation Laboratories.

Table 4.3. Continued.

	Low-K Basalt Series												
	070721	070721	**080573**	080573	080546	**070701**	070701	**080585**	080585	080522	080562	080582	**080512**
Ba	**998**	983	**783**	831	1014	**472**	521	**482**	572	528	694	839	**368**
Rb	**15**	14	**18**	15	26	**9**	9	**8**	8	14	11	14	**10**
Sr	**1348**	1218	**972**	944	843	**675**	682	**621**	641	600	642	1060	**541**
Zr	**186**	182	**166**	153	196	**114**	125	**96**	104	124	107	144	**125**
Hf	**3.9**		**4.1**			**2.4**		**2.4**					**3.0**
Y	**26.2**	25	**26.5**	26	25	**22.7**	26	**24.1**	25	28	20	28	**21.6**
Nb	**31.2**	33	**13.3**	14	39	**13.5**	17	**13.7**	15	18	15	25	**16.4**
Th	**5.62**	4	**1.89**	2	7	**2.65**	3	**2.67**	2	1	1	5	**2.11**
Zn	**123**		**165**			**91**		**143**					**60**
V	**223**		**201**			**203**		**209**					**194**
Ni	**215**	208	**124**	125	36	**141**	158	**143**	126	180	80	175	**201**
Sc	**22.5**	27	**20.6**	22	19	**27.2**	28	**27.5**	27	25	19	25	**24.1**
La	**53.7**		**35.0**			**30.1**		**24.6**					**20.0**
Ce	**100.1**		**83.2**			**58.0**		**53.4**					**41.2**
Pr	**10.32**		**10.04**			**6.02**		**6.03**					**4.97**
Nd	**35.6**		**35.9**			**21.4**		**21.9**					**19.8**
Sm	**7.09**		**7.63**			**4.72**		**4.75**					**4.35**
Eu	**2.36**		**2.34**			**1.62**		**1.61**					**1.39**
Gd	**6.25**		**6.55**			**4.50**		**4.78**					**4.74**
Tb	**0.90**		**0.93**			**0.69**		**0.77**					**0.74**
Dy	**4.85**		**4.90**			**3.91**		**4.47**					**4.25**
Ho	**0.89**		**0.93**			**0.76**		**0.86**					**0.84**
Er	**2.38**		**2.62**			**2.14**		**2.50**					**2.31**
Tm	**0.324**		**0.363**			**0.298**		**0.357**					**0.342**
Yb	**1.92**		**2.23**			**1.82**		**2.25**					**2.11**
Lu	**0.270**		**0.329**			**0.264**		**0.326**					**0.314**

Table 4.3. Continued.

	Low-K Basalt Series			Alkaline Basalt Series								
	080521	080511	080515	**070901**	070901	070714	070722	080551	**080523**	080523	**080543**	080543
SiO_2	**47.35**	50.59	55.48	**50.24**	49.91	51.93	48.83	49.68	**48.76**	48.78	**56.13**	58.49
TiO_2	**1.64**	1.55	1.36	**1.76**	1.63	1.68	1.65	1.38	**1.46**	1.48	**0.95**	0.80
Al_2O_3	**14.64**	13.52	16.60	**15.10**	16.72	16.30	15.44	14.68	**15.43**	15.77	**18.28**	18.29
FeO	**8.69**	8.44	8.41	**9.05**	8.14	8.51	8.75	7.47	**10.14**	9.75	**6.27**	5.41
MnO	**0.19**	0.16	0.14	**0.14**	0.14	0.14	0.15	0.11	**0.19**	0.17	**0.16**	0.14
MgO	**8.99**	8.21	4.69	**7.51**	6.66	5.61	9.30	11.03	**7.99**	8.82	**2.56**	2.36
CaO	**12.57**	10.78	7.20	**9.01**	8.60	8.83	9.43	9.11	**10.59**	9.89	**6.48**	5.81
Na_2O	**2.48**	3.62	3.95	**3.95**	4.81	3.71	3.72	3.91	**3.41**	3.44	**5.65**	5.07
K_2O	**2.19**	1.79	1.78	**2.41**	2.42	2.25	1.87	1.54	**1.12**	1.01	**2.58**	2.76
P_2O_5	**1.27**	1.33	0.39	**0.82**	0.97	1.05	0.86	1.10	**0.90**	0.90	**0.94**	0.87
Total	**100.00**	100	100	**100.00**	100	100	100	100	**100.00**	100	**100.00**	100
Sm ppm							9.61					
Nd ppm							60.7					
$^{147}Sm/^{144}Nd$							0.096					
$^{143}Nd/^{144}Nd$							0.512					
+/-							3					
εNd							-3.16					

Table 4.3. Continued.

	Low-K Basalt Series			Alkaline Basalt Series								
	080521	080511	080515	**070901**	070901	070714	070722	080551	**080523**	080523	**080543**	080543
Ba	**2024**	1739	777	**1437**	1404	1580	1709	1589	**1140**	1170	**2230**	2227
Rb	**33**	29	26	**40**	36	31	30	22	**15**	15	**53**	48
Sr	**2811**	2255	644	**1669**	1511	1669	1739	1880	**1324**	1272	**2089**	1910
Zr	**143**	243	173	**212**	212	219	224	209	**128**	174	**322**	291
Hf	**3.2**			**4.7**					**3.0**		**5.9**	
Y	**28.7**	29	23	**23.1**	24	23	25	25	**27.8**	32	**29.3**	28
Nb	**53.3**	51	28	**36.8**	40	38	41	37	**30.4**	33	**58.8**	67
Th	**14.02**	11	5	**3.62**	2	4	5	4	**9.92**	8	**25.29**	24
Zn	**72**			**123**					**81**		**94**	
V	**218**			**194**					**215**		**105**	
Ni	**186**	139	43	**134**	124	120	132	165	**172**	129	**0**	29
Sc	**20.6**	21	20	**18.5**	21	24	21	27	**25.2**	25	**7.3**	12
La	**113.4**			**58.9**					**74.5**		**132.7**	
Ce	**200.0**			**114.1**					**132.2**		**226.8**	
Pr	**21.34**			**11.92**					**14.43**		**22.05**	
Nd	**74.4**			**42.0**					**51.3**		**60.1**	
Sm	**11.96**			**7.83**					**8.91**		**9.94**	
Eu	**3.29**			**2.53**					**2.47**		**2.85**	
Gd	**10.15**			**6.22**					**7.98**		**7.99**	
Tb	**1.20**			**0.85**					**1.05**		**1.00**	
Dy	**5.92**			**4.39**					**5.49**		**5.13**	
Ho	**1.05**			**0.79**					**1.04**		**0.98**	
Er	**2.76**			**2.10**					**2.82**		**2.87**	
Tm	**0.361**			**0.287**					**0.393**		**0.403**	
Yb	**2.35**			**1.67**					**2.50**		**2.45**	
Lu	**0.332**			**0.237**					**0.363**		**0.341**	

Table 4.3. Continued.

	Xenocrystic Basalt Series									Hornblende Dacite Series		
	85909	85909	**070706**	070706	**070702**	070702	070705	080516	080517	**070715**	070715	**080542**
SiO_2	**56.74**	56.35	**48.15**	47.61	**50.08**	49.21	47.38	55.01	50.68	**69.68**	67.25	**69.34**
TiO_2	**1.12**	1.15	**1.46**	1.48	**1.41**	1.42	1.44	1.32	1.63	**0.39**	0.39	**0.39**
Al_2O_3	**15.65**	16.41	**15.88**	17.13	**16.03**	16.75	16.55	16.66	16.43	**14.93**	16.25	**15.49**
FeO	**7.25**	7.39	**10.54**	10.27	**9.95**	9.80	9.74	8.59	10.19	**2.80**	2.65	**2.80**
MnO	**0.13**	0.13	**0.18**	0.18	**0.17**	0.17	0.17	0.14	0.17	**0.05**	0.05	**0.05**
MgO	**5.88**	5.38	**8.43**	8.05	**7.33**	7.59	7.93	5.04	7.08	**1.35**	2.63	**1.15**
CaO	**7.00**	6.83	**10.18**	9.81	**9.37**	9.25	8.41	7.75	8.10	**3.63**	3.28	**3.20**
Na_2O	**3.69**	4.05	**3.48**	3.74	**3.62**	3.88	3.90	3.64	4.04	**4.20**	4.70	**4.47**
K_2O	**2.13**	2.00	**1.08**	1.17	**1.40**	1.36	1.20	1.49	1.31	**2.74**	2.60	**2.91**
P_2O_5	**0.41**	0.31	**0.61**	0.54	**0.64**	0.57	3.29	0.36	0.38	**0.22**	0.20	**0.20**
Total	**100.00**	100	**100.00**	100	**100.00**	100	100	100	100	**100.00**	100	**100.00**
Sm ppm							4.63			2.66		
Nd ppm							23.2			17.45		
$^{147}Sm/^{144}Nd$							0.121			0.092		
$^{143}Nd/^{144}Nd$							0.513			0.513		
+/-							2			4		
εNd							1.39			-1.24		

Table 4.3. Continued.

	Xenocrystic Basalt Series									Hornblende Dacite Series		
	85909	85909	**070706**	070706	**070702**	070702	070705	080516	080517	**070715**	070715	**080542**
Ba	**947**	977	**613**	662	**785**	797	591	671	657	**1325**	1378	**1204**
Rb	**32**	31	**17**	16	**20**	19	17	22	20	**33**	34	**37**
Sr	**750**	728	**802**	825	**854**	831	587	621	617	**772**	809	**694**
Zr	**166**	168	**73**	162	**166**	172	152	163	169	**122**	134	**102**
Hf	**3.5**		**2.1**		**3.7**					**2.9**		**2.9**
Y	**19.4**	21	**27.0**	26	**24.5**	25	24	23	25	**7.7**	9	**8.2**
Nb	**26.4**	30	**21.8**	28	**23.5**	28	20	25	26	**14.5**	15	**17.7**
Th	**6.80**	5	**2.77**	2	**4.37**	4	4	5	3	**8.78**	12	**7.05**
Zn	**80**		**81**		**132**					**51**		**61**
V	**139**		**211**		**198**					**44**		**43**
Ni	**90**	92	**111**	126	**101**	113	76	49	33	**0**	23	**0**
Sc	**18.0**	18	**24.3**	29	**25.4**	25	26	20	26	**5.1**	6	**4.1**
La	**37.3**		**43.6**		**38.8**					**35.8**		**25.6**
Ce	**67.4**		**81.5**		**80.6**					**57.7**		**46.9**
Pr	**6.44**		**9.60**		**9.00**					**5.10**		**4.63**
Nd	**21.0**		**32.0**		**30.4**					**15.3**		**14.3**
Sm	**4.36**		**6.22**		**5.78**					**2.68**		**2.75**
Eu	**1.51**		**1.97**		**1.90**					**0.84**		**0.82**
Gd	**4.01**		**5.68**		**5.46**					**1.94**		**2.08**
Tb	**0.62**		**0.87**		**0.83**					**0.26**		**0.29**
Dy	**3.43**		**4.68**		**4.54**					**1.37**		**1.48**
Ho	**0.65**		**0.92**		**0.87**					**0.25**		**0.28**
Er	**1.82**		**2.67**		**2.54**					**0.68**		**0.78**
Tm	**0.258**		**0.377**		**0.367**					**0.094**		**0.109**
Yb	**1.65**		**2.40**		**2.25**					**0.57**		**0.68**
Lu	**0.236**		**0.354**		**0.325**					**0.082**		**0.104**

Table 4.3. Continued.

	Hornblende Dacite Series					Strongly Alkaline Basalt Series					
	080542	080541	**080544**	080544	080545	**080536**	080536	080513	**080563**	080563	080502
SiO_2	71.01	71.59	**68.05**	68.56	71.39	**42.38**	40.39	43.32	**41.19**	39.75	42.49
TiO_2	0.37	0.38	**0.41**	0.40	0.34	**1.68**	1.57	1.57	**1.70**	1.52	1.49
Al_2O_3	14.25	14.08	**16.46**	16.33	14.97	**13.78**	13.94	13.33	**13.59**	13.57	13.32
FeO	2.45	2.49	**2.99**	2.69	2.20	**10.04**	9.88	8.06	**10.97**	9.85	10.16
MnO	0.05	0.05	**0.06**	0.05	0.04	**0.22**	0.20	0.13	**0.23**	0.21	0.23
MgO	2.15	2.09	**1.25**	1.87	1.76	**10.38**	13.49	17.63	**10.23**	14.90	11.37
CaO	3.02	2.94	**3.42**	3.31	2.60	**13.90**	12.71	10.19	**14.34**	12.64	14.72
Na_2O	3.61	3.36	**4.31**	3.86	3.48	**4.05**	4.70	3.74	**4.59**	4.96	3.03
K_2O	2.91	2.85	**2.85**	2.75	3.06	**1.67**	1.41	0.82	**0.93**	0.76	0.79
P_2O_5	0.18	0.18	**0.20**	0.18	0.15	**1.90**	1.70	1.21	**2.23**	1.83	2.41
Total	100	100	**100.00**	100	100	**100.00**	100	100	**100.00**	100	100
Sm ppm						14.89					
Nd ppm						97.8					
$^{147}Sm/^{144}Nd$						0.092					
$^{143}Nd/^{144}Nd$						0.513					
+/-						2					
εNd						1.55					

Table 4.3. Continued.

	Hornblende Dacite Series					Strongly Alkaline Basalt Series					
	080542	080541	**080544**	080544	080545	**080536**	080536	080513	**080563**	080563	080502
Ba	1193	1185	**1286**	1305	1257	**1548**	1459	1788	**1616**	1485	1769
Rb	37	36	**33**	33	40	**29**	21	24	**13**	11	10
Sr	703	689	**748**	752	601	**2397**	2034	2315	**2565**	2171	2268
Zr	116	114	**111**	120	105	**117**	200	249	**237**	237	237
Hf			**3.1**			**2.1**			**4.4**		
Y	9	9	**8.2**	8	8	**42.8**	36	29	**39.2**	37	40
Nb	19	19	**18.4**	19	14	**44.2**	53	49	**58.5**	69	69
Th	7	8	**7.68**	9	9	**16.32**	13	11	**19.60**	14	15
Zn			**62**			**135**			**175**		
V			**48**			**225**			**247**		
Ni	16	15	**0**	22	16	**177**	171	144	**165**	160	154
Sc	7	4	**5.2**	5	4	**22.9**	29	20	**22.7**	25	29
La			**25.8**			**159.0**			**155.8**		
Ce			**48.5**			**305.6**			**300.2**		
Pr			**4.78**			**32.12**			**31.16**		
Nd			**15.1**			**97.0**			**91.1**		
Sm			**2.76**			**17.05**			**16.30**		
Eu			**0.85**			**4.85**			**4.58**		
Gd			**2.22**			**12.89**			**12.28**		
Tb			**0.32**			**1.66**			**1.56**		
Dy			**1.66**			**8.13**			**7.63**		
Ho			**0.30**			**1.47**			**1.36**		
Er			**0.79**			**3.94**			**3.64**		
Tm			**0.105**			**0.525**			**0.494**		
Yb			**0.64**			**3.04**			**2.90**		
Lu			**0.092**			**0.439**			**0.401**		

Table 4.3. Continued.

	Two Pyroxene Andesite Series											
	060951	060951	**080534**	080534	080531	080532	080533	080535	080572	070713	070712	070711
SiO_2	**58.82**	57.47	**62.42**	63.43	63.23	62.25	63.09	61.88	62.07	61.47	61.65	62.46
TiO_2	**1.08**	1.05	**0.82**	0.81	0.79	0.84	0.81	0.82	0.89	0.80	0.80	0.84
Al_2O_3	**16.13**	17.07	**16.15**	15.93	15.91	16.17	15.69	16.78	15.59	16.22	16.40	15.96
FeO	**6.13**	6.00	**5.09**	4.95	4.78	4.91	4.90	4.93	4.80	4.80	4.61	4.73
MnO	**0.10**	0.10	**0.08**	0.09	0.09	0.09	0.08	0.09	0.08	0.08	0.08	0.08
MgO	**3.81**	4.40	**2.67**	2.50	2.84	2.96	2.81	2.83	3.16	3.81	3.30	2.26
CaO	**6.38**	6.26	**5.50**	5.13	5.22	5.46	5.43	5.33	5.40	5.43	5.32	6.09
Na_2O	**4.46**	4.57	**4.39**	4.22	4.24	4.41	4.28	4.36	4.63	4.43	4.57	4.06
K_2O	**2.16**	2.17	**2.39**	2.50	2.47	2.44	2.46	2.42	2.71	2.46	2.68	2.98
P_2O_5	**0.93**	0.90	**0.48**	0.45	0.43	0.48	0.45	0.57	0.68	0.48	0.59	0.53
Total	**100.00**	100	**100.00**	100	100	100	100	100	100	100	100	100
Sm ppm			4.96									
Nd ppm			30.8									
$^{147}Sm/^{144}Nd$			0.097									
$^{143}Nd/^{144}Nd$			0.512									
+/-			3									
εNd			-2.86									

Table 4.3. Continued.

	Two Pyroxene Andesite Series											
	060951	060951	**080534**	080534	080531	080532	080533	080535	080572	070713	070712	070711
Ba	**1502**	1532	**1425**	1379	1407	1400	1327	1377	1643	1469	1674	1642
Rb	**24**	23	**29**	28	27	23	27	22	31	28	31	30
Sr	**1297**	1277	**1077**	1055	1050	1110	1053	1069	1457	1107	1242	1241
Zr	**173**	200	**194**	178	178	177	174	179	194	181	188	188
Hf	**4.5**		**4.7**									
Y	**20.0**	20	**15.1**	15	19	16	16	16	17	16	17	16
Nb	**27.1**	32	**20.4**	24	23	23	23	23	26	23	23	22
Th	**7.58**	8	**6.79**	5	5	4	5	6	7	5	8	8
Zn	**82**		**72**									
V	**127**		**104**									
Ni	**61**	78	**31**	58	58	62	58	64	60	63	64	64
Sc	**13.3**	15	**11.3**	14	15	16	16	14	14	13	11	12
La	**66.8**		**49.6**									
Ce	**118.3**		**93.6**									
Pr	**12.54**		**9.69**									
Nd	**45.7**		**29.7**									
Sm	**7.04**		**5.41**									
Eu	**2.20**		**1.63**									
Gd	**4.92**		**4.32**									
Tb	**0.75**		**0.59**									
Dy	**3.87**		**3.06**									
Ho	**0.71**		**0.55**									
Er	**1.95**		**1.49**									
Tm	**0.272**		**0.207**									
Yb	**1.68**		**1.23**									
Lu	**0.235**		**0.171**									

Table 4.4. Calculations of temperature, pressure, and depth (Albarede, 1992; Sugawara, 2000; Lee et al., 2009) based on the results of the olivine back calculation method of Parker et al., (2010), which follows the method of Leeman et al. (2009). Samples listed in normal font are XRF analyses, while those in bold print are ICP analyses.

Series	Sample	Ln P (Kbar) *	P (Kbar) *	T(°C) of Segregation †	Depth (Km)
Low-K	070721	3.58	35.87	1581	121
	070701	3.45	31.5	1581	107
	080573	2.67	14.44	1452	52
	080585	3.20	24.54	1544	84
	080522	3.23	25.28	1548	87
	080582	3.12	22.65	1498	78
	080511	2.76	15.8	1430	56
	080512	3.21	24.78	1551	85
	080521	3.15	23.34	1479	81
	070721	3.46	31.82	1580	108
	070701	3.38	29.37	1587	100
	080573	3.08	21.76	1538	75
	080585	3.46	31.82	1614	108
Alkaline	080523	3.14	23.1	1512	80
	080551	2.60	13.46	1378	49
	070722	2.97	19.49	1460	68
	080523	3.22	25.03	1535	86
Strongly Alkaline	080536	4.08	59.15	1708	197
	080563	4.18	65.37	1741	217
	080502	3.85	46.99	1648	157
	080513	3.73	41.68	1630	140
	080536	3.87	47.94	1652	160
	080563	4.09	59.74	1743	198

* - Albarede, 1992

† - Sugawara, 2000

Table 4.5. NCI calculation results following the procedure of DePaolo et al. (1992).

Sample	Series	εNd	NCI *	NCI †
070701	Low-K	-1.78	23.6	35.7
070722	Alkaline	-3.16	32.3	43.0
070705	Xenocrystic	1.39	3.8	19.0
080536	Strongly Alkaline	1.55	2.8	18.2
080534	Two Pyroxene	-2.86	30.4	41.4
070715	Hornblende Dacite	-1.24	20.3	32.8

* - crustal εNd of -14, lithosphere εNd of 2

† - crustal εNd of -14, asthenosphere εNd of 5

REFERENCES CITED

Albarede, F., 1992. How deep do common basaltic magmas form and differentiate?, Journal of Geophysical Research, v. 97, p. 10997-11009

Anderson, D.J., Lindsley, D.H., and Davidson, P.M., 1993. QUILF: a PASCAL program to assess equilibria among Fe-Mg-Mn-Ti oxides, pyroxenes, olivine and quartz: Computers and Geoscience, v. 19, p. 1333-1350.

Aubele, J.C., and Crumpler, L.S., 2001. Raton-Clayton and Ocate Volcanic Fields. New Mexico Geological Society Guidebook, 52nd Field Conference, Geology of the Llano Estacado, 69-76

Baldridge, W.S., 2004. Pliocene-Quaternary volcanism in New Mexico and a model for genesis of magmas in continental extension, *In* Mack, G.H., and Giles, K.A., (*eds*.), The Geology of New Mexico: A Geologic History. New Mexico Geological Society Special Publication 11, p. 313-330

Baldridge, W.S., Keller, G.R., Haak, V., Wendlandt, E., Jiracek, G.R., and Olsen, K.H., 1995. The Rio Grande Rift. *In* Olsen, K.H., (*ed.*), Continental rifts: evolution, structure, tectonics: Amsterdam, Elsevier. p. 233-275

Baldridge, W.S., Perry, F.V., Vaniman, D.T., Nealey, L.D., Leavy, B.D., Laughlin, A.W., Kyle, P., Bartov, Y., Steinitz, G., and Gladney, E.S., 1991. Middle to late Cenozoic magmatism of the southeastern Colorado Plateau and central Rio Grande rift (New Mexico and Arizona, USA): A model for continental rifting. Tectonophysics, 197: 327-354

Baldwin, B., and Muehlberger, W.R., 1959. Geologic studies of Union County, New Mexico: New Mexico Bureau of Mines and Mineral Resources Bulletin 63, 171 p.

Barker, D.S., 1979. Cenozoic magmatism in the Trans-Pecos Province: relation to the Rio Grande Rift *in* Riecker, R.E., (*ed.*), Rio Grande Rift; tectonics and magmatism: American Geophysical Union, p. 382-392.

CD-ROM Working Group, 2002. Structure and evolution of the lithosphere beneath the Rocky Mountains: initial results from the CD-ROM experiment, GSA Today, p. 4-10

Chapin, C.E., 1971. The Rio Grande Rift, Part I: Modifications and additions, *in* James, H.L., (*ed.*), Guidebook of the San Luis Basin, Colorado: New Mexico Geological Society, Twenty-second Annual Field Conference, Guidebook, v. 22, p. 191-201

Chapin, C.E., 1979. Evolution of the Rio Grande Rift - A summary, *in* Riecker, R.E., ed., Rio Grande Rift: Tectonics and magmatism: Washington, D.C., American Geophysical Union, p. 1-5

Chapin, C.E., and Cather, S.M., 1994. Tectonic setting of the axial basins of the northern and central Rio Grande rift, *In* Keller, G.R., and Cather, S.M., (*eds.*), Basins of the Rio Grande Rift: Structure, Stratigraphy, and Tectonic Setting, Boulder, Colorado, Geological Society of America Special Paper 291

Chapin, C.E., Wilks, M., and McIntosh, W.C., 2004. Space-time patterns of Late Cretaceous to present magmatism in New Mexico-comparison with Andean volcanism and potential for future volcanism. New Mexico Bureau of Geology and Mineral Resources, Bulletin 160, 13-40

Collins, R.F., 1949. Volcanic rocks of Northeastern New Mexico, Bulletin of the Geological Society of America, v. 60, p. 1017-1040

Davidson, J.P., 1996. Deciphering mantle and crustal signatures in subduction zone magmatism. *In* Bebout, G.E., Scholl, D.W., Kirby, S.H., Platt, J.P., (*eds*.), Subduction: Top to Bottom. Monogr. Am. Geophys. Union 96, 251-262

Davidson, J.P., Dungan, M.A., Ferguson, K.M., and Colucci, M.T., 1987. Crust-magma interactions and the evolution of arc magmas: the San Pedro-Pellado volcanic complex, southern Chilean Andes, Geology, 15, 443-446

Davis, L.L., Smith, D., McDowell, F.W., Walker, N.W., and Borg, L.E., 1996. Eocene potassic magmatism at Two Buttes, Colorado, with implications for Cenozoic tectonics and magma generation in the western United States: Geological Society of America Bulletin, v. 108, p. 1567-1579.

DePaolo, D.J., Perry, F.V., and Baldridge, W.S., 1992. Crustal versus mantle sources of granitic magmas: a two-parameter model based on Nd isotope studies: Royal Society of Edinburgh Transactions: Earth Sciences, v. 83, p. 439-446

Dungan, M.A., Thompson, R.A., Stormer, J.S., and O'Neill, J.M., 1989. Excursion 18B: Rio Grande rift volcanism: Northeastern Jemez zone, New Mexico. *In* Chapin, C.E., and Zidek, J., (*eds*.), Field Excursions to volcanic terranes in the western United States, Volume I: Southern Rocky Mountain region. NM Bureau of Mines and Mineral Resources, Memoir 46, 435-486

Fitton, J.G., James, D., Kempton, P.D., Ormerod, D.S., and Leeman, W.P., 1988. The role of lithospheric mantle in the generation of late Cenozoic basifc magmas in the western United States: Journal of Petrology, Special Lithosphere Issue, p. 331-349.

Gibson, S.A., Thompson, R.N., Leat, P.T., Morrison, M.A., Hendry, G.L., Dickin, A.P., and Mitchell, J.G., 1992. Asthenosphere-derived magmatism in the Rio Grande rift, western USA: implications for continental break-up, *in* Storey, B.C., Alabaster, T., and Pankhurst, R.J., (eds.) Magmatism and the causes of continental break-up, Geological Society Special Publication no. 68, p. 61-89

Gibson, S.A., Thompson, R.N., Leat, P.T., Morrison, M.A., Hendry, G.L., Dickin, A.P., and Mitchell, J.G., 1993. Ultrapotassic magmas along the flanks of the Oligo-Miocene Rio Grande Rift, USA: Monitors of the zone of lithospheric mantle extension and thinning beneath a continental rift, Journal of Petrology, v. 34, p. 187-228

Gilbert, H., 2012. Crustal structure and signatures of recent tectonism as influenced by ancient terranes in the western United States, Geosphere, v. 8, no. 1, p. 141-157

Jones, L.M., Walker, R.L., and Stormer, J.C., 1974. Isotope composition of strontium and origin of volcanic rocks of the Raton-Clayton district, northeastern New Mexico, Geological Society of America Bulletin, v. 85, p. 33-36

Karlstrom, K.E., and Humphreys, E.D., 1998. Persistent influence of Proterozoic accretionary boundaries in the tectonic evolution of southwestern North America: interaction of cratonic grain and mantle modification events, Rocky Mountain Geology, v. 33, p. 161-179

Keller, G.R., and Baldridge, W.S., 1999. The Rio Grande rift: a geological and geophysical overview, Rocky Mountain Geology, v. 34, p. 121-130

Kluth, C.F., and Schaftenaar, C.H., 1994. Depth and geometry of the northern Rio Grande rift in the San Luis Basin, south-central Colorado, *In* Keller, G.R., and Cather, S.M., (*eds.*), Basins of the Rio Grande Rift: Structure, Stratigraphy, and Tectonic Setting: Boulder, Colorado, Geological Society of America Special Paper 291, p. 27-37

Le Bas, M.J., Le Maitre, R.W., Streckeisen, A., and Zanettin, B., 1986. A chemical classification of volcanic rocks based on the total alkali-silica diagram. Journal of Petrology 27, p. 745-750

Leeman, W.P., Schutt, D.L., Hughes, S.S., 2009. Thermal structure beneath the Snake River Plain: implications for the Yellowstone Hotspot, Journal of Volcanology and Geothermal Research, v. 188, p. 57-67

Leeman, W.P., Lewis, J.F., Evarts, R.C., Conrey, R.M., Streck, M.J., 2005. Petrologic constraints on the thermal structure of the Cascade arc, Journal of Volcanology and Geothermal Research, v. 140, p. 67-105

Le Maitre, R.W. (ed.), 1989. A classification of igneous rocks and glossary of terms, Blackwell Scientific, Oxford, 193 p.

Lindsley, D.H., 1983. Pyroxene thermometry, American Mineralogist, v. 68, p. 477-493

Luedke, R.G., and Smith, R.L., 1978. Map showing distribution, composition, and age of the late Cenozoic volcanic centers in Arizona and New Mexico, US Geological Survey Miscellaneous Investigation Series Map I-1091-A

Magnani, M.B., Miller, K.C., Levander, A., and Karlstrom, K., 2004. The Yavapai-Mazatzal boundary: a long-lived tectonic element in the lithosphere of southwestern North America, Geological Society of America Bulletin, v. 116, p. 1137-1142

McDonough, W.F., and Sun, S.S., 1995. The composition of the Earth. Chemical Geology 120, p. 223-253

Menzies, M.A., Kyle, P.R., Jones, M., and Ingram, G., 1991. Enriched and depleted source components for tholeiitic and alkaline lavas from Zuni-Bandera, New Mexico: Inferences about intraplate processes and stratified lithosphere, Journal of Geophysical Research, v. 96, p. 13645-13671

Mutschler, F.E., Larson, E.E., and Bruce, R.M., 1987. Laramide and younger magmatism in Colorado – new petrologic and tectonic variations on old themes. *In* Drexler, J.W., and Larson, E.E., (*eds*.), Cenozoic volcanism in the southern Rocky Mountains updated: a tribute to Rudy C. Epis – Part I. Colorado School of Mines Quarterly 82, p. 1-47

Parker, D.F., Hodges, F.N., Perry, A., Mitchener, M.E., Barnes, M.A., and Ren, M., 2010. Geochemistry and petrology of late Eocene Cascade Head and Yachats Basalt and alkalic intrusions of the central Oregon Coastal Range, U.S.A., Journal of Volcanology and Geothermal Research, v. 198, p. 311-324

Parker, D.F., and McMillan, N., 2007. Early onset of Rio Grande Rift magmatism in West Texas: Geological Society of America, Abstracts with programs, v. 39, no. 6, p. 511.

Perry, F.V., Baldridge, W.S., and DePaolo, D.J., 1987. Role of asthenosphere and lithosphere in the genesis of late Cenozoic basaltic rocks from the Rio Grande rift and adjacent regions of the southwestern United States. Journal of Geophysical Research, 92: 9193-9213

Phelps, D.W., Gust, D.A., and Wooden, J.L., 1983. Petrogenesis of the mafic feldspathoidal lavas of the Raton-Clayton volcanic field, New Mexico, Contributions to Mineralogy and Petrology, v. 84, p. 182-190

Shaw, C.A., and Karlstrom, K.E., 1999. The Yavapai-Mazatzal crustal boundary in the southern Rocky Mountains, Rocky Mountain Geology, v. 34, p. 37-52

Sinno, Y.A., Daggett, P.H., Keller, G.R., Morgan, P., and Harder, S.H., 1986. Crustal structure of the southern Rio Grande rift determined from seismic refraction profiling, Journal of Geophysical Research, v. 91, p. 6143-6156

Stormer, J.C., Jr., 1972. Mineralogy and petrology of the Raton-Clayton volcanic field, northeastern New Mexico. GSA Bulletin 83, p. 3299-3322

Stormer, J.C., 1987. Capulin Mountain Volcano and the Raton-Clayton Volcanic Field, northeastern New Mexico, Geological Society of America Centennial Field Guide - Rocky Mountain Section, p. 421-424

Stroud, J.R., 1997. The volcanic history and landscape evolution of the Raton-Clayton volcanic field [M.S. Thesis], Socorro, NM Institute of Mining and Technology, 49p.

Sugawara, T., 2000. Empirical relationships between temperature, pressure, and MgO content in olivine and pyroxene saturated liquid, Journal of Geophysical Research, v. 105, p. 8457-8472

Wakita, H., Rey, P., and Schmitt, R.A., 1971. Abundances of the 14 rare-earth elements and 12 other rare elements in Apollo 12 samples: Five igneous and one breccia rocks and four soils: Proceedings of the Second Lunar Science Conference, v. 2, p. 1319-1329

White, J.C., Holt, G.S., Parker, D.F., and Ren, M., 2003. Trace-element partitioning between alkali feldspar and peralkalic quartz trachyte to rhyolite magma, part I: Systematics of trace-element partitioning: American Mineralogist, v. 88, p. 316-329.

White, J.C., Ren, Minghua, and Parker, D.F., 2005. Variation in mineralogy, temperature, and oxygen fugacity in a suite of strongly peralkaline lavas and tuffs, Pantelleria, Italy: Canadian Mineralogist, v. 43, p. 1331-1347.

Yuan, H., and Dueker, K., 2005. Upper mantle tomographic V_p and V_s images of the Rocky Mountains in Wyoming, Colorado, and New Mexico: evidence for a thick heterogeneous chemical lithosphere, Geophysical Monograph Series 154, p. 329-345

CHAPTER FIVE

Conclusions

Volcanic rocks, from a variety of locations throughout Colorado and New Mexico, exhibit subduction-like geochemical signatures even though they were formed far from the edge of the continent. Each of these volcanic centers was created by a different set of processes, however, all magmas have undergone differentiation during ascent, with fractional crystallization being the predominant process.

The εNd_t values from McDermott Formation trachyandesite indicate that lithospheric mantle is the probable source for this volcanic material. Upper and lower crustal xenolith analyses reported in literature suggest much higher εNd_t values for crustal material, ruling out crustal anatexis as a source for the McDermott magmas. However, NCI calculations do indicate some crustal Nd contribution to the magmas and xenocrysts were observed in one sample. General geochemical trends suggest a possible relationship between the McDermott Formation trachyandesite and the La Plata Mountains intrusive complex, though weathering and sericitization of both sets of rock have made geochemical modelling impossible.

The Nathrop Domes erupted a low temperature (~650-670 ^{o}C) rhyolite with a strongly negative εNd_t value. The similarity between the εNd_t value from the rhyolite and that of the local Precambrian granite suggest a crustal source for these lava domes. Trace element patterns lack the subduction-like signature and show evidence of high degrees of fractional crystallization. The location of these rhyolite domes at the edge of the Arkansas Valley Graben suggests that rift-related magmatism likely provided the heat

to create the relatively low volume of rhyolite erupted at this locality. NCI calculations also suggest mantle contributions to the Nathrop magmas of 20-30%.

The six series from the Raton-Clayton volcanic field all contain this subduction-like signature despite their widely varied compositions. εNd_t values from all series, combined with trace element data, suggest a lithospheric mantle source for these magmas. Depth calculations suggest typical lithospheric depths for most magmas, though depths as great as 217 km were calculated for some strongly alkaline series magmas. These calculations also support current literature estimates for the thickness of the lithosphere being approximately 200 km beneath the RGR. Temperature and pressure calculations also support a greater depth of melting for the strongly alkaline series magmas. All magmas from this field evolved through open-system processes including assimilation and fractional crystallization. The varying degrees of assimilation, unknown assimilant compositions, and apparent formation as numerous individual magma systems made geochemical modelling impossible.

The correlation between the presence of the subduction-like signature and εNd_t values similar to lithospheric mantle indicates that this signature is likely a lithospheric mantle feature. Partial melting of this ancient, subduction-modified lithosphere produced magmas with this subduction-like signature far from the areas of concurrent subduction.

BIBLIOGRAPHY

Albarede, F., 1992. How deep do common basaltic magmas form and differentiate?, Journal of Geophysical Research, v. 97, p. 10997-11009

Andersen, D. J., Lindsley, D. H., Davidson, P. M., 1993, QUILF: A PASCAL program to assess equilibria among Fe–Mg–Mn–Ti oxides, pyroxenes, olivine, and quartz: Computers and Geosciences, v. 19, p. 1333–1350.

Aubele, J.C., and Crumpler, L.S., 2001. Raton-Clayton and Ocate Volcanic Fields. New Mexico Geological Society Guidebook, 52nd Field Conference, Geology of the Llano Estacado, 69-76

Bacon, C. R., and Hirschmann, M. M., 1988, Mg/Mn partitioning as a test for equilibrium between coexisting Fe–Ti oxides: American Mineralogist, v. 73, p. 57–61.

Baldridge, W.S., 2004. Pliocene-Quaternary volcanism in New Mexico and a model for genesis of magmas in continental extension, *In* Mack, G.H., and Giles, K.A., (*eds*.), The Geology of New Mexico: A Geologic History. New Mexico Geological Society Special Publication 11, p. 313-330

Baldridge, W. S., Keller, G. R., Haak, V., Wendlandt, E., Jiracek, G. R., and Olsen, K. H., 1995, The Rio Grande Rift, *in* Olsen, K. H., ed., Continental rifts: Evolution, structure, and tectonics: Developments in Geotectonics, v. 25, Amsterdam, Elsevier, p. 233–275.

Baldridge, W. S., Olsen, K. H., and Callender, J. F., 1984, Rio Grande Rift: Problems and perspectives, *in* Baldridge, W. S., Dickerson, P. W., Riecker, R. E., and Zidek, J., eds., Rio Grande Rift: Northern New Mexico: New Mexico Geological Society Thirty-fifth Annual Field Conference, Guidebook, v. 35, p. 1–12.

Baldridge, W.S., Perry, F.V., Vaniman, D.T., Nealey, L.D., Leavy, B.D., Laughlin, A.W., Kyle, P., Bartov, Y., Steinitz, G., and Gladney, E.S., 1991. Middle to late Cenozoic magmatism of the southeastern Colorado Plateau and central Rio Grande rift (New Mexico and Arizona, USA): A model for continental rifting. Tectonophysics, 197: 327-354

Baldwin, B., and Muehlberger, W.R., 1959. Geologic studies of Union County, New Mexico: New Mexico Bureau of Mines and Mineral Resources Bulletin 63, 171 p.

Baltz, E.H., Ash, S.R., and Anderson, R.Y., 1966, History of nomenclature and stratigraphy of rocks adjacent to the Cretaceous-Tertiary boundary, western San Juan Basin, New Mexico: United States Geological Survey Professional Paper, p. D1-D23.

Barker, D.S., 1979. Cenozoic magmatism in the Trans-Pecos Province: relation to the Rio Grande Rift *in* Riecker, R.E., (*ed.*), Rio Grande Rift; tectonics and magmatism: American Geophysical Union, p. 382-392.

Bickford, M. E., and Boardman, S. J., 1984, A Proterozoic volcano–plutonic terrane, Gunnison and Salida areas, Colorado: The Journal of Geology, v. 92, p. 657–666.

Burt, D. M., Sheridan, M. F., Bikun, J. V., and Christiansen, E. H., 1982, Topaz rhyolites—Distribution, origin, and significance for exploration: Economic Geology, v. 77, p. 1818–1836.

CD-ROM Working Group, 2002. Structure and evolution of the lithosphere beneath the Rocky Mountains: initial results from the CD-ROM experiment, GSA Today, p. 4-10

Chapin, C. E., 1971, The Rio Grande Rift, Part I: Modifications and additions, *in* James, H. L., ed., Guidebook of the San Luis Basin, Colorado: New Mexico Geological Society, Twenty-second Annual Field Conference, Guidebook, v. 22, p. 191–201.

Chapin, C. E., 1979, Evolution of the Rio Grande Rift—A summary, *in* Riecker, R. E. ed., Rio Grande Rift: Tectonics and magmatism: Washington, D.C., American Geophysical Union, p. 1–5.

Chapin, C. E., and Cather, S. M., 1994, Tectonic setting of the axial basins of the northern and central Rio Grande Rift, *in* Keller, G. R., and Cather, S. M., eds., Basins of the Rio Grande Rift: Structure, stratigraphy, and tectonic setting: Boulder, Colorado, Geological Society of America Special Paper 291, p. 5–25.

Chapin, C.E., Wilks, M., and McIntosh, W.C., 2004, Space-time patterns of Late Cretaceous to present magmatism in New Mexico-comparison with Andean volcanism and potential for future volcanism: New Mexico Bureau of Geology and Mineral Resources Bulletin 160, p. 13-40.

Christiansen, E. H., Sheridan, M. F., and Burt, D. M., 1986, The geology and geochemistry of Cenozoic topaz rhyolites from the western United States: Geological Society of America Special Paper 205, 82 p.

Collins, R.F., 1949. Volcanic rocks of Northeastern New Mexico, Bulletin of the Geological Society of America, v. 60, p. 1017-1040

Condie, K.C., Latysh, N., Van Schmus, W.R., Kozuch, M., and Selverstone, J., 1999, Geochemistry, Nd and Sr isotopes, and U/Pb zircon ages of granitoid and metasedimentary xenoliths from the Navajo Volcanic Field, Four Corners area, southwestern United States: Chemical Geology, v. 156, p. 95-133.

Condie, K.C., and Selverstone, J., 1999, The crust of the Colorado Plateau: new views of an old arc: Journal of Geology, v. 107, p. 387-397.

Condon, S.M., 1990, Geologic and structure contour map of the Southern Ute Indian Reservation and adjacent areas, southwestern Colorado and northwest New Mexico: United States Geological Survey Miscellaneous Investigations Series Map I-1958, 1:100,000 scale.

Cowan, D.S., and Bruhn, R.L., 1992, Late Jurassic to early Late Cretaceous geology of the U.S. Cordillera, i*n* Burchfiel, B.C., Lipman, P.W., and Zoback, M.L., (*eds.*), The Cordilleran Orogen: Conterminous U.S.: Boulder, Colorado, Geological Society of America, The Geology of North America, v. G-3, p. 169-203.

Cunningham, C.G., Naeser, C.W., Marvin, R.F., Luedke, R.G., and Wallace, A.R., 1994, Ages of selected intrusive rocks and associated ore deposits in the Colorado Mineral Belt: U.S. Geological Survey Bulletin 2109, 31 p.

Davidson, J. P., 1996, Deciphering mantle and crustal signatures in subduction zone magmatism, *in* Bebout, G. E., Scholl, D. W., Kirby, S. H., and Platt, J. P., eds., Subduction: Top to bottom: American Geophysical Union Monograph Series, v. 96, p. 251–262.

Davidson, J.P., Dungan, M.A., Ferguson, K.M., and Colucci, M.T., 1987. Crust-magma interactions and the evolution of arc magmas: the San Pedro-Pellado volcanic complex, southern Chilean Andes, Geology, 15, 443-446

Davis, L.L., Smith, D., McDowell, F.W., Walker, N.W., and Borg, L.E., 1996. Eocene potassic magmatism at Two Buttes, Colorado, with implications for Cenozoic tectonics and magma generation in the western United States: Geological Society of America Bulletin, v. 108, p. 1567-1579.

DePaolo, D. J., Perry, F. V., and Baldridge, W. S., 1992, Crustal versus mantle sources of granitic magmas: A two-parameter model based on Nd isotopic studies: Royal Society of Edinburgh Transactions: Earth Sciences, v. 83, p. 439–446.

Dickinson, W.R., Klute, M.A., Hayes, M.J., Janecke, S.U., Lundin, E.R., McKittrick, M.A., and Olivares, M.D., 1988, Paleogeographic and paleotectonic setting of Laramide sedimentary basins in the central Rocky Mountain region: Geological Society of America Bulletin, v. 100, p. 1023-1039.

Dickinson, W.R., and Snyder, W.S., 1978, Plate tectonics of the Laramide orogeny: Geological Society of America, Memoir 151, p. 355-366.

Dungan, M.A., Thompson, R.A., Stormer, J.S., and O'Neill, J.M., 1989. Excursion 18B: Rio Grande rift volcanism: Northeastern Jemez zone, New Mexico. *In* Chapin, C.E., and Zidek, J., (*eds*.), Field Excursions to volcanic terranes in the western United States, Volume I: Southern Rocky Mountain region. NM Bureau of Mines and Mineral Resources, Memoir 46, 435-486

Eckel, E.B., Williams, J.S., and Galbraith, F.W., 1949, Geology and ore deposits of the La Plata district, Colorado, with sections by G.M. Schwartz, D.J. Varnes, and E.N. Goddard: U.S. Geological Survey Professional Paper 219, 179 p.

Feeley T.C., and Cosca, M.A., 2003, Time vs. composition trends of magmatism at Sunlight volcano, Absaroka volcanic province, Wyoming: Geological Society of America Bulletin, v. 115, p. 714-728.

Fitton, J.G., James, D., Kempton, P.D., Ormerod, D.S., and Leeman, W.P., 1988, The role of lithospheric mantle in the generation of late Cenozoic basic magmas in the western United States: Journal of Petrology, Special Lithosphere Issue, p. 331-349

Gibson, S. A., Thompson, R. N., Leat, P. T., Dickin, A. P., Morrison, M. A., Hendry, G. L., and Mitchell, J. G., 1992, Asthenosphere-derived magmatism in the Rio Grande Rift, western USA: Implications for continental break-up, *in* Storey, B. C., Alabaster, T., and Pankhurst, R. J., eds., Magmatism and the causes of continental break-up: Geological Society Special Publication, v. 68, p. 61–89.

Gibson, S. A., Thompson, R. N., Leat, P. T., Morrison, M. A., Hendry, G. L., Dickin, A. P., and Mitchell, J. G., 1993, Ultrapotassic magmas along the flanks of the Oligo–Miocene Rio Grande Rift, USA: Monitors of the zone of lithospheric mantle extension and thinning beneath a continental rift: Journal of Petrology, v. 34, p. 187–228.

Gilbert, H., 2012, Crustal structure and signatures of recent tectonism as influenced by ancient terranes in the western United States: Geosphere, v. 8, p. 141–157.

Gutscher, M.-A., Spakman, W., Bijwaard, H., and Engdahl, E.R., 2000, Geodynamics of flat subduction: Seismicity and tomographic constraints from the Andean margin: Tectonics, v. 19, p. 814-833

Harlan, S.S., Snee, L.W., and Geissman, J.W., 1996, $^{40}Ar/^{39}Ar$ geochronology and paleomanetism of Independence volcano, Absaroka volcanic supergroup, Beartooth Mountains, Montana: Canadian Journal of Earth Science, v. 33, p. 1648-1654.

Halliday, A. N., Davidson, J. P., Hildreth, W., and Holden, P., 1991, Modelling the petrogenesis of high Rb/Sr silicic magmas: Chemical Geology, v. 92, p. 107–114.

Jones, L.M., Walker, R.L., and Stormer, J.C., 1974. Isotope composition of strontium and origin of volcanic rocks of the Raton-Clayton district, northeastern New Mexico, Geological Society of America Bulletin, v. 85, p. 33-36

Karlstrom, K. E., and Humphreys, E. D., 1998, Persistent influence of Proterozoic accretionary boundaries in the tectonic evolution of southwestern North America: Interaction of cratonic grain and mantle modification events: Rocky Mountain Geology, v. 33, p. 161–179.

Karlstrom, K.E., Amato, J.M., Williams, M.L., Heizler, M., Shaw, C.A., Read, A.S., and Bauer, P., 2004, Proterozoic tectonic evolution of the New Mexico region: A synthesis, *In* Mack, G.H., and Giles, K.A., (*eds*.), The Geology of New Mexico: A Geologic History: New Mexico Geological Society Special Publication 11, p. 1-34.

Keller, J. W., McCalpin, J. P., and Lowry, B. W., 2004, Geologic map of the Buena Vista east quadrangle, Chaffee County, Colorado: Colorado Geological Survey Open-File Report OF04-04.

Kluth, C.F., and Schaftenaar, C.H., 1994. Depth and geometry of the northern Rio Grande rift in the San Luis Basin, south-central Colorado, *In* Keller, G.R., and Cather, S.M., (*eds.*), Basins of the Rio Grande Rift: Structure, Stratigraphy, and Tectonic Setting: Boulder, Colorado, Geological Society of America Special Paper 291, p. 27-37

Le Bas, M. J., Le Maitre, R. W., Streckeisen, A., and Zanettin, B., 1986, A chemical classification of volcanic rocks based on the total alkali-silica diagram: Journal of Petrology, v. 27, p. 745–750.

Leeman, W.P., Schutt, D.L., Hughes, S.S., 2009. Thermal structure beneath the Snake River Plain: implications for the Yellowstone Hotspot, Journal of Volcanology and Geothermal Research, v. 188, p. 57-67

Leeman, W.P., Lewis, J.F., Evarts, R.C., Conrey, R.M., Streck, M.J., 2005. Petrologic constraints on the thermal structure of the Cascade arc, Journal of Volcanology and Geothermal Research, v. 140, p. 67-105

Le Maitre, R.W. (ed.), 1989. A classification of igneous rocks and glossary of terms, Blackwell Scientific, Oxford, 193 p.

Lipman, P.W., Prostka, H.J., and Christiansen, R.L., 1972, Cenozoic volcanism and plate-tectonic evolution of the Western United States. I. Early and Middle Cenozoic: Philosophical Transactions of the Royal Society of London, v. 271, p. 217-248.

Lindsley, D.H., 1983. Pyroxene thermometry, American Mineralogist, v. 68, p. 477-493

Luedke, R.G., and Smith, R.L., 1978. Map showing distribution, composition, and age of the late Cenozoic volcanic centers in Arizona and New Mexico, US Geological Survey Miscellaneous Investigation Series Map I-1091-A, 1:1,000,000 scale

Magnani, M.B., Miller, K.C., Levander, A., and Karlstrom, K., 2004, The Yavapai-Mazatzal boundary: a long-lived tectonic element in the lithosphere of southwestern North America: Geological Society of America Bulletin, v. 116, p. 1137-1142.

Mattie, P.D., Condie, K.C., Selverstone, J., and Kyle, P.R., 1997, Origin of the continental crust in the Colorado Plateau: Geochemical evidence from mafic xenoliths from the Navajo Volcanic Field, southwestern USA: Geochimica et Cosmochimica Acta, v. 61, p. 2007-2021.

McCoy, A.M., Karlstrom, K.E., Shaw, C.A., Williams, M.L., 2005, The Proterozoic Ancestry of the Colorado Mineral Belt: 1.4 Ga shear zone system in central Colorado, *in* Keller, G.R., (*ed.*), The Rocky Mountain Region: An Evolving Lithosphere: American Geophysical Union Geophysical Monograph Series 154, p. 71-90.

McDonough, W. F., and Sun, S. S., 1995, The composition of the Earth: Chemical Geology, v. 120, p. 223–253.

McIntosh, W. C., and Chapin, C. E., 2004, Geochronology of the central Colorado volcanic field: New Mexico Bureau of Geology and Mineral Resources, Bulletin 160, p. 205–237.

McIntosh, W. C., and Chapin, C. E., 2007, Geochronology of the early southern Rocky Mountain volcanic field, *in* The Volcanoes of Colorado: A Colorado Scientific Society Symposium Honoring Thomas A. Steven: Greeley, Colorado, University of Northern Colorado, p. 13–14.

McMillan, N.J., 2004, Magmatic record of Laramide subduction and the trasnition to Tertiary extension: upper Cretaceous through Eocene igneous rocks of New Mexico, *In* Mack, G.H., and Giles, K.A., (*eds*.), The Geology of New Mexico: A Geologic History: New Mexico Geological Society Special Publication 11, p. 249-270.

Meen, J.K., and Eggler, D.H., 1987, Petrology and geochemistry of the Cretaceous Independence volcanic suite, Absaroka Mountains, Montana: clues to the composition of the Archean sub-Montanan mantle: Geological Society of America Bulletin, v. 98, p. 238-247.

Menzies, M.A., Kyle, P.R., Jones, M., and Ingram, G., 1991, Enriched and depleted source components for tholeiitic and alkaline lavas from Zuni-Bandera, New Mexico: Inferences about intraplate processes and stratified lithosphere: Journal of Geophysical Research, v. 96, p. 13645-13671.

Miller, D.M., Nilsen, T.H., and Bilodeau, W.L., 1992, Late Cretaceous to early Eocene geologic evolution of the U.S. Cordillera, *in* Burchfiel, B.C., Lipman, P.W., and Zoback, M.L., (*eds.*), The Cordilleran Orogen: Conterminous U.S.: Boulder, Colorado, Geological Society of America, The Geology of North America v. G-3, p. 205-260.

Mutschler, F. E., Larson, E. E., and Bruce, R. M., 1987, Laramide and younger magmatism in Colorado—New petrologic and tectonic variations on old themes, *in* Drexler, J. W., and Larson, E. E., eds., Cenozoic volcanism in the southern Rocky Mountains updated: A tribute to Rudy C. Epis—Part I: Colorado School of Mines Quarterly, v. 82, p. 1–47.

Parker, D. F., Ghosh, A., Price, C. W., Rinard, B. D., Cullers, R. L., and Ren, M., 2005, Origin of rhyolite by crustal melting and the nature of parental magmas in the Oligocene Conejos Formation, east–central San Juan Mountains, Colorado, USA: Journal of Volcanology and Geothermal Research, v. 139, p. 185–210.

Parker, D.F., Hodges, F.N., Perry, A., Mitchener, M.E., Barnes, M.A., and Ren, M., 2010. Geochemistry and petrology of late Eocene Cascade Head and Yachats Basalt and alkalic intrusions of the central Oregon Coastal Range, U.S.A., Journal of Volcanology and Geothermal Research, v. 198, p. 311-324

Parker, D.F., and McMillan, N., 2007. Early onset of Rio Grande Rift magmatism in West Texas: Geological Society of America, Abstracts with programs, v. 39, no. 6, p. 511.

Pearce, J. A., Harris, N. B. W., and Tindle, A. G., 1984, Trace element discrimination diagrams for the tectonic interpretation of granitic rocks: Journal of Petrology, v. 25, p. 956–983.

Perry, F. V., Baldridge, W. S., and DePaolo, D. J., 1987, Role of asthenosphere and lithosphere in the genesis of late Cenozoic basaltic rocks from the Rio Grande Rift and adjacent regions of the southwestern United States: Journal of Geophysical Research, v. 92, p. 9193–9213.

Perry, F.V., Baldridge, W.S., and DePaolo, D.J., 1988, Chemical and isotopic evidence for lithosphere thinning beneath the Rio Grande rift. Nature, 332: 432-434

Perry, F. V., DePaolo, D. J., and Baldridge, W. S., 1993, Neodymium isotopic evidence for decreasing crustal contributions to Cenozoic ignimbrites of the western United States: Implications for the thermal evolution of the Cordilleran crust: Geological Society of America Bulletin, v. 105, p. 872–882.

Phelps, D.W., Gust, D.A., and Wooden, J.L., 1983. Petrogenesis of the mafic feldspathoidal lavas of the Raton-Clayton volcanic field, New Mexico, Contributions to Mineralogy and Petrology, v. 84, p. 182-190

Putirka, K. D., 2008, Thermometers and barometers for volcanic systems: Reviews in Mineralogy and Geochemistry, v. 69, p. 61–120.

Reeside, J.B. Jr., 1924, Upper Cretaceous and Tertiary formations of the western part of the San Juan Basin Colorado and New Mexico: United States Geological Survey, Professional Paper 134, p. 1-70.

Rollinson, H.R., 1993, Using geochemical data; evaluation, presentation, interpretation: Longman Scientific and Technical, Harlow, United Kingdom, 352 p.

Schooler, R. A., 1982, Interpretation of rock and vapor phase relations in the Ruby Mountain Volcanic Complex, Chaffee County, Colorado [Master's thesis]: Bowling Green, Ohio, Bowling Green State University, 104 p.

Shaw, C. A., and Karlstrom, K. E., 1999, The Yavapai–Mazatzal crustal boundary in the southern Rocky Mountains: Rocky Mountain Geology, v. 34, p. 37–52.

Sinno, Y.A., Daggett, P.H., Keller, G.R., Morgan, P., and Harder, S.H., 1986. Crustal structure of the southern Rio Grande rift determined from seismic refraction profiling, Journal of Geophysical Research, v. 91, p. 6143-6156

Stormer, J.C., Jr., 1972. Mineralogy and petrology of the Raton-Clayton volcanic field, northeastern New Mexico. GSA Bulletin 83, p. 3299-3322

Stormer, J.C., 1987. Capulin Mountain Volcano and the Raton-Clayton Volcanic Field, northeastern New Mexico, Geological Society of America Centennial Field Guide - Rocky Mountain Section, p. 421-424

Stroud, J.R., 1997. The volcanic history and landscape evolution of the Raton-Clayton volcanic field [M.S. Thesis], Socorro, NM Institute of Mining and Technology, 49p.

Sugawara, T., 2000. Empirical relationships between temperature, pressure, and MgO content in olivine and pyroxene saturated liquid, Journal of Geophysical Research, v. 105, p. 8457-8472

Taylor, S. R., and McLennan, S. M., 1985, The Continental Crust: Its composition and evolution. Blackwell, Oxford, 312 p.

Tweto, O., 1979, Geologic map of Colorado: United States Geological Survey, 1:500,000 scale.

Tweto, O., 1979, The Rio Grande Rift system in Colorado, *in* Riecker, R. E., ed., Rio Grande Rift: Tectonics and magmatism: Washington, D.C., American Geophysical Union, p. 33–56.

Tweto, O., and Sims, P. K., 1963, Precambrian ancestry of the Colorado mineral belt: Geological Society of America Bulletin, v. 74, p. 991–1014.

Van Alstine, R. E., 1969, Geology and mineral deposits of the Poncha Springs NE quadrangle, Chaffee County, Colorado, with a section on fluorspar mines and prospects: U.S. Geological Survey Professional Paper 626, 52 p.

Wakita, H., Rey, P., and Schmitt, R. A., 1971, Abundances of the 14 rare-earth elements and 12 other rare elements in Apollo 12 samples: Five igneous and one breccia rocks and four soils: Proceedings of the Second Lunar Science Conference, v. 2, p. 1319–1329.

Werle, J.L., Ikramuddin, M, and Mutschler, F.E., 1984, Allard stock, La Plata Mountains Colorado – an alkaline rock-hosted porphyry copper – precious metal deposit: Canadian Journal of Earth Science v. 21, p. 630-641.

Whalen, J. B., Currie, K. L., and Chappell, B. W., 1987, A-type granites: Geochemical characteristics, discrimination and petrogenesis: Contributions to Mineralogy and Petrology, v. 95, p. 407–419.

White, J.C., Holt, G.S., Parker, D.F., and Ren, M., 2003. Trace-element partitioning between alkali feldspar and peralkalic quartz trachyte to rhyolite magma, part I: Systematics of trace-element partitioning: American Mineralogist, v. 88, p. 316-329.

White, J.C., Ren, Minghua, and Parker, D.F., 2005. Variation in mineralogy, temperature, and oxygen fugacity in a suite of strongly peralkaline lavas and tuffs, Pantelleria, Italy: Canadian Mineralogist, v. 43, p. 1331-1347.

Wilson, A.B., and Sims, P.K., 2003, Colorado mineral belt revisited – an analysis of new data: U.S. Geological Survey Open-File Report 03-046, 7 p.

Wobus, R. A., and 11 others, 1990, Geochemistry of high-potassium rocks from the mid-Tertiary Guffey volcanic center, Thirtynine Mile Volcanic Field, central Colorado: Geology, v. 18, p. 642–645.

Yuan, H., and Dueker, K., 2005. Upper mantle tomographic V_p and V_s images of the Rocky Mountains in Wyoming, Colorado, and New Mexico: evidence for a thick heterogeneous chemical lithosphere, Geophysical Monograph Series 154, p. 329-345